

UNIVERSITY OF OKLAHOMA

GRADUATE COLLEGE

VARIABLE TEMPERATURE DIFFUSE REFLECTION INFRARED
SPECTROSCOPY AND THERMOGRAVIMETRY- MASS SPECTROMETRY
INVESTIGATIONS OF BENZOIC ACID INTERACTIONS WITH SODIUM AND
CALCIUM MONTMORILLONITE CLAYS

A DISSERTATION

SUBMITTED TO THE GRADUATE FACULTY

in partial fulfillment of the requirements for the

Degree of

DOCTOR OF PHILOSOPHY

By

TARA MICHELLE NICKELS

Norman, Oklahoma

2015

VARIABLE TEMPERATURE DIFFUSE REFLECTION INFRARED
SPECTROSCOPY AND THERMOGRAVIMETRY- MASS SPECTROMETRY
INVESTIGATIONS OF BENZOIC ACID INTERACTIONS WITH SODIUM AND
CALCIUM MONTMORILLONITE CLAYS

A DISSERTATION APPROVED FOR THE
DEPARTMENT OF CHEMISTRY AND BIOCHEMISTRY

BY

Dr. Robert White, Chair

Dr. Wai-Tak Yip

Dr. Charles Rice

Dr. Shaorong Liu

Dr. Mark Nanny

© Copyright by TARA MICHELLE NICKELS 2015
All Rights Reserved.

I would like to dedicate my work to my husband, Logan. He has brought me more joy than he may ever know. Graduate school at the University of Oklahoma is the best decision I have ever made because it is here that I met my wonderful husband, my partner in crime.

Acknowledgements

I would like to thank Dr. Robert White for all of his guidance, support, and constructive criticism. I am honored to have learned from such a wonderful chemist and person. The skills I have gained from his teachings are invaluable. I would like to thank my graduate committee: Dr. Shaorong Liu, Dr. Wai Tak Yip, Dr. Charles Rice, Dr. Mark Nanny, and Dr. Frederike Jentoft for their guidance and input to my PhD program career. In addition, I would like to thank Audrey Ingram and Dalia Maraoulaite for their stimulating discussion and contribution to this project.

I would like to thank my parents Rusty and Tina Gann, Deborah Davis and Rod Cummins, and my grandparents. Their love and support has always been there in my times of need. I would like to say a very special thank you to my husband, Logan, and his wonderful family. My husband has been the support that I have needed to get to where I am today. I would also like to thank John Kennedy. He has been an enormous influence in my life and his words of wisdom and encouragement have meant a lot to me through my educational journey.

Table of Contents

Acknowledgements	iv
Table of Contents	v
List of Tables	viii
List of Figures	ix
Abstract.....	xii
1 Chapter 1: Background	1
1.1 Pharmaceuticals and Personal Care Products.....	3
1.1.1 Environmental Exposure	4
1.1.2 Recent Investigations	6
1.2 Benzoic Acid	10
1.2.1 Benzoic Acid Structure and Properties	10
1.2.2 Benzoic Acid Sources	11
1.2.3 Environmental Exposure	12
1.3 Montmorillonite Clay.....	14
1.3.1 Montmorillonite Clay Structure.....	14
1.3.2 Montmorillonite Interlayer	17
1.4 Variable Temperature Diffuse Reflection Infrared Fourier Transform Spectroscopy as a Method for Analysis of Soil Contaminants	19
1.5 Thermogravimetric- Mass Spectrometric Analysis as a Method for Analysis of Soil Contaminants.....	23
1.6 Research Objectives	23
2 Chapter 2: Experimental	25

2.1	Chemicals and Reagents.....	25
2.2	Sample Preparation	26
2.2.1	Sodium and Calcium Montmorillonite Samples	26
2.2.2	Benzoic Acid Loadings of Sodium and Calcium Montmorillonite Clays	27
2.2.3	Variable Temperature-Diffuse Reflection Infrared Fourier Transform Spectroscopy Sample Preparation.....	28
2.3	Instrumentation.....	31
2.3.1	Variable Temperature Diffuse Reflection Infrared Fourier Transform Spectroscopy.....	31
2.3.2	Thermogravimetry-Mass Spectrometry	35
2.4	Molecular Modeling.....	37
2.5	Data Manipulation	39
2.5.1	Variable Temperature Diffuse Reflection Infrared Fourier Transform Spectroscopy Data.....	39
2.5.2	Thermogravimetry Mass Spectrometry Data.....	40
3	Chapter 3: Variable Temperature Diffuse Reflection Infrared Spectroscopy Investigation of Benzoic Acid Interactions with Montmorillonite Clay Interlayer Water.....	43
3.1	Introduction	43
3.2	Results and Discussion.....	45
3.3	Conclusions	57
4	Chapter 4: Thermogravimetry – Mass Spectrometry Investigation of Benzoic Acid Interactions with Sodium and Calcium Montmorillonite Clays	59
4.1	Introduction	59
4.2	Results and Discussion.....	60
4.3	Conclusions	86

5	Chapter 5: Variable Temperature Infrared Spectroscopy Investigations of Benzoic Acid Desorption from Sodium and Calcium Montmorillonite Clays ...	88
5.1	Introduction	88
5.2	Results and Discussion.....	89
5.3	Conclusions	107
6	Chapter 6: Conclusions and Future Implications	110
6.1	Benzoic Acid and Water Molecular Environments	111
6.2	Subsequent Soil Contaminant Investigations	123
6.2.1	Thermogravimetric-Mass Spectrometric Data Predictions for Salicylic Acid loaded montmorillonites	124
6.2.2	Variable Temperature- Diffuse Reflection Infrared Fourier Transform Spectroscopy Data predictions for salicylic acid loaded montmorillonites	125
6.3	Future Applications.....	126
	References.....	130
	Appendix I: Molecular Modeling	141
	Appendix II: Thermogravimetry-Mass Spectrometry Time and Temperature Correlation	151

List of Tables

Table 1.1 Selected PPCP Organic Acid Contaminant Risk Ranking	8
Table 2.1 Preparation of Na and Ca Cation Exchanged Montmorillonites	27
Table 2.2 Benzoic Acid Loadings on Sodium Montmorillonite	28
Table 2.3 Benzoic Acid Loadings on Calcium Montmorillonite	28
Table 2.4 Silver Powder Dilutions	29
Table 3.1 Carboxylic Acid Functionality Vibrational Frequencies (cm^{-1})	54
Table 3.2 Measured and Calculated Vibrational Frequencies for Benzoic Acid Adsorbed on CaMMT (cm^{-1})	56
Table 3.3 Measured and Calculated Vibrational Frequencies for Benzoic Acid Adsorbed on NaMMT (cm^{-1})	57
Table 5.1 Benzoic Acid Vibration Band Assignments (cm^{-1})	92
Table 6.1 Salicylic Acid Predicted and Experimental Infrared Frequencies	126

List of Figures

Figure 1.1 Fate of Pharmaceuticals and Personal Care Products in Waste Water.....	5
Figure 1.2 Benzoic Acid Dimer	11
Figure 1.3 Montmorillonite Structure	17
Figure 1.4 VT-DRIFTS Perturbation Method	22
Figure 2.1 Diffuse Reflection	30
Figure 2.2 Reflectance spectra measured for neat (solid line) and 5% (w/w) clay diluted in silver powder (dashed line).	30
Figure 2.3 VT-DRIFTS Schematic	33
Figure 2.4 VT-DRIFTS Sample Holder Diagram.....	34
Figure 2.5 Thermogravimetry Apparatus Cross-Section	36
Figure 2.6 Molecular Modeling Schematic of Benzoic Acid Monomer, Water Molecule, and Na ⁺ or Ca ²⁺ cation	38
Figure 2.7 Molecular Modeling Schematic of Benzoic Acid Monomer and Na ⁺ or Ca ²⁺ cation.....	38
Figure 3.1 Benzoic acid deposited on Ca (solid) and Na (dashed) montmorillonites.....	46
Figure 3.2 Rate of O-H stretching vibration intensity loss as a function of sample temperature.....	48
Figure 3.3 VT-DRIFTS spectra representing loss of interlayer water	50
Figure 4.1 Mass loss curves for sodium (dashed line) and calcium (solid line) montmorillonites.....	62
Figure 4.2 Mass spectrometric m/z 18 ion signal intensity profiles representing water desorption from sodium (dashed line) and calcium (solid line) montmorillonite	65
Figure 4.3 Neat sodium montmorillonite mass spectrometric m/z 18 ion signal intensity profile (solid line) overlaid with first derivative of weight loss curve (dashed line)	66

Figure 4.4 Neat calcium montmorillonite mass spectrometric m/z 18 ion signal intensity profile (solid line) overlaid with first derivative of weight loss curve (dashed line)	66
Figure 4.5 Curve fitting for the neat sodium montmorillonite m/z 18 ion intensity temperature profile	67
Figure 4.6 Curve fitting for the neat calcium montmorillonite m/z 18 ion intensity temperature profile	67
Figure 4.7 Mass loss curves for samples containing 10% (w/w) benzoic acid adsorbed on sodium (dashed line) and calcium (solid line) montmorillonites	69
Figure 4.8 Mass spectrometric m/z 18 ion signal intensity profiles representing water desorption from samples containing 10% (w/w) benzoic acid adsorbed on sodium (dashed line) and calcium (solid line) montmorillonites	71
Figure 4.9 Low temperature mass spectrometric m/z 18 ion signal intensity profile overlays for benzoic acid loaded calcium montmorillonites	73
Figure 4.10 High temperature mass spectrometric m/z 18 ion signal intensity profile overlays for benzoic acid loaded calcium montmorillonites	73
Figure 4.11 Low temperature mass spectrometric m/z 18 ion signal intensity profile overlays for benzoic acid loaded sodium montmorillonites	74
Figure 4.12 High temperature mass spectrometric m/z 18 ion signal intensity profile overlays for benzoic acid loaded sodium montmorillonites	74
Figure 4.13 Mass spectrometric ion signal intensity profiles representing water (18), benzoic acid (122), benzene (78), and carbon dioxide (44) measured during TG-MS analysis of samples containing 10% (w/w) benzoic acid adsorbed on (a) sodium and (b) calcium montmorillonite	77
Figure 4.14 TG-MS analysis of Benzoic Acid Deposited on Silver Powder	78
Figure 4.15 Mass spectrometric m/z 122 ion signal intensity temperature profiles for samples containing different amounts of benzoic acid adsorbed on (a) sodium and (b) calcium montmorillonites	81
Figure 4.16 Mass spectrometric m/z 44 ion signal intensity temperature profiles for samples containing different amounts of benzoic acid adsorbed on calcium montmorillonites	84
Figure 4.17 Mass spectrometric m/z 78 ion signal intensity temperature profiles for samples containing different amounts of benzoic acid adsorbed on calcium montmorillonites	84

Figure 4.18 Mass spectrometric m/z 44 ion signal intensity temperature profiles for samples containing different amounts of benzoic acid adsorbed on sodium montmorillonites	85
Figure 4.19 Mass spectrometric m/z 78 ion signal intensity temperature profiles for samples containing different amounts of benzoic acid adsorbed on sodium montmorillonites	85
Figure 5.1 Ambient temperature DRIFTS spectra for benzoic acid/clay samples and for neat clay (top) and benzoic acid (bottom)	91
Figure 5.2 VT-DRIFTS spectra for sodium (left) and calcium (right) montmorillonites containing 10% (w/w) benzoic acid. The overlaid spectra shown at the top were subtracted to produce the difference spectra at the bottom	97
Figure 5.3 VT-DRIFTS spectra for sodium (left) and calcium (right) montmorillonites containing 10% (w/w) benzoic acid. The overlaid spectra shown at the top were subtracted to produce the difference spectra at the bottom	100
Figure 5.4 VT-DRIFTS spectra for sodium (left) and calcium (right) montmorillonites containing 10% (w/w) benzoic acid. The overlaid spectra shown at the top were subtracted to produce the difference spectra at the bottom	103
Figure 5.5 Plots of -C=O stretching vibration band wavenumber as a function of sample temperature obtained from VT-DRIFTS analyses of samples containing 10% (w/w) benzoic acid adsorbed on (a) sodium and (b) calcium montmorillonites	106
Figure 6.1 Adsorbed Benzoic Acid	114
Figure 6.2 Clustered Benzoic Acid: (a) benzoic acid interacting through a water bridge, (b) benzoic acid interacting through long range hydrogen bonding	116
Figure 6.3 Benzoate-Cation Interaction	118
Figure 6.4 Water Bridge	121

Abstract

Molecular interactions between benzoic acid and cations and water contained within montmorillonite clay interlayer spaces and processes involved in thermal desorption of benzoic acid from sodium and calcium montmorillonite clays are characterized by using variable temperature diffuse reflection infrared Fourier transform spectroscopy (VT-DRIFTS) and thermogravimetry-mass spectrometry (TG-MS). The availability of high stability Fourier transform infrared interferometers make it possible to conduct experiments designed to identify subtle sample structure changes resulting from external perturbations. In particular, infrared spectrum measurements obtained while heating samples can be used to associate specific structure changes with incremental additions of thermal energy. By using sample perturbation and difference spectroscopy, infrared spectral changes resulting from removal of interlayer water are associated with changes in local benzoic acid environments. Additionally, desorption of benzoic acid is identified and subtle changes in molecular vibrations are detected and employed to characterize specific benzoic acid adsorption sites. Difference spectra features can be correlated with changes in specific molecular vibrations that are characteristic of benzoic acid molecular orientation. Results suggest that the carboxylic acid functionality of benzoic acid interacts with interlayer cations through a bridging water molecule and that this interaction is affected by the nature of the cation present in the clay interlayer space. These interactions can also be disrupted by the presence of organic anions, in particular, benzoate. Abrupt changes in benzoic acid adsorption properties occur for both clay samples at about 125 °C.

Results from thermogravimetric-mass spectrometric analyses of sodium and calcium montmorillonites containing adsorbed benzoic acid are used to characterize adsorption sites and elucidate thermal desorption processes. Desorption of interlayer water is affected by the presence of benzoic acid, which disrupts cation-water interactions. Multiple benzoic acid desorption environments are indicated, which depend on the clay interlayer cation. Benzoic acid desorption occurs at higher temperatures for clays containing calcium ions compared to those containing sodium ions, presumably due to stronger interactions between the adsorbate and calcium ions. Benzoic acid desorption profiles, as well as the detection of decomposition products, suggest that benzoic acid persists on clays to temperatures as high as 550 °C. Above 300 °C, benzoic acid decomposes, yielding benzene and carbon dioxide.

Chapter 1: Background

Concerns about water purity and the inability to remove pharmaceuticals and personal care products (PPCPs) by waste water plants were first raised more than 50 years ago. In 1965, Stumm-Zollinger and Fair published findings that steroid hormones were present in wastewaters. [1] Reporting that steroid contaminated waste waters were released into the environment through waste water treatment plants (WWTP), they postulated that mixing with groundwater was inevitable. [1] However, despite evidence of environmental contamination through waste water release into natural water supplies, little attention was paid to this issue until the 1990s. At that time, the first analytical techniques for quantification of low concentrations of pharmaceuticals and personal care products in aqueous environments were developed. [2-6] Early studies provided evidence to suggest that contaminant concentrations significantly below 1 ppb could negatively affect an ecological community. [7-9] Over the past two decades, the issue of PPCPs release into the environment has become a public health concern and therefore the subject of scientific scrutiny. [10-15] Still, PPCPs remain largely unregulated in waste water, so there continues to be a need for understanding the fate of PPCPs in the environment. [16] Analytical techniques can be used to provide information regarding the environmental

impact of improper disposal of pharmaceuticals and personal care product pollutants. Methods for analysis of contaminated wastewaters have been well developed. [17] However, the development of analytical techniques for studying contaminated soils and for elucidating molecular interactions between contaminants and soils is still needed.

To develop the method presented here for investigation of PPCP soil contaminants, a model soil/contaminant system was selected. The Environmental Protection Agency has identified organic acids as a primary source of contamination. [18] Benzoic acid is often employed for surface adsorption studies due to its simple structure, which is representative of organic acids in general. [19-22] Entering the environment primarily through WWTPs, benzoic acid is diluted to low concentrations, and introduced into natural water supplies. The ubiquitous nature of benzoic acid justifies its uses as a test contaminant. Through soil contact with released waste water, benzoic acid is typically adsorbed on the clay component, [23] which provides a barrier to natural decomposition pathways. [10-11] Consequently, benzoic acid interactions with clays have been extensively studied. [18, 21, 23-27] These studies have primarily focused on montmorillonites, because this clay structure is ubiquitous in soils. Specific molecular interactions between benzoic acid and montmorillonite clays presented here were characterized by variable temperature diffuse reflection infrared Fourier transform spectroscopy (VT-DRIFTS), [28, 29] and thermogravimetry- mass spectrometry (TG-MS). [30]

1.1 Pharmaceuticals and Personal Care Products

Pharmaceuticals and personal care products (PPCPs) is a classification including copious numbers of diverse compounds. Pharmaceuticals are developed and produced for their use as biologically active chemicals, encompassing prescription and over the counter medications for human, veterinary, and agricultural purposes. [31] Personal care products primarily include over the counter commodities intended for external use. This includes cosmetics, fragrances, lotions, shampoos, toothpastes, and sunscreens. [32] Additionally, agricultural pesticides and food preservatives are included in the PPCPs classification. A great number of these compounds are designed to be stable, long lasting, and water soluble, ultimately leading to their persistence in the environment. Pharmaceuticals have greatly contributed to the advancement of our society over the last century. However, it should come as no surprise that as the world population continues to grow, PPCP production rate increase. The rate at which pharmaceutical usage has increased compared to population growth is staggering. The world population expanded approximately 14% from 1999 [33] to 2009; [34] whereas, pharmaceutical use increased by 95% over this time frame. [35] A similar positive correlation is likely for the production of personal care products. This trend will only continue in the future, increasing the need for a better understanding of the environmental fates of PPCPs.

1.1.1 Environmental Exposure

Primarily unregulated, many PPCPs are pervasive in the environment. [1-6] Unfortunately, the environmental and human health consequences of increasing amounts of these contaminants have yet to be fully realized. Hundreds of different PPCPs have been identified in water supplies including: drinking water, agricultural irrigation sources, lakes, rivers, and rainwater. [15, 35-37] Often, these substances are detected at low concentrations. The long-term health effects of chronic exposure to low concentrations of PPCPs have yet to be determined. [38] However, it can be reasonably extrapolated that the previously mentioned trend toward increased pharmaceutical usage will result in increased environmental PPCP concentrations, making chronic exposure worse. Pharmaceuticals and personal care products reach the environment by three main pathways: waste water, refuse and landfills, and industrial release. [15, 39]

Figure 1.1 shows potential pathways by which residential contaminants enter the environment from waste water. Residential contaminants arise from two main sources: improper disposal of unused and expired PPCPs, and human or animal excretion of metabolized and unmetabolized pharmaceuticals. [15, 39] The problem of improper disposal of pharmaceuticals has been widely recognized and protocols for safely disposing of pharmaceuticals have been employed in some areas. [40, 41] However, proper disposal protocols and drop-off sites go largely unused by the public. [40-42] Residential PPCP contaminant wastes can collect in septic tanks or waste water treatment plant holding pools, both of which are susceptible to overflow. [31] Overflow introduces contaminants into the environment. After waste water reaches treatment plants, it is

separated into sludge and liquid. Sludge is often used as fertilizer by farmers, leading to environmental contamination by agricultural run-off. [32] After treating the liquid component, it is released into natural sources. [32] Agricultural run-off and release of treated waste waters are the leading sources of environmental contamination because waste water treatment plants are not designed to remove PPCPs. [31] Altering existing waste water treatment plants so that they could effectively remove PPCPs would be costly. Additionally, any modifications that would be made may not be effective for future decontaminations because of rapid development of new pharmaceuticals and personal care products.

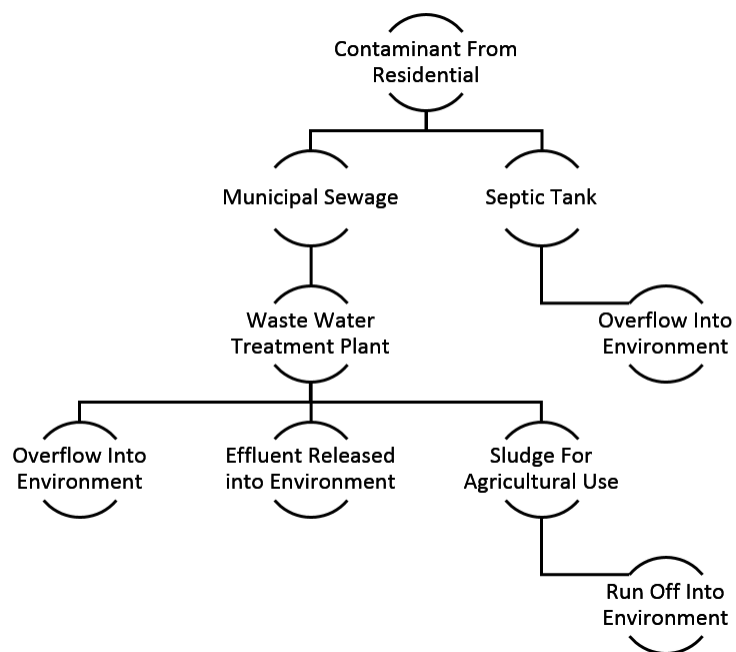


Figure 1.1 Fate of Pharmaceuticals and Personal Care Products in Waste Water

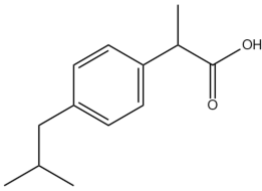
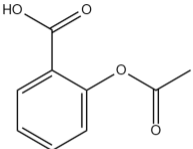
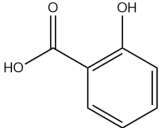
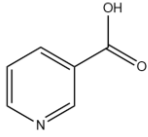
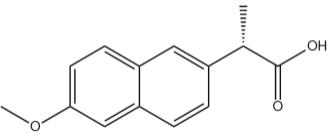
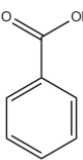
Release of PPCPs into groundwater through refuse disposal and landfilling has been documented over the last two decades. [10, 43, 44] This is of particular concern due to the lack of operating regulations for landfill sites with regard to the types of wastes that are accepted. In fact, most landfills are open dump sites with no closed borders, allowing anonymous disposal of contaminated refuse without consequences. [10] As a result of this lack of regulation, landfills contain the largest number of PPCP contaminants by volume. [45] Rainfall provides a constant pathway for contaminants to enter ground water via land-fill run off. [46] Pharmaceuticals and personal care products have been found in landfill run off at concentrations ranging from 100 to 10,000 ng/L. [15] Although waste waters typically contain the largest total amounts of pharmaceuticals and personal care products, landfill run off is responsible for the highest local concentrations of PPCP environmental contaminants. This is a particularly important problem, because the combination of several pharmaceutical contaminants may pose a greater health risk than the individual substances by themselves. [15] Thus, large PPCP environmental concentrations pose an increased risk to both human health and environmental biosystems. [15]

1.1.2 Recent Investigations

Recently, the number of reported studies involving environmental PPCPs has increased exponentially. [47] A review of the literature from the last decade reveals the detection of an increasing number of PPCP derived compounds in the environment. [38]

Consequently, several attempts have been made to rank known PPCP derived pollutants by their estimated environment and human health risk. [48-50] The purpose of this ranking is to better focus future studies on those substances that potentially pose the greatest risk. Some organic acid contaminants identified by Copper et al are listed in Table 1.1. Although benzoic acid was not included in the organic acids ranked by the Cooper et al study, it is often included in risk rankings because of its wide-spread use and abundance in the environment [51]. Often, decomposition products of high risk compounds are also ranked as potential environmental contaminants. [51] Salicylic acid, for example, is a decomposition product of acetylsalicylic acid. It is also found in over the counter personal care products. However, the leading source of salicylic acid environmental contamination is as an acetylsalicylic acid decomposition product. For reference, benzoic acid [52] and salicylic acid[53] are included in Table 1.1.

Table 1.1 Selected PPCP Organic Acid Contaminant Risk Ranking

Compound/Structure	Environmental Risk Rank (All Data Categories) [48]	Water Solubility (25 °C)	pK _a (25 °C)
 Ibuprofen	1	0.021 mg/mL	4.9
 Acetylsalicylic Acid	125	4.6 mg/mL	3.49
 Salicylic Acid	Not Listed	2.24 mg/mL	2.97
 Nicotinic Acid	135	18.0 mg/mL	4.75
 Naproxen	268	0.0159 mg/mL	4.15
 Benzoic Acid	Not Listed	3.44 mg/mL	4.2

As a result of increased efforts to identify PPCPs at lower concentrations, new analysis methods have been developed for their detection and for investigating the fates of these substances in the environment. Techniques typically employed include: x-ray diffraction, infrared spectroscopy, thermal analysis, and nuclear magnetic resonance. X-ray diffraction studies have been shown to be of use in measuring changes in soil dimensions in response to adsorption of contaminant species. [18, 54-57] While x-ray diffraction is a useful tool for identifying contaminant adsorption, it provides little information regarding the contaminant identity or information concerning specific interactions between contaminants and soils. Thus x-ray diffraction studies are limited to confirming that soils have been contaminated. Nuclear magnetic resonance is often used to characterize soil contaminant environments, including adsorbate configurations. [58-61] However, the sensitive nature of this technique requires that sample compositions be carefully controlled to eliminate interferences. Thus, NMR is not an ideal technique for soil types that are often found in the environment. Several thermal analysis techniques have been utilized to study soil-contaminant interactions, including thermogravimetry and differential scanning calorimetry [18, 62, 63]. These techniques provide information regarding sample changes caused by application of increasing energy (i.e. heat); however, they do not provide information regarding the mechanisms responsible for observed changes. Infrared spectroscopy is a commonly used technique for characterization of contaminant-soil interaction, [24, 25, 64-68] and is often used in combination with sample heating. Samples can be analyzed as thin films or pellets. However, necessary sample

compositions needed to form thermally stable thin films can make interpretations of spectral changes in terms of contaminant-soil interactions difficult.

1.2 Benzoic Acid

The Environmental Protection Agency has identified organic acids as a primary source of contamination. [18] Benzoic acid is the simplest aromatic carboxylic acid, and is often employed for surface adsorption studies because it has a simple structure that is representative of organic acids in general. [19-22] In several studies, including the work presented here, benzoic acid was selected for initial experiments because of its simple structure, which is found in numerous PPCPs.

1.2.1 Benzoic Acid Structure and Properties

Represented in Figure 1.2, neat benzoic acid is a crystalline solid consisting of hydrogen bonded dimers. [69, 70] It exists in a dimerized, planar spatial arrangement, stacked with the carboxylic acid groups arranged in an alternating orientation. [71, 72] Benzoic acid dimers exhibit tautomerization. [73] Based on molecular structure calculations, the benzoic acid dimer is 16 Angstroms in length and the monomer is approximately 7 Angstroms in length. With a pK_a of 4.2, benzoic acid is a weak acid with low solubility in water. [52] It sublimates at 100 °C, melts at 122 °C, and boils at 249 °C. Above 300 °C, benzoic acid can decompose into benzene and carbon dioxide. [74]

Sodium benzoate, which is the conjugate base sodium salt of benzoic acid, is also commonly found in the environment. [52] Sodium benzoate is produced by the reaction of benzoic acid and sodium hydroxide. [52]

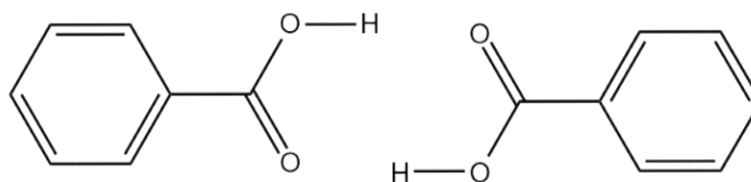


Figure 1.2 Benzoic Acid Dimer

1.2.2 Benzoic Acid Sources

Benzoic acid is produced through several processes. It occurs naturally in many plants, berries, dairy products, tubers, honey, and as an intermediate in metabolite biosynthetic pathways. [52] The primary source of benzoic acid derives from commercial synthesis. Synthetic benzoic acid is used in a variety of manufacturing processes, including production of pharmaceuticals. [52] The World Health Organization estimated the 1998 annual production of benzoic acid to be in excess of 600,000,000 kg worldwide. [52] This estimation includes only industrial benzoic acid production and does not include quantities resulting from decomposition of food, pharmaceuticals, and personal

care products. Current benzoic acid production is most likely much greater than the 1998 estimate.

Widely used as a food preservative, benzoic acid inhibits the growth of mold, yeast, and bacteria. [75-79] Due to its higher solubility compared to benzoic acid (1:200), sodium benzoate is preferred as a preservative, but both forms are employed. [52] Sodium benzoate readily converts to benzoic acid at low pH (<~4.2). Thus, it is often used in foods and beverages that have high acid contents such as fruit juices, soft drinks, pickles, and condiments. [52] Personal care products such as toothpastes, cosmetics, perfumes, lotions, and deodorants, as well as antifungal creams and pharmaceuticals, both prescribed and over the counter, and cigarettes, often contain added benzoic acid or sodium benzoate. [52] Industrially, benzoic acid is used as an antifreeze additive for corrosion inhibition in automobiles and water based cooling systems, [80] and as a stabilizer for photograph processing baths and for packaging plastics. Industrial applications of benzoic acid lead to environmental contamination by its release into air and water supplies.

1.2.3 Environmental Exposure

Benzoic acid has been detected in air, water, and sediments. [37, 81, 82] The primary pathway for human exposure to benzoic acid is from its use as a food preservative. [52] Studies performed to estimate benzoic acid content in food stuffs report that single serving size concentrations range from undetectable to 2100mg/kg. [83, 84]

After ingestion, benzoic acid and sodium benzoate are rapidly absorbed. [52] Although subsequent metabolism can occur rapidly, incomplete metabolism of benzoic acid is common. Metabolism as low as 75% of initial uptake has been reported. Thus, it is to be expected that benzoic acid originating from food sources can be introduced to waste water streams by human and animal eliminations. Furthermore, because large amounts of benzoic acid are used as a food preservatives, discarded food stuffs can contribute significantly to environmental benzoic acid contamination due to landfilling. Benzoic acid can also enter the environment as an industrial waste product. In 1995, Germany released a report citing the amount of benzoic acid environmental contaminant derived solely from industrial processes. At the time it was estimated that as much as 525 kg was introduced into the atmosphere, 3000 kg into natural water sources, and 8000 kg into waste water treatment plants each year. [52] These quantities are likely much higher today.

Treated waste water returned to the environment constitutes yet another pathway for contamination. Benzoic acid is not removed during waste water treatment. Several studies report findings of detectable amounts of benzoic acid in natural water sources such as lakes, rainwater, seawater, and ground water. [37, 85-87] Geoaccumulation of benzoic acid in soils and transport of benzoic acid through soils following rainfall has also been reported. Soils have been found to stabilize contaminants contained in treated waste water. The presence of these substances would otherwise not be concerning because effective water-based decomposition pathways result in short lifetimes. Benzoic acid transport through soils is of great concern for agriculture and wildlife. [88] Although

benzoic acid is not currently thought to represent a significant risk to human health, it does pose a risk to some wildlife and environmental biomes. [52]

1.3 Montmorillonite Clay

Because of significant diversity, soil characterizations are based on complicated classifications that include descriptions of the parent rock (inorganic materials) that is chemically or physically weathered, and the organic matter content. [89] Soil content varies with location and is influenced by many factors, including the parent material and climate effects. [89] Due to the wide range of soil compositions, a single formulation that adequately represents all soils is not available. However, organic acids are typically adsorbed on the clay soil component. [23] Consequently, many studies are simplified by focusing on the clay soil component, instead of a particular soil. These studies often employ montmorillonites, because this type of clay is ubiquitous in soils. [18, 21, 23-26].

1.3.1 Montmorillonite Clay Structure

Montmorillonite clays consist of two negatively charged oxide layers separated by an interlayer space containing exchangeable cations and water. [90-92] The accepted formula for montmorillonite is $(Al_{3.33}Mg_{0.67})Si_8O_{20}(OH)_4$. [93] The clay structure is depicted in Figure 1.3. Montmorillonite is a species of clay in the Phyllosilicate, or sheet

silicate, category, which is a class of soil minerals. [93, 94] Phyllosilicates are characterized by structures containing sheets with six-membered SiO_4 rings arranged in a tetrahedral pattern. [93, 94] Montmorillonite is a member of the smectite subgroup within the Phyllosilicate class. [93] Clays in the smectite group are characterized by a 2:1 layer structure, where two tetrahedral silicate layers surround a single octahedral layer. [93] This 2:1 sheet arrangement is illustrated in Figure 1.3. In addition, clays in the smectite group contain inorganic oxides with an approximate 1:5 ratio of magnesium ions to aluminum ions. [92] Clays in the smectite group are further differentiated by the types of ions occupying octahedral positions. [92, 93] In montmorillonite, these locations are predominantly filled by Al^{3+} . Montmorillonite is a member of the dioctahedral smectite subgroup. [92, 93] The substitution Mg^{2+} for Al^{3+} in some octahedral sites gives these smectites a charge imbalance, which requires the presence of interlayer cations for charge balance. [93] This arrangement allows for the well-known expansion of the montmorillonite interlayer with increased hydration. [91, 94] Because the clay classification system is primarily based on a sliding scale representing different cation substitutions, many clays with different designations have similar properties and behaviors.

The clay characterization system has evolved over time to include new clay discoveries as well as synthetic clays. [89, 93] Specifically, more detailed differentiations between members of the smectite group have been established over the past 50 years. [95, 96] In early classification schemes, smectites were broadly referred to as montmorillonite clays with no further differentiation within this group [93]. Consequently, early literature references do not differentiate between montmorillonites in terms of group, subgroup, or

species. This has led to a broad and somewhat variable description of montmorillonites in literature references over time. Fortunately, this is not too concerning because members of the smectite group, which are structurally similar, have similar properties. Often, montmorillonites originate from the weathering of clays with similar structural properties. [91, 92] This creates a wide variety of naturally occurring mixed layer clays that vary in composition depending on geographical location. [89, 93] Because of the wide diversity of clays, commercially available montmorillonite harvested from specific locations was named based on the source, such as Wyoming, California, and Mississippi montmorillonites. [97] Due to similarities of clays in the smectite group, and the abundance of montmorillonite in the environment, [92] different montmorillonite clays are often employed as “representative” clays in order to characterize chemical and physical processes that occur in the environment [18, 21, 23-26].

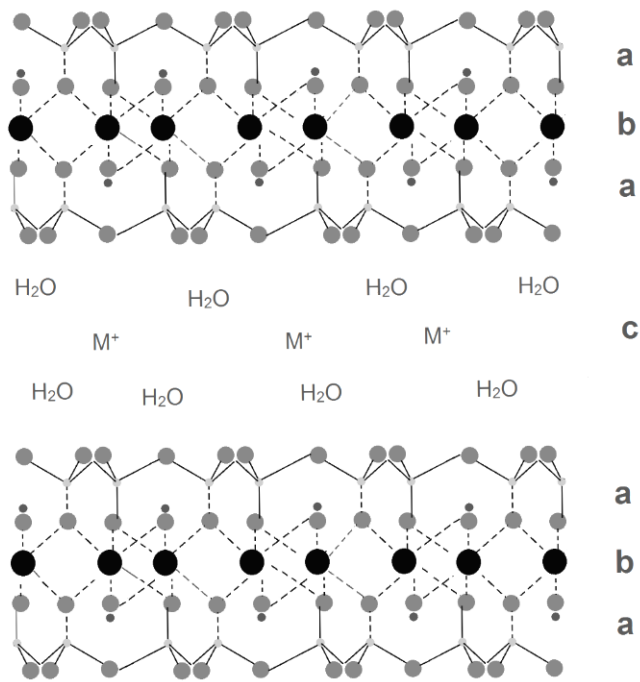


Figure 1.3 Montmorillonite Structure
(a) Tetrahedral layer (b) Dioctahedral layer (c) Interlayer

1.3.2 Montmorillonite Interlayer

Montmorillonite interlayer thickness can vary, being approximately 1 nm minimally, [92] and expanding with increased hydration. The interlayer space contains water and exchangeable cations, [91-93] which are represented by H₂O and M⁺ respectively in Figure 1.3c. The interlayer space is formed as a consequence of the octahedral layer substitution of Mg²⁺ ions for approximately 1/6th of the Al³⁺ ions in the structure. Interlayer cations balance the resulting negative charges carried by the octahedral sheets. The degree to which charge substitution occurs determines the cation

exchange capacity (CEC), which can also be described as the number of positive charge equivalents needed to balance the negatively charged sheets. [92] Montmorillonites typically have CEC values between 80-120 meq/100 g. [92] Naturally occurring cations found within clay interlayer spaces are determined by the parent material and geographical location. However, interlayer cations are exchangeable. Thus, octahedral sheet negative charges can be balanced by combinations of different cations. The total number of cations is dictated by cation charge and clay CEC. [97] As shown in Figure 1.3, silicate sheets are held together in a sandwich structure by electrostatic interactions. [89] This basic sandwich structure is repeated to yield a particle containing approximately 10-20 sheets, depending on hydration and the nature of the cation present. In the environment, the most commonly found interlayer cations are Na^+ and Ca^{2+} . Although a mixture of these ions is common, depending on location, other ions can be found. The rigidity of the silicate sheet sandwich structure is determined by the interlayer cation, and increases with increasing cation charge.

The quantity of clay interlayer water depends on the cation and humidity. [92] Cations have different hydration sphere dimensions, where some water molecules reside inside the clay interlayer space. Consequently, the clustering of water, which has been extensively studied, differs depending on interlayer cation. [98] Typically, the strength with which the water is held increases with increasing cation charge. [99] Clays swell and shrink with changing interlayer hydration, which depends on the cation, environmental conditions, and the amount of water available. [92, 97] At the extreme, hydration can separate the silicate layer sheets so much that they are no longer organized

into a stack. [93] Clay swelling and shrinking processes dictate water transport mechanisms, by which impurities move among soil particles.

1.4 Variable Temperature Diffuse Reflection Infrared Fourier Transform Spectroscopy as a Method for Analysis of Soil Contaminants

Infrared diffuse reflection spectroscopy is an analytical technique based on the principle that molecules can absorb energy through resonance interactions between infrared radiation electromagnetic field oscillations and bond vibrations, which are characteristic of molecular structure. [100] Thus, infrared spectral features are representative of molecular structure, and are often used for molecular structure identifications. Several studies based on the use of reflection spectroscopy for analysis of soils have been reported over the past 20 years. [101] In the 1980s a spectral library of various soil samples was produced for use by soil scientists working in the field. As technology improved and internet access became available, a similar, but more detailed soil spectra library was constructed. [102] A few recent soil contaminant studies conducted by using near- IR were referenced in section 1.1.2. Often, soil characterization is done with near-IR due to its lower cost, portability, and ease of sample preparation. In contrast, mid-IR spectra provide more information, but are often not utilized for soil analysis due to its lack of sample-to-sample reproducibility. [101]

In the studies described here, a new method for characterizing soil contaminants in the mid-IR range is introduced. This methodology is outlined by the diagram in Figure

1.4. As described in section 1.3, montmorillonite can be considered to be a representative soil clay material. In the part A of the diagram, the contaminant is represented by X inside the oval, and may exist as either a neutral or charge carrying species. The presence of charge carrying species depends on soil pH and the properties of the specific contaminant. Grey double arrows represent interactions between the contaminant and clay components, water (H₂O) and the exchangeable interlayer cation (Cation). The infrared spectrum measured for the sample configuration shown in part A of Figure 1.4 would contain spectrum features corresponding to all of the solid state components interacting with the contaminant. Typically, information regarding the contaminant is buried under overlapping spectral contributions from the other constituents. Most IR studies are based on comparisons between the spectrum corresponding to the system designated in part A and reference infrared spectra corresponding to the substances interacting with the contaminant molecule. Information regarding the contaminant based on spectral subtractions is difficult to obtain because of artifacts introduced by sample-to-sample variability. To avoid this problem, spectral subtractions using spectra obtained from the same sample can be employed. With this approach, spectral features from the sample components that do not change are eliminated, leaving behind only spectral features characteristic of the contaminant. Application of this method to analysis of a single solid sample requires the introduction of a “sample perturbation” during spectral measurements. The purpose of the perturbation is to cause a change in the contaminant without significantly changing its surroundings.

By perturbing the sample by heating, a different contaminant configuration (Figure 1.4 part B) can be achieved, in this instance through loss of water. Subtracting the

spectrum obtained for the sample when configured as shown in part A from the spectrum associated with the part B configuration results in a difference spectrum that contains only information about the sample that have changed. In the subtracted spectrum, positive features identify new sample interactions, and negative features identify sample interactions that were lost due to the perturbation. The absorptivity and the number of molecules affected by the perturbation will determine the intensity of the positive and negative difference spectra features. Subtracted spectra obtained after continued heating (parts C & D) will contain negative features representative of the loss of the contaminant. Subtracting the spectrum measured for the part B configuration from the spectrum obtained for the part C configuration would provide information about the contaminant environment before desorption. Similarly, subtracting the spectrum measured for the part B configuration from the spectrum obtained for the part D configuration would provide information about the contaminant decomposition process, yielding Y + Z products. Difference spectra produced in this manner will aid in determining the mechanisms by which the contaminant desorbs and/or decomposes while heating the sample. This procedure can be used to detect subtle changes in a single sample at different degrees of perturbation (i.e. temperature) with greater sensitivity than what can be obtained by subtracting library reference spectra.

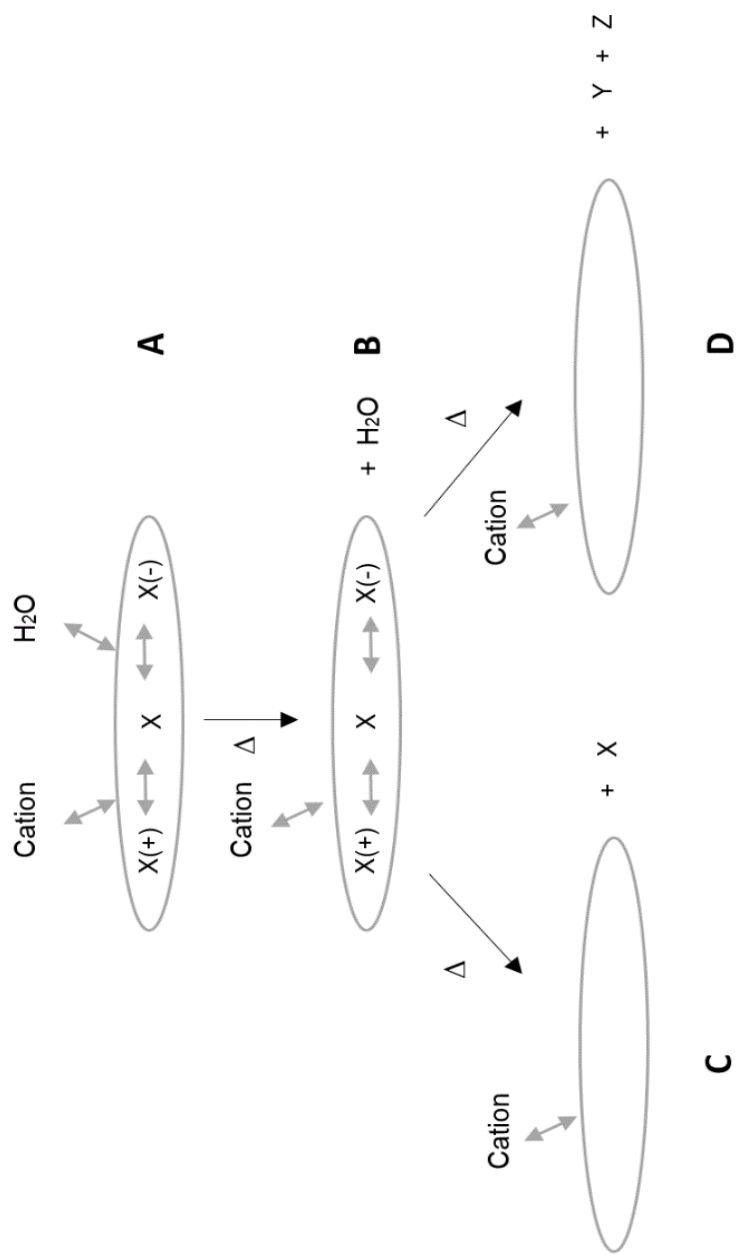


Figure 1.4 VT-DRIFTS Perturbation Method

1.5 Thermogravimetric- Mass Spectrometric Analysis as a Method for Analysis of Soil Contaminants

Thermogravimetry is a commonly used technique for soil and clay analysis. [18, 63, 97, 103] It is often used to characterize neat clay water content and dihydroxylation temperature unique to certain clays. [103] TG-MS technique has also been used to identify soils that have been contaminated. [18] Mass spectrometric analysis of volatiles released during pyrolysis can allow for specific molecular interactions to be characterized.

1.6 Research Objectives

The overall goal of this research project is to elucidate molecular-level interactions between pharmaceutical and personal care product contaminants and clays. Studies of molecular interactions of PPCPs with soils is necessary to evaluate long-term environmental impacts as well as for developing appropriate methods to remedy this problem. The short-term objective of the research presented here is to create a working theory of the molecular interactions between montmorillonite clay and the benzoic acid model compound, which represents the first step toward the overall goal. To characterize benzoic acid-clay interactions, benzoic acid was adsorbed onto montmorillonite clays and in-situ analysis was performed by using variable temperature diffuse reflection infrared Fourier transform spectroscopy (VT-DRIFTS) as well as by using thermogravimetry-

mass spectrometry (TG-MS). Results from VT-DRIFTS sample perturbation studies permit access to vibrational information regarding the benzoic acid environment and how vibrations change with temperature. Evaluating VT-DRIFTS results in combination with TG-MS data allows for specific benzoic acid-clay interactions to be determined. These interactions dictate the environmental fate of benzoic acid in the presence of montmorillonite clay.

Chapter 2: Experimental

2.1 Chemicals and Reagents

Montmorillonite (K10) and benzoic acid were purchased from Sigma-Aldrich. Sodium Chloride was purchased from Mallinckrodt. Calcium Chloride was purchased from Fischer Scientific. Silver powder (100 mesh, 99.95%) was purchased from Alfa Aesar. Carbon tetrachloride was purchased from JT Baker Chemical Company. All chemicals were used as received without additional purification. Helium was purchased from AirGas.

2.2 Sample Preparation

2.2.1 Sodium and Calcium Montmorillonite Samples

Montmorillonite (MMT) clays with Na^+ (NaMMT) and Ca^{2+} (CaMMT) interlayer ions were prepared by cation exchange with the corresponding metal chloride solution by following previously described procedures. [104, 105] The weights of clays and metal chloride used to prepare samples are listed in Table 2.1. Metal chloride solutions contained three times the estimated maximum cation exchange capacity of montmorillonite, which is reported to be 150 meq/100g. [105] The clay/metal chloride slurry was stirred for 2-3 hours at room temperature and then allowed to stand overnight. In the suspension, clay particles form quasi-crystals, with structures that depend on the local cation. [106] After allowing sufficient time for the clay to settle, the supernatant (salt solution) was discarded and the sodium and calcium clays were washed 3-4 times with 250 mL of distilled water to remove excess salts. To avoid loss of interlayer water, the cation exchanged clay was then allowed to dry at room temperature. During the drying process, quasi-crystals present in the suspension coalesce to form larger particles. [107]

Table 2.1 Preparation of Na and Ca Cation Exchanged Montmorillonites

	MMT K10 (g)	Ca AND Na CHLORIDE (g)	WATER VOLUME (mL)
CaMMT	10.0010	3.0111	50
NaMMT	9.9936	2.9913	50

2.2.2 Benzoic Acid Loadings of Sodium and Calcium Montmorillonite Clays

Cation exchanged clays, prepared as described in section 2.2.1, were loaded with benzoic acid by incipient wetness. For loading benzoic acid on the sodium montmorillonite clay, 0.1002 grams of benzoic acid was dissolved in 10 milliliters of carbon tetrachloride. Different amounts of this solution was mixed with sodium montmorillonite clay to produce samples containing variable amounts of adsorbate (Table 2.2). For loading benzoic acid on calcium montmorillonite clay, 0.1002 grams of benzoic acid was dissolved in 10 milliliters of carbon tetrachloride. Various amounts of this benzoic acid solution was mixed with calcium montmorillonite clays as described by Table 2.3. The mixtures were stirred for 30 minutes at room temperature, then the solvent was removed by roto-evaporation for 90 minutes at room temperature.

Table 2.2 Benzoic Acid Loadings on Sodium Montmorillonite

BENZOIC ACID SOLUTION (mL)	ADDITIONAL CCl₄ (mL)	NaMMT (g)	% (w/w) BENZOIC ACID LOADING
3.4	6.6	0.2996	10.18
1.6	8.4	0.3001	5.06
1.3	8.7	0.3009	4.15
0.9	9.1	0.2997	2.92
0.3	9.7	0.2997	0.99

Table 2.3 Benzoic Acid Loadings on Calcium Montmorillonite

BENZOIC ACID SOLUTION (mL)	ADDITIONAL CCl₄ (mL)	CaMMT (g)	% (w/w) BENZOIC ACID LOADING
3.4	6.6	0.2993	10.19
1.6	8.4	0.3000	5.07
1.3	8.7	0.3132	3.99
0.9	9.1	0.2910	3.01
0.6	9.4	0.3024	1.96
0.3	9.7	0.3004	1.00

2.2.3 Variable Temperature-Diffuse Reflection Infrared Fourier Transform

Spectroscopy Sample Preparation

The VT-DRIFTS samples were prepared from benzoic acid loaded clays by mixing the clay powder with silver powder in a 5-95 ratio by weight. The montmorillonite clay silver dilution is described in Table 2.4. Approximately 15 mg samples were employed for VT-DRIFTS analysis. Silver powder diluent, which is highly scattering and inert for this application, was employed to eliminate spectral artifacts that appeared in infrared

spectra when neat clays were analyzed by VT-DRIFTS. These spectral artifacts are caused by the diffuse reflectance spectrum collection method. As illustrated by Figure 2.1, incident radiation is focused onto the powdered sample, where it is either reflected, scattered, or transmitted through the sample. The part of the incident radiation that is scattered through and reflected by the sample and returned to the surface is diffuse reflectance. Diffuse reflectance is then collected and directed toward the infrared detector. Specular reflectance, particle size variations, refractive index effects, and sample packing differences are responsible for spectral artifacts, such as band distortion and inversions. Band inversions in DRIFTS measurements can occur due to the Reststrahlen. [108] Increased sample reflectance is observed near the intense 1050 cm^{-1} montmorillonite inorganic oxide absorption band due to high sample refractive index, which results in an apparent loss of absorbance (i.e. an increase in reflectance). Figure 2.2 shows that this phenomenon results in a distorted reflectance spectrum when the neat clay is analyzed by DRIFTS. Fortunately, as illustrated by the dashed line spectrum in Figure 2.2, sample dilution can reduce the sample refractive index and eliminate this artifact. Thus, to avoid Reststrahlen effects, samples used for VT-DRIFTS studies were diluted in silver powder.

Table 2.4 Silver Powder Dilutions

	% (w/w)	MMT (g)	SILVER POWDER (g)	% (w/w) SILVER DILUTED
CaMMT	Neat	0.0246	0.4699	4.97
	10.19	0.0256	0.4750	5.11
NaMMT	Neat	0.0256	0.4510	5.37
	10.18	0.0261	0.4752	5.21

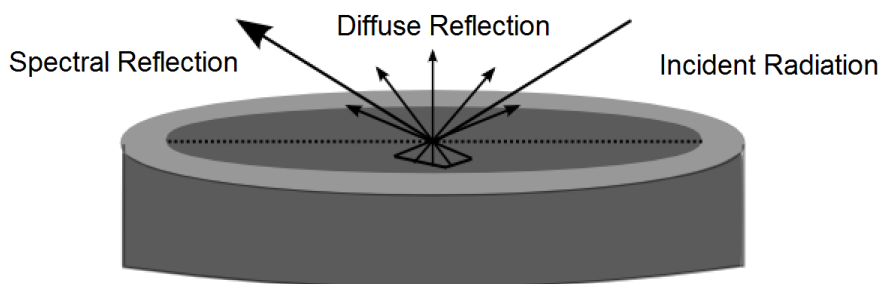


Figure 2.1 Diffuse Reflection

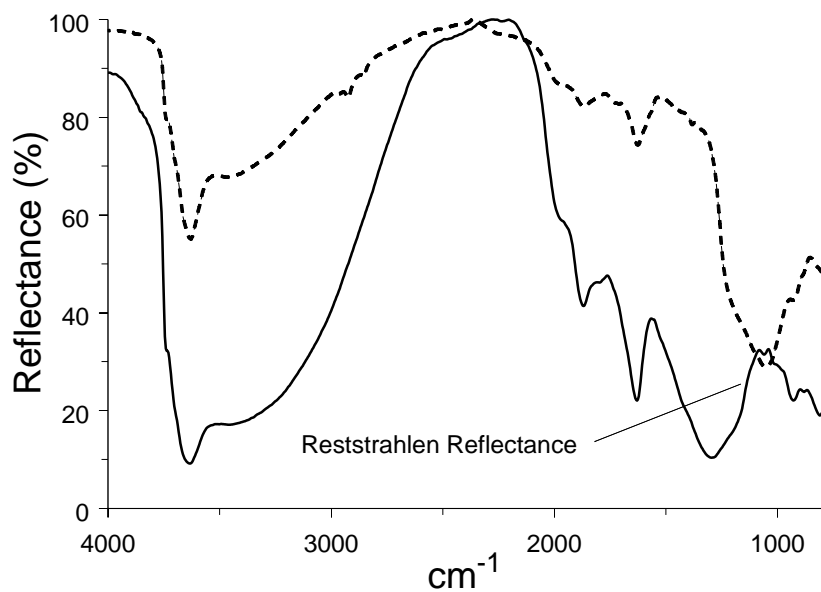


Figure 2.2 Reflectance spectra measured for neat (solid line) and 5% (w/w) clay diluted in silver powder (dashed line).

2.3 Instrumentation

A Mettler Toledo AB104-S/FACT analytical balance was used to weigh solid chemicals to the nearest 0.1 mg. A Buchler Instruments VV-micro rotary evaporator was used to prepare cation exchanged montmorillonite samples. The rotary evaporator was connected to a house vacuum.

2.3.1 *Variable Temperature Diffuse Reflection Infrared Fourier Transform Spectroscopy*

VT-DRIFTS measurements were made on a Mattson Instruments Inc. Nova Cygni 120 instrument with a modified Harrick Scientific Inc. praying mantis diffuse reflection accessory and environmental chamber. The VT-DRIFTS schematic is shown in Figure 2.3. Changes were made to the praying mantis diffuse reflection sample holder accessory [109] and a diagram of the sample holder is shown in

Figure 2.4. The sample holder is mounted on a stainless steel base. The base contains an o-ring so that a sealed sample compartment can be formed when the stainless steel cover is attached. The sample holder base contains three fittings used as gas inlet and outlets during purging. The sample holder consists of a stainless steel ring placed on top of a platinum foil. An Omega CHAL-010 precision fine wire thermocouple runs through the stainless steel base and touches the back side of the sample holder platinum foil. The sample heater consists of a coil of nickel-chromium wire sandwiched between

a quartz tube covering the stainless steel base supporting the sample holder. A Eurotherm temperature controller was utilized to program heating ramps. A software macro program was employed to acquire sample temperature readings from the temperature controller. Temperature readings were taken before and after each spectrum measurement. Temperatures before and after each measurement were averaged and correlated with acquired spectra. An InfraRed Associated, Inc. J-5385-2 liquid nitrogen cooled Mercury-Cadmium-Telluride (MCT) detector was used. The MCT detector has a spectral range of 666-4762 cm^{-1} . A Madison Instruments, Inc. 0200-0004 (Middleton, WI) water-cooled globar (silicon carbide) infrared radiation source was utilized. The water-cooled globar source allows for higher signal to noise ratio at high wavenumber compared to air cooled sources.

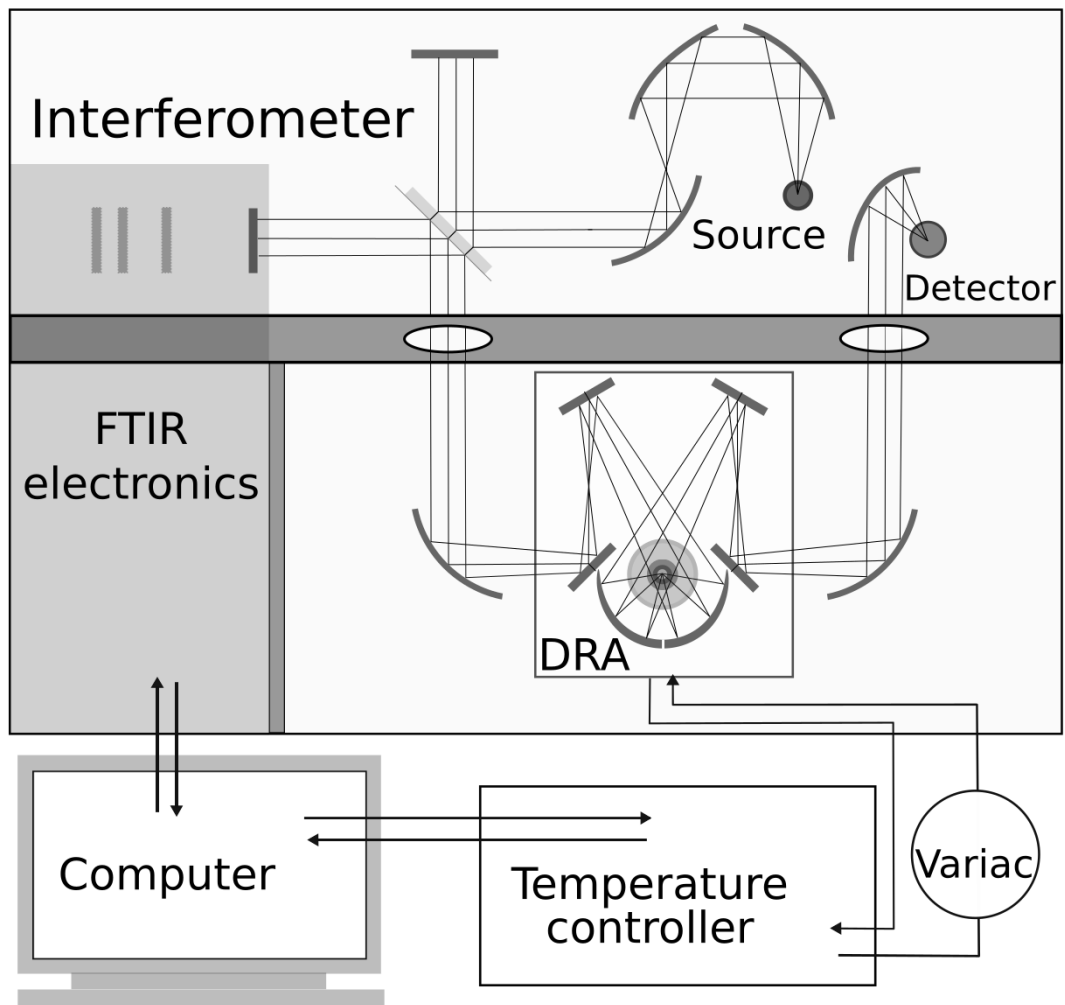


Figure 2.3 VT-DRIFTS Schematic

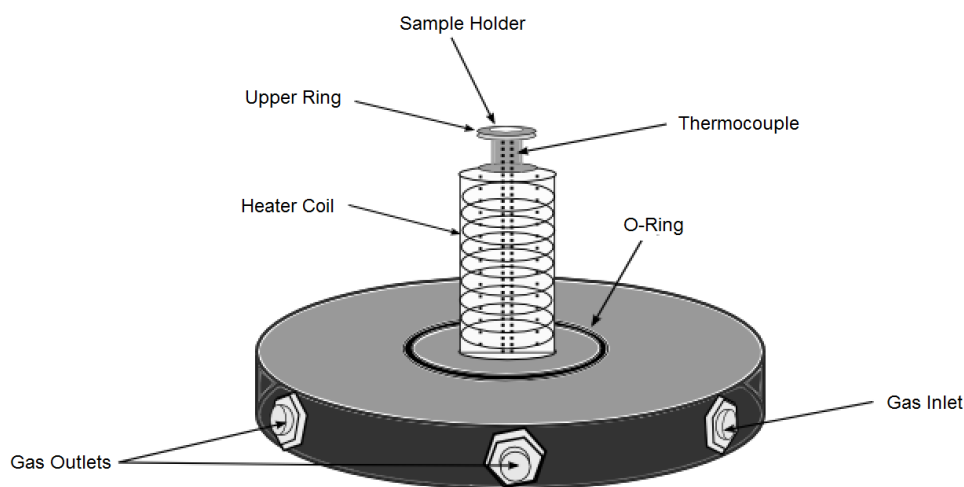


Figure 2.4 VT-DRIFTS Sample Holder Diagram

Neat calcium and sodium montmorillonite clays and 10 % (w/w) benzoic acid loaded sodium and calcium montmorillonite clays were analyzed by variable temperature diffuse reflection Fourier transform spectroscopy (VT-DRIFTS). This allowed for in situ analysis of sample changes resulting from thermal perturbation of the sample. Samples were prepared for VT-DRIFTS analysis according to the method outlined in section 2.2.2. After the sample was loaded, the environmental chamber was helium purged at 10 mL/min for at least 45 minutes prior to heating to remove any residual water and carbon dioxide. A linear heating ramp of 5 °C per minute was employed from room temperature to 500 °C. A software macro was employed so that spectra and sample temperature measurements could be saved while heating samples. The number of signal averaged scans was set to 100 at 8cm⁻¹ resolution so that measurements were taken at 1 minute (5 °C) intervals.

2.3.2 *Thermogravimetry-Mass Spectrometry*

Thermogravimetry – mass spectrometry (TG-MS) measurements were made by using a DuPont Instruments 951 Thermogravimetric Analyzer attached to a HP 5973 MSD quadrupole mass spectrometer so that gases evolved during sample heating in the thermogravimetric analyzer could be detected by the mass spectrometer. The TG-MS interface was heated to 200 °C to prevent condensation of volatiles before they reached the mass spectrometer. The samples were prepared as described in section 2.2.2. The thermogravimetric analyzer was purged with helium gas at 50 mL/min. Samples were heated using a linear temperature ramp of 5 °C/min from ambient temperature to at least 550 °C. The flow of volatiles evolved by sample heating, which were mixed with the helium purge gas, was split and approximately 15 mL/min of this mixture was directed into the mass spectrometer for analysis. The thermogravimetric analyzer contains a sample pan attached to a balance arm. Balance arm movements were recorded as changes in voltage, which were correlated to mass loss. Temperature and sample mass readings were collected at 3 second (0.25 °C) intervals. Mass spectra were collected at every 0.1 minute (0.5 °C) intervals.

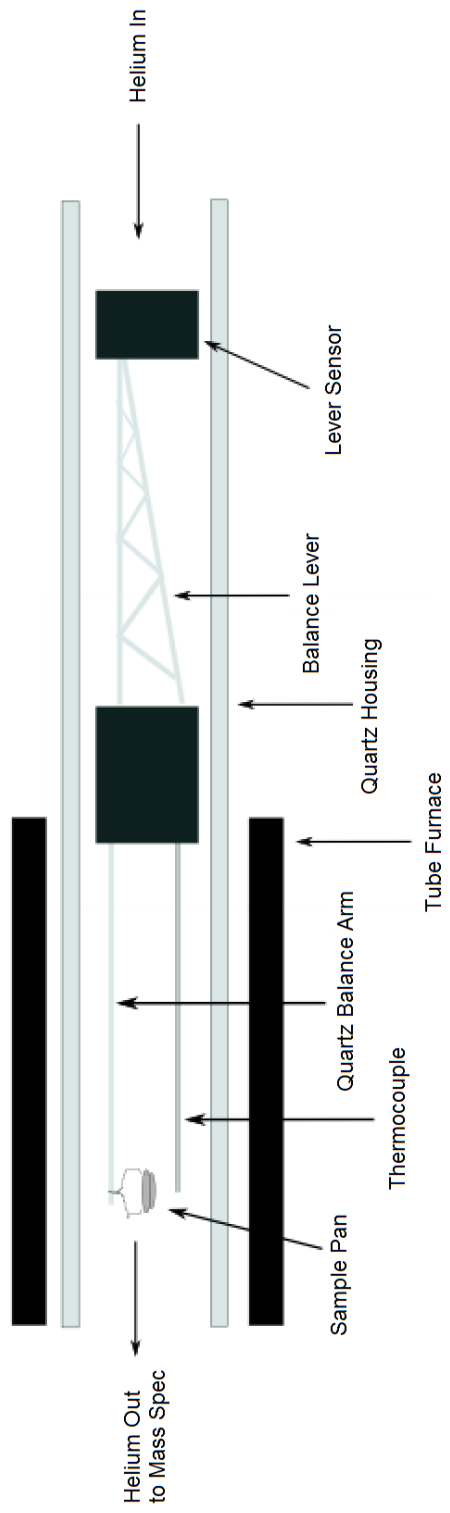


Figure 2.5 Thermogravimetry Apparatus Cross-Section

2.4 Molecular Modeling

Molecular modeling was performed by using the GAUSSIAN program. Benzoic acid and water molecules were individually geometry optimized at the B3LYP/cc-pVTZ level. After optimization, the molecules were arranged with the appropriate ion in the two-body and three-body models shown in Figure 2.6 and Figure 2.7. Distances between the cation and molecules were systematically varied to determine spatial arrangements that resulted in vibrational frequencies that best fit experimental results. Na^+ and Ca^{2+} two and three body models employed the same x, y, z coordinates for vibrational frequency calculations. Vibrational frequencies were calculated for the benzoic acid three-body and two-body models at the B3LYP/cc-pVTZ level, which has previously been used to obtain vibrational frequencies similar to those measured for the benzoic acid monomer and dimer. [110] Calculated vibrational frequencies for Na^+ and Ca^{2+} three-body models (Figure 2.4) and calculated vibrational frequencies for Na^+ and Ca^{2+} two-body models (Figure 2.5) can be found in Appendix I.

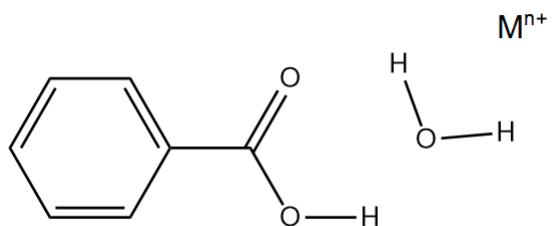


Figure 2.6 Molecular Modeling Schematic of Benzoic Acid Monomer, Water Molecule, and Na⁺ or Ca²⁺ cation

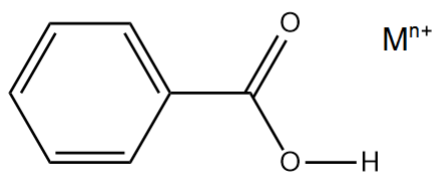


Figure 2.7 Molecular Modeling Schematic of Benzoic Acid Monomer and Na⁺ or Ca²⁺ cation

2.5 Data Manipulation

2.5.1 Variable Temperature Diffuse Reflection Infrared Fourier Transform

Spectroscopy Data

Infrared spectra were collected as interferograms and converted to single beam spectra by Fourier transformation. Single beam spectra were then converted to reflectance spectra, R_{∞} (eq 2.1). Reflectance spectrum calculations require a non-absorbing reference spectrum, R_{∞} (reference). [100] Single beam spectral intensities decrease with increasing sample temperature due to detector saturation effects. Therefore, multiple reference single beams were required for use in calculating reflectance spectra for samples at different temperatures. Reference spectra were obtained by heating silver powder, a highly scattering material, and collecting spectra at 1 °C intervals. Reflectance spectra were computed by dividing single beam sample measurements by a reference single beam spectrum obtained at the same temperature. To baseline slopes in calculated reflectance spectra, spectra were converted to apparent absorbance (eq 2.2) and then baseline corrected. Reflectance spectral intensities are not linearly proportional to concentration. [100] Therefore, spectrum manipulations to accurately reflect spectral changes in relation to concentration is necessary. The Kubelka-Munk function, $f(R_{\infty})$, was utilized because it can be linearly related to concentration. Derivation of the Kubelka-Munk function assumes infinite dilution of samples in a non-absorbing diluent, a constant scattering coefficient, and an infinitely thick sample. [100] While these conditions can never be

fully met, the dilution factors employed for studies described here provided acceptable results. After baseline correction in apparent absorbance format, spectra were converted back to reflectance and then converted to Kubelka-Munk format (eqn 2.3) for display and subtractions. [109]

$$R_{\infty} = R_{\infty} (\text{sample}) / R_{\infty} (\text{reference}) \quad (2.1)$$

$$\text{Apparent Absorbance} = -\log(R_{\infty}) \quad (2.2)$$

$$f(R_{\infty}) = (1-R_{\infty})^2 / 2R_{\infty} \quad (2.3)$$

2.5.2 *Thermogravimetry Mass Spectrometry Data*

Thermogravimetry and mass spectral data were collected by two different data collection systems that were started simultaneously so that elapsed time measurements could be correlated. A minimal error of 1 second (<0.1 °C) or less was associated with data collection start times. Raw thermogravimetry data consisted of sets of three variable measurements which included elapsed time (minutes), sample temperature (°C), and sample mass (mg). Absolute masses were converted to % sample mass values by dividing them by the initial sample mass and multiplying the result by 100% (eqn 2.3). Percent mass was plotted as a function of temperature (°C). Thermogravimetry first derivatives

$$\% \text{ Weight} = \text{Weight}_{\text{remaining}}/\text{Weight}_{\text{initial}}*100 \quad (2.3)$$

were obtained by calculating the slope between data points. For plots, 15 consecutive slope values were averaged and then multiplied by -1 to convert the resulting negative values to positive values. Averaging 15 slope data points smoothed the data and significantly reduced the noise of the plots. Thermogravimetry first derivative averages were plotted against the lowest sample temperature in each 15 data point range. The heating ramp was set to attain a linear 5 °C increase, but the temperature controller introduced some variability. Mass spectral raw data was saved as two variable parameters: elapsed time (minutes) and ion intensity. Mass spectral data and thermogravimetry data measurement intervals were not the same, so a time to temperature correlation was used to convert mass spectral measured times to sample temperatures. To accurately correlate thermogravimetry measured temperatures (°C) with time (minutes), a fifth degree polynomial was fit to a plot of temperature (°C) versus time (minutes). Mass spectral measured times (minutes) were then converted to sample temperature (°C) values by using the fifth order polynomial. Although a linear fit to the temperature vs. time data provided an R² value of 0.999, it resulted in an error of up to ± 20 °C at high temperatures. The polynomial equation reduced this conversion error to less than ± 5 °C. Sample temperatures for each mass spectrometry data set were computed by unique equations to account for the variability of TG-MS heating ramps. An example of a time to temperature correlation with the linear and fifth degree polynomial equations can be found in Appendix II. At a temperature of 601.34 °C recorded by the thermogravimetry apparatus in that example, the linear equation yields a temperature of 614.84 °C for the mass

spectrometry measurement. The polynomial predicted a temperature of 597.58 °C for the same elapsed time. These fitted values represent errors of 13.5 °C and 3.75 °C respectively. Temperature (°C), derived from thermogravimetry polynomial fitting of sample temperature versus time data, was plotted versus specific ion intensity for the mass spectral ion signal plots shown here. Unfortunately, peak intensities in mass spectral plots obtained for one sample could not be directly correlated with intensities obtained for a different sample because numerous factors affected sample-to-sample ion intensities that could not be controlled. Alternatively, mass spectral ion intensity versus sample temperature plots were scaled by using the m/z 18 ion intensity profile representing water evolution for reference. To ensure reproducibility when comparing mass spectral plots within the same run, the same scaling factor was used for all plots collected during the same data collection run. Thermogravimetry first derivative plots were overlaid onto mass spectral ion intensity temperature profiles for comparisons. Examples of these overlay plots can be found in Figure 4.3 and 4.4. The close correlations between the thermogravimetry mass loss first derivatives and ion signal temperature profiles validate this data manipulation methodology.

Chapter 3: Variable Temperature Diffuse Reflection Infrared Spectroscopy Investigation of Benzoic Acid Interactions with Montmorillonite Clay Interlayer Water

3.1 Introduction

Specific molecular interactions between benzoic acid and montmorillonite clays were previously characterized by thermo-IR. [24] By using NIR, Lu et al. compared the interactions of benzoic acid with sodium and calcium montmorillonites. [57] They assigned NIR bands to different types of water molecules within the hydrated clay interlayer space and determined that water molecule hydrogen bonding was enhanced after benzoic acid was adsorbed. By using thermo-IR, Yariv et al. reported that the -C=O stretching vibration frequency of benzoic acid adsorbed on montmorillonite is dependent on the cation present in the clay interlayer space and the extent of clay dehydration. [24] They found that singly charged cations, such as Na⁺, perturbed the -C=O stretching vibration the least relative to neat benzoic acid (dimer), whereas multiply charged cations,

such as Ca^{2+} , produced the largest wavenumber shifts. They proposed a model to explain their spectroscopic findings in which a water molecule bridges between the acid and cation. After prolonged heating in vacuum, the -C=O stretching vibration band was found to shift to lower wavenumbers and ultimately split into two peaks that were assigned to benzoic anhydride. Yariv et al. reported that benzoic acid was still bound to clay even after heating in vacuum to temperatures above $150\text{ }^{\circ}\text{C}$, suggesting the presence of strong interactions. [24]

The thermo-IR technique used for previous studies of benzoic acid adsorbed on montmorillonites was based on transmission infrared spectroscopy of clay thin films. Because these films are typically fragile, a better approach is the use of diffuse reflection infrared Fourier transform spectroscopy (DRIFTS), which can be directly applied to powders. DRIFTS has been shown to be sensitive to small amounts of adsorbates, with detection limits as low as 1-10 molecules per 100 nm^2 . [26] Typically, DRIFTS spectra measured for the mineral are subtracted from spectra obtained for the same mineral, but also containing adsorbates, to generate difference spectra containing only adsorbate spectral features. As pointed out by Thomas and Kelley, [26] careful reference and adsorbate spectrum measurements are critical for obtaining accurate difference spectra. For this reason, they reportedly avoided studies with montmorillonites. Unlike many other minerals, montmorillonite structures consist of a sandwich of two inorganic sheets around a variable thickness water layer. In order to measure an appropriate reference spectrum, it is necessary to precisely control the water content, which is difficult to accomplish. Thus, depending on environmental conditions, samples may contain different amounts of water and infrared spectra would therefore contain varying water

absorbance contributions, which would be difficult to remove by using spectral subtractions.

To characterize benzoic acid-clay interactions in greater detail, in-situ analyses were performed by using variable temperature diffuse reflection infrared Fourier transform spectroscopy (VT-DRIFTS). Perturbation studies were employed to obtain vibrational information regarding subtle changes in the benzoic acid environment caused by heating. In particular, interactions between the acid and montmorillonite interlayer cations and the effects of water on molecular vibrations were characterized. The difficulty in accurately measuring reference spectra is avoided because the reference is the same sample, but at a different temperature. Spectral variations detected by using this methodology reveal benzoic acid vibration changes that occur as a result of interlayer water loss, which are indicative of changes to the local molecular environment that result from partial dehydration of the clay.

3.2 Results and Discussion

Figure 3.1 shows ambient temperature DRIFTS spectra for the sodium and calcium clays containing benzoic acid adsorbate. These spectra are consistent with those reported by Yariv et al. for benzoic acid deposited on sodium and calcium montmorillonites. [25] The inset plot in Figure 3.1 shows scale expansions for the spectral region spanning the benzoic acid -C=O and -C-C- stretching vibrational modes. The -C=O stretching vibration bands ($1650 - 1750 \text{ cm}^{-1}$) are significantly different for the two clay materials.

The -C=O band for benzoic acid adsorbed on NaMMT consists of overlapping features and extends to higher wavenumber than the -C=O band obtained from the CaMMT sample, which appears to be a single peak with a small shoulder on the high wavenumber side. Overlapping bands in the $1400\text{-}1500\text{ cm}^{-1}$ range have similar shapes for the two clay samples but are slightly offset on the wavenumber axis. A band near 1560 cm^{-1} , which represents -COO^- , is more evident in the sodium montmorillonite clay spectrum. Above 2500 cm^{-1} , the sodium montmorillonite sample spectrum exhibits somewhat higher -O-H stretching vibration band intensities, indicating that the sodium montmorillonite contained more interlayer water.

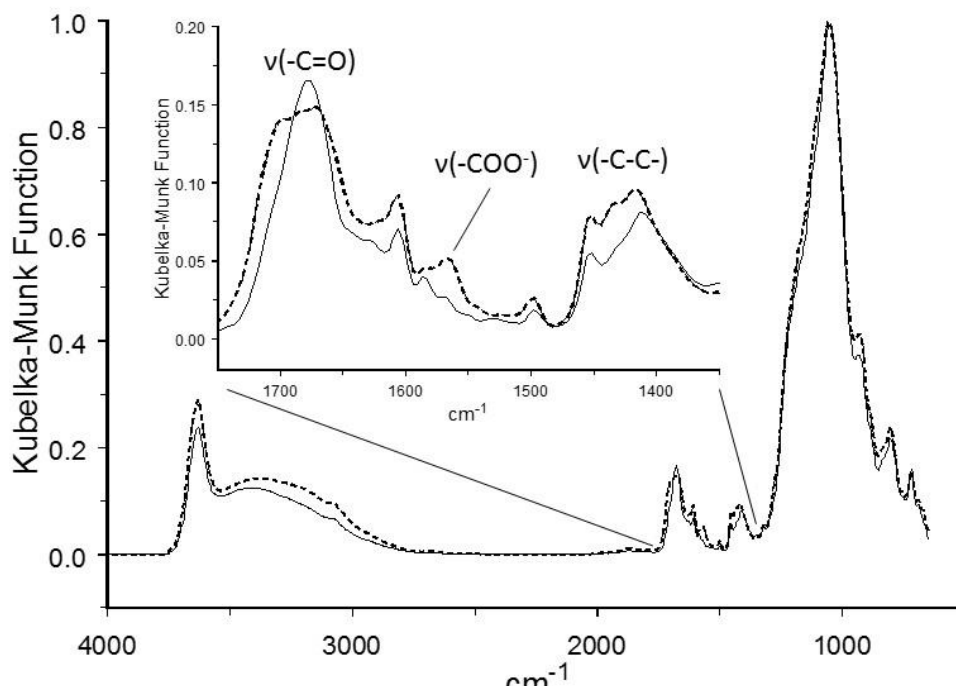


Figure 3.1 Benzoic acid deposited on Ca (solid) and Na (dashed) montmorillonites

Upon heating, changes to clay sample VT-DRIFTS spectra were immediately apparent. The largest spectral changes were associated with loss of O-H stretching vibration band intensity (2800-3800 cm^{-1}). TG-MS analyses confirmed that these spectral changes could be correlated with water evolution, most likely from the clay interlayer space. Integrating the 2800 – 3800 cm^{-1} spectral region of VT-DRIFTS spectra and plotting integrated values as a function of temperature yielded trends that resembled the TG-MS mass loss curves obtained for the benzoic acid loaded clay samples. Figure 3.2 shows the absolute value of the first derivative of these plots, which reflects the rate of O-H stretching vibration intensity loss as a function of sample temperature. Both plots maximize in the 30-40 $^{\circ}\text{C}$ temperature range, indicating that water evolved from clay samples most rapidly at these relatively low temperatures.

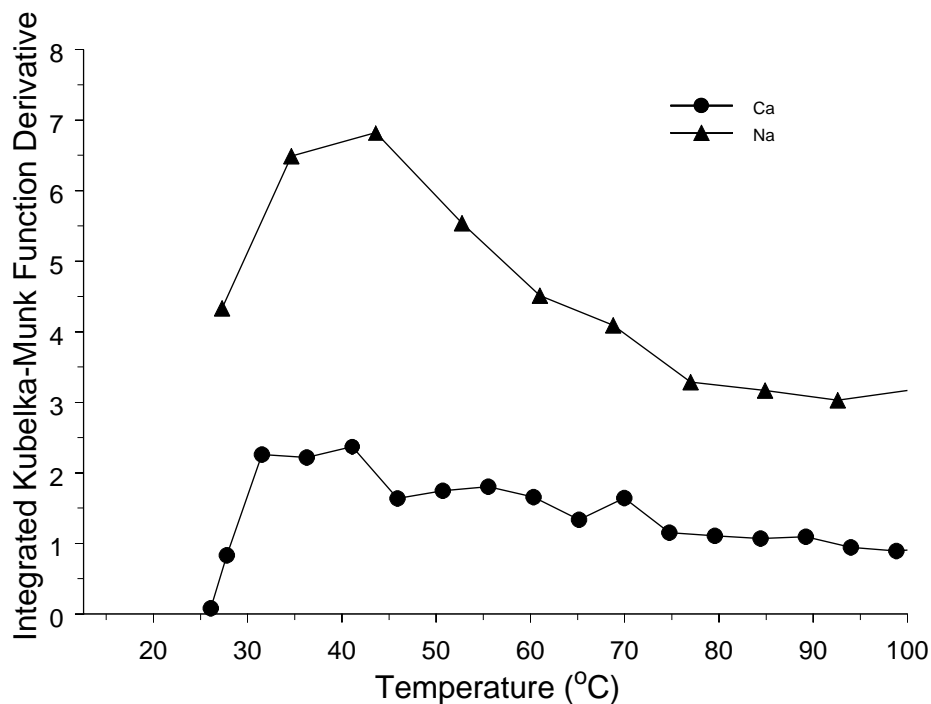
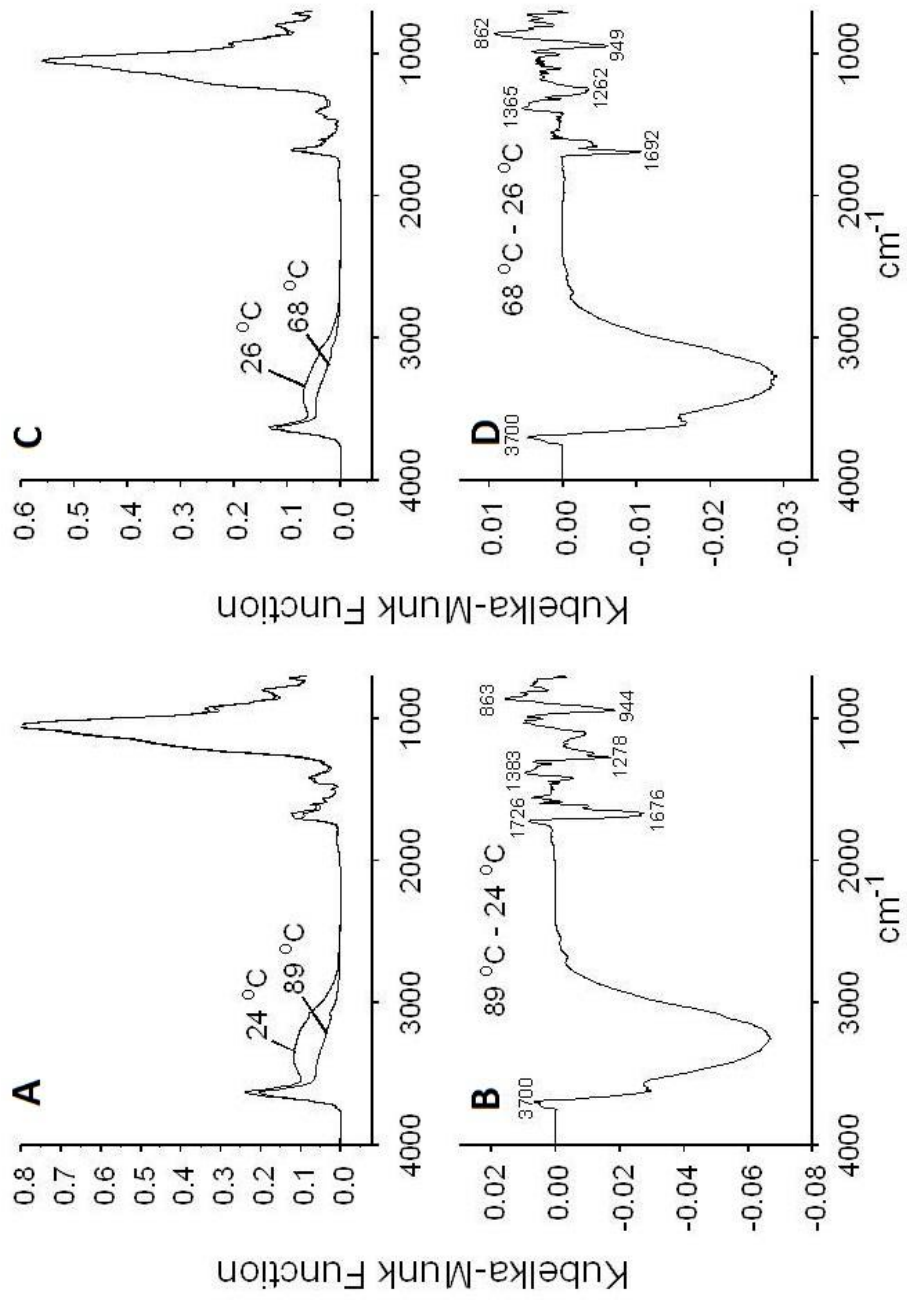


Figure 3.2 Rate of O-H stretching vibration intensity loss as a function of sample temperature

Figure 3.3 (A&C) shows overlays of VT-DRIFTS spectra measured before heating and at temperatures high enough to drive off most of the clay interlayer water for each sample. The bottom plots in Figure 3.3 (B&D) show difference spectra calculated by subtracting the top spectra. Vibrational bands that did not change in frequency or absorptivity when the sample was heated do not appear in difference spectra. The 89 °C (NaMMT) and 68 °C (CaMMT) spectra were selected after subtracting the ambient temperature spectrum from each successively acquired VT-DRIFTS spectrum and

comparing difference spectra features. Spectra obtained at the specified temperatures produced the same difference spectral features, but with greater intensity than the spectra measured at lower temperatures. Difference spectra calculated by using VT-DRIFTS spectra acquired above these temperatures contained new features, indicating that additional temperature dependent processes were contributing to spectral changes. Negative features in difference spectra represent vibrational motions as they existed at ambient temperature, but were lost when the sample was heated. Positive features indicate a gain in intensity that resulted from heating the sample. The loss of -O-H stretching vibration intensity (2800-3800 cm^{-1}), which was due to water desorption, is apparent in the overlaid spectra and also appears as dominant negative features in difference spectra. Small positive features near 3700 cm^{-1} are indicative of hydroxyl functionalities that have lost hydrogen bonded water molecules due to sample heating and consequently experienced a blue shift in -O-H stretching vibration frequency. Small negative features near 1625 cm^{-1} correspond to loss of water bending vibration intensity and are indicative of water desorption. Although negative features indicating a loss of benzoic acid vibrational modes were observed, TG-MS analysis of the gases evolved when these samples were heated revealed that no benzoic acid was released at these temperatures. In fact, only water vapor was detected. Thus, benzoic acid vibrational changes revealed by difference spectra must result from solid-state configuration changes, and not from benzoic acid desorption.



Benzoic Acid/Sodium Montmorillonite Benzoic Acid/Calcium Montmorillonite

Figure 3.3 VT-DRIFTS spectra representing loss of interlayer water

Benzoic acid local environment changes that occur in these low temperature ranges most likely result from the loss of hydrogen bonding interactions with interlayer water molecules, which would primarily affect the vibrations of the polar carboxylic acid functionality. Negative peaks at 1692 cm^{-1} for the calcium montmorillonite (CaMMT) and at 1676 cm^{-1} for the sodium montmorillonite (NaMMT) samples represent a net loss of -C=O stretching vibration intensity. These negative features are more narrow and less intense than the -C=O bands in ambient temperature spectra, indicating that only some of the benzoic acid molecules in the sample were responsible for these bands. A small positive feature at 1726 cm^{-1} in the sodium montmorillonite difference spectrum suggests a slight blue shift for the -C=O stretching vibration after water desorption. However, the otherwise negative -C=O stretching vibration band suggests that the positive -C=O band, which would represent the molecular environment after water removal, had a lower absorptivity than the negative -C=O stretching vibration band, which characterizes the vibration before heating. A similar overlap of positive and negative bands may have occurred for the calcium montmorillonite sample, but no positive features were detected that would confirm this.

The negative -C=O stretching vibration bands appeared at 1676 cm^{-1} (NaMMT) and 1692 cm^{-1} (CaMMT), which is the opposite of what would be expected if the carboxylic acid groups were directly interacting with interlayer cations. If direct interactions occurred, the higher Ca^{2+} charge would be expected to draw more electron density away from the carbonyl functionality and lower the -C=O stretching vibration frequency more than Na^+ . Alternatively, these relative -C=O stretching frequencies would be predicted

if benzoic acid were hydrogen bonded to water molecules bridging between the interlayer cation and benzoic acid, as previously proposed by Yariv et al.[24]

Because loss of hydrogen bonded water is expected to primarily impact the polar carboxylic acid vibrations, positive features near 1383 (NaMMT) and 1365 cm^{-1} (CaMMT) and negative features at 1278 (NaMMT) and 1262 cm^{-1} (CaMMT) most likely represent in-plane benzoic acid -C-O-H bending vibrations. Removal of interlayer water results in an intensity loss for the lower wavenumber in-plane bending motions, which is replaced by intensity gains at the higher wavenumbers. Thus, the frequency for the -C-O-H in-plane bending vibration undergoes a blue shift by slightly more than 100 cm^{-1} that can be correlated with water loss for both clay samples. The negative 944 (NaMMT) and 949 cm^{-1} (CaMMT) features can similarly be correlated with the positive 863 (NaMMT) and 862 cm^{-1} (CaMMT) bands and attributed to a red shift in benzoic acid out-of-plane -C-O-H bending vibration wavenumber. A small negative band appears in the benzoic acid/NaMMT difference spectrum at 1115 cm^{-1} but is not present in the benzoic acid/CaMMT spectrum. This feature likely resulted from incomplete canceling of the large clay absorbance attributed to overlapping inorganic oxide vibration bands that appears in this region of ambient temperature spectra. Interestingly, none of the difference spectra features can be attributed to the benzoic acid aromatic ring. This is consistent with the hypothesis that water lost by heating these samples was interacting exclusively with the polar carboxylic acid functional group. The frequencies of the negative peaks corresponding to the in-plane and out-of-plane -C-O-H bending vibrations are characteristic of the functional group motions of affected benzoic acid molecules before the water desorbed. These vibrations have similar frequencies for the sodium and

calcium montmorillonites, suggesting that $-C-O-H$ local environments are similarly impacted by the two interlayer cations.

Table 3.1 provides a comparison between benzoic acid adsorbate vibrational frequencies derived from VT-DRIFTS measurements and the corresponding vibrational mode frequencies for benzoic acid monomer and dimer. Values for $-C=O$ stretching vibration frequencies associated with the affected benzoic acid adsorbates after removal of clay interlayer water (e.g. above ambient temperature) are not listed in the table because they could not be extracted from difference spectra. The $-C=O$ stretching vibration frequency shifts caused by the loss of hydrogen bonded water were small and therefore were mostly or entirely canceled by the overlapping negative peak, which had a higher absorptivity. Although the difference spectrum for benzoic acid adsorbed on NaMMT (Figure 3.3B) exhibits a small positive feature at 1726 cm^{-1} , this most likely represents a residual after most of the shifted peak intensity was canceled. Because positive $-C=O$ stretching vibration peaks were effectively absent from difference spectra, the shifts (if they occurred) were much smaller than bending vibration shifts, which were in the range of $90\text{-}100\text{ cm}^{-1}$. In fact, the $-C-O-H$ vibration is known to be significantly impacted by hydrogen bonding. Comparing monomer and dimer frequencies for the out-of-plane $-C-O-H$ bending vibration shows that it occurs at 592 cm^{-1} in the benzoic acid monomer, but appears as a doublet at 917 and 952 cm^{-1} in spectra for the hydrogen bonded benzoic acid dimer.^[111] Thus, the $\sim 90\text{ cm}^{-1}$ red shift of this band (Figure 3.3) after removal of interlayer water suggests that the carboxylic acid functional group local environment changed from one with more hydrogen bonding to one with less hydrogen bonding, but that the isolated monomer (free from hydrogen bonding) was not formed.

Table 3.1 Carboxylic Acid Functionality Vibrational Frequencies (cm⁻¹)

Vibration	Benzoic Acid - CaMMT		Benzoic Acid - NaMMT		Neat Benzoic Acid Monomer[111]	Neat Benzoic Acid Dimer[111]
	26 °C	68 °C	24 °C	89 °C		
-C=O Stretch	1692	N/A	1676	1726	1764	1696
In-Plane -C-O-H Bend	1262	1365	1278	1383	1194	1288/1297
Out-Of-Plane -C-O-H Bend	949	862	944	863	592	917/952

Quantum mechanical molecular modeling was employed to characterize benzoic acid environments that might contribute to the observed difference spectra changes. Vibrational frequencies were calculated for a three body model consisting of Ca²⁺, a single water molecule, and benzoic acid, with the water molecule located between the cation and acid. To simulate the loss of water from this arrangement, calculated vibration frequencies were compared to those obtained for a two body model consisting of only Ca²⁺ and benzoic acid. Although these simple models ignore the effects of inorganic clay components and the potential for multiple hydrogen bond formation, the trends in calculated vibration frequencies are consistent with the observed difference spectra features. Table 3.2 lists measured vibrational frequencies for benzoic acid adsorbed on CaMMT and frequencies calculated for the same vibrational modes by using the (Ca²⁺ - H₂O - benzoic acid) and (Ca²⁺ - benzoic acid) models. Vibration frequencies associated with -C=O stretching and in-plane -C-O-H bending are similar to those associated with benzoic acid adsorbed at ambient temperature, but the calculated out-of-plane -C-O-H

bending vibration frequency is about 90 cm^{-1} below the measured value. However, calculated frequency changes for the -C-O-H bending vibrations resulting from removal of water are in the same direction and of similar magnitude as was found by using VT-DRIFTS measurements. Molecular modeling predicts that loss of the bridging water molecule should result in a -C=O stretching vibration frequency increase of about 20 cm^{-1} , whereas the in-plane -C-O-H bending vibration frequency should increase by about 100 cm^{-1} and the out-of-plane -C-O-H bending vibration frequency should decrease by about 90 cm^{-1} . Table 3.3 shows similar frequency shifting trends when Na^+ is employed as the molecular model cation. In fact, the predicted -C=O stretching vibration for the (cation – H_2O – benzoic acid) system differed by only 3 cm^{-1} when the cation was Ca^{2+} compared to Na^+ , and the calculated -C-O-H bending vibration frequencies were identical, suggesting that carboxylic acid perturbations were overwhelmingly due to the bridging water molecule. In both cases, the calculated -C=O stretching vibration frequency increased when the bridging water was removed. For the model containing Ca^{2+} , this increase was 20 cm^{-1} , whereas the shift was somewhat larger ($\sim 35\text{ cm}^{-1}$) when the model contained Na^+ . These trends are consistent with the appearance of the small positive feature at 1726 cm^{-1} for the benzoic acid/ NaMMT VT-DRIFTS difference spectrum in Figure 3.3 and the lack of a corresponding positive feature for the benzoic acid/ CaMMT difference spectrum. Apparently, the increase in -C=O stretching vibration frequency in spectra obtained for the benzoic acid/ CaMMT sample was too small for the high wavenumber side of the positive peak to be visible. In addition to predicting -C=O stretching vibration band shifts that were consistent with difference spectra results, calculations indicated that the removal of the bridging water should result in dramatic –

C=O stretching vibration absorptivity decreases; by a factor of four when Ca²⁺ was present and by about a factor of 3 when Na⁺ was selected as the model cation. The combined effects of the predicted small increase in –C=O stretching vibration frequency and dramatic loss in absorptivity resulting from removal of the bridging water is consistent with the negative difference spectrum features associated with the –C=O functionality in VT-DRIFTS difference spectra.

Table 3.2 Measured and Calculated Vibrational Frequencies for Benzoic Acid Adsorbed on CaMMT (cm⁻¹)

Vibration	Benzoic Acid - CaMMT 26 °C	Benzoic Acid - CaMMT 68 °C	Benzoic Acid – H ₂ O - Ca ²⁺ Model	Benzoic Acid - Ca ²⁺ Model
-C=O Stretch	1692	N/A	1678	1698
In-Plane -C-O-H Bend	1262	1365	1296	1397
Out-Of-Plane -C-O-H Bend	949	862	862	748

Table 3.3 Measured and Calculated Vibrational Frequencies for Benzoic Acid Adsorbed on NaMMT (cm⁻¹)

Vibration	Benzoic Acid - NaMMT 24 °C	Benzoic Acid - NaMMT 89 °C	Benzoic Acid – H ₂ O - Na ⁺ Model	Benzoic Acid - Na ⁺ Model
-C=O Stretch	1676	N/A	1675	1710
In-Plane -C-O-H Bend	1278	1383	1296	1420
Out-Of-Plane -C-O-H Bend	944	863	862	774

3.3 Conclusions

The VT-DRIFTS analysis methodology described here is an effective aid for interpreting spectral changes that result from subtle sample perturbations. Difference spectra shown in Figure 3.3 reveal information regarding only those benzoic acid molecules that exhibited vibration band changes in response to loss of clay interlayer water. The ~15 mg samples employed for VT-DRIFTS contained about 75 µg of benzoic acid, of which only a fraction was responsible for the observed spectral changes. Using the approach described here, the need for precisely controlling reference mineral spectrum measurement conditions to assure accurate difference spectrum calculations is avoided, making it possible to study more complicated systems, such as montmorillonite clays. Although our results are consistent with the bridging water molecule model proposed by Yariv et al.,[24] difference spectrum features shown here represent only a fraction of the total benzoic acid adsorbate, suggesting that the Yariv et al. model is

incomplete. Other benzoic acid molecules likely experience a wide range of different adsorption environments. In fact, by continuing to heat benzoic acid/clay samples above 100 °C, additional structure changes can be induced involving: further dehydration, dehydroxylation, benzoic acid desorption, benzoic acid decomposition, and other surface reactions. A detailed assessment of the higher temperature vibrational changes associated with benzoic acid desorption/decomposition from montmorillonite clays, based on the methodology outlined here, is provided in Chapter 5.

Chapter 4: Thermogravimetry – Mass Spectrometry Investigation of Benzoic Acid Interactions with Sodium and Calcium Montmorillonite Clays

4.1 Introduction

In a thermogravimetry study of benzoic acid/clay interactions, Lu et al. reported that benzoic acid desorption from sodium montmorillonite maximized at 140 °C, which was lower than when the clay contained calcium interlayer cations (179 °C). [18] They attributed the higher desorption temperature to stronger interactions between calcium ions and benzoic acid molecules. Thus, thermo-IR and thermogravimetry studies both reached the same general conclusion, that benzoic acid more strongly interacts with interlayer cations with higher charge.

Previous work has demonstrated the utility of employing thermal analysis techniques to probe benzoic acid interactions with montmorillonite clays. Results described here were obtained by using thermogravimetry – mass spectrometry (TG-MS) to study benzoic acid desorption from sodium and calcium montmorillonites. The use of

mass spectrometric detection of the vapors generated during thermogravimetric analysis permits selected monitoring of specific volatiles during sample heating. This capability facilitates detailed investigations of the processes involved in temperature-dependent mass loss steps. Based on results from TG-MS analyses, a stepwise mechanism for benzoic acid desorption/decomposition is proposed.

4.2 Results and Discussion

TG-MS analyses were conducted to characterize neat clays and the same clays containing adsorbed benzoic acid. As shown in Figure 4.1, neat clay samples exhibited mass loss profiles that were qualitatively similar. For comparisons, vertical arrows in Figure 4.1 denote specific mass losses between 40 and 100 °C and between 100 and 400 °C. Both samples lost about 4% mass when heated to 550 °C. Mass spectrometric analysis of volatiles released from the neat clay samples while heating confirmed that water loss was primarily responsible for the sample mass changes. For both neat clays, the rate of water evolution maximized below 100 °C, but continued throughout sample heating. The mass loss profiles shown in Figure 4.1 indicate that water loss occurred in three sequential steps. A steep mass loss occurred below 100 °C, followed by a more gradual loss between 100 and 400 °C. Above 400 °C, the mass loss rate increased. The low temperature mass loss (< 100°C) can be attributed to water loss from clay interlayer spaces. [97, 112] These desorbing water molecules were involved in hydrogen bonding with other water molecules and may also have been interacting with interlayer cations

and negative clay surfaces. [99, 113] The 100-400 °C temperature range mass loss likely results from desorption of water molecules that were more strongly interacting with polar clay moieties than those that evolved at lower temperatures. [103] Loss of interlayer water upon heating causes a gradual decrease in clay basal layer spacing, [114] therefore the specific interactions between clay surfaces and the water molecules that desorb above 100 °C may be a consequence of increased confinement due to a reduction of interlayer thickness. Above 400 °C, mass loss mechanisms likely include dehydroxylation, [103] in which condensation reactions between neighboring clay surface hydroxyl groups result in water formation. [18] Depending on the type of montmorillonite and prior treatments, these three mass loss steps can shift over wide temperature ranges. [103] Figure 4.1 indicates that the CaMMT sample employed for studies described here contained more interlayer water but exhibited a lower dehydroxylation rate above 400 °C when compared to the NaMMT sample.

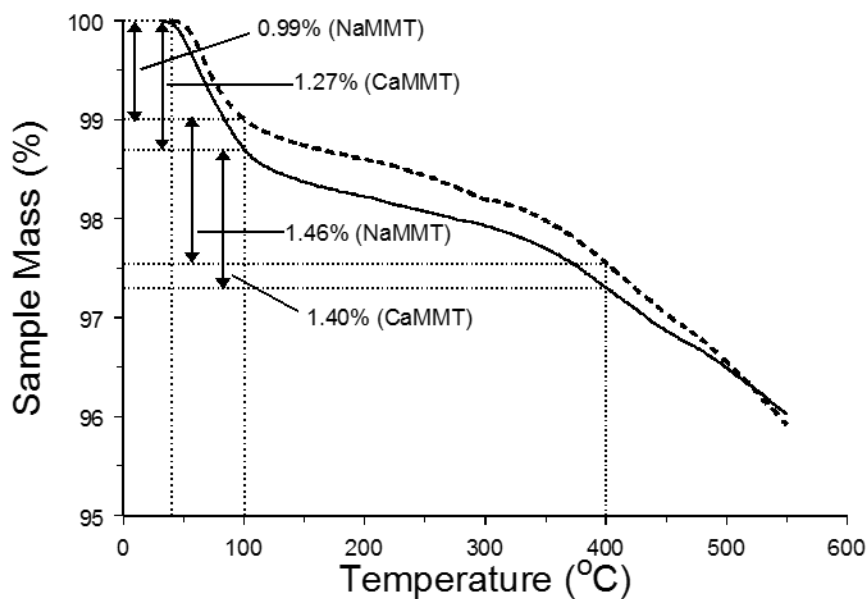


Figure 4.1 Mass loss curves for sodium (dashed line) and calcium (solid line) montmorillonites

TG-MS m/z 18 ion signal intensity profiles representing water evolution for the two clay samples were qualitatively similar, but contained distinct differences, particularly in the temperature range corresponding to interlayer water desorption (Figure 4.2). When the first derivative plots of the corresponding mass loss profiles were overlaid on the m/z 18 profiles, the shapes of the curves matched well, as shown in Figure 4.3 and Figure 4.4, suggesting that water evolution was solely responsible for these mass losses. However, interlayer water desorption for the CaMMT sample persisted to higher temperatures compared to the NaMMT sample, resulting in a discernible shoulder on the high

temperature side of the CaMMT m/z 18 profile in Figure 4.2. Curve fitting was performed on MS m/z 18 peaks for neat CaMMT and NaMMT, shown in Figure 4.5 and Figure 4.6. A single curve was successfully fit to the neat NaMMT m/z 18 ion intensity temperature profile below 100 °C. In contrast, three curves were necessary to fit the neat CaMMT m/z 18 ion intensity temperature profiles to a similar degree. The necessity of multiple peaks for curve fitting of neat CaMMT water evolution profile suggests differences in water behavior during thermal treatment when the interlayer cation was Ca²⁺ compared to Na⁺. The m/z 18 ion intensity temperature profile differences for NaMMT and CaMMT may be rationalized by considering results from recent studies of water diffusion in confined clay interlayer spaces. For instance, by combining nuclear spin echo experiments with molecular dynamics simulations, Marry et al. postulated that activation energies for water molecule diffusion within the interlayer space of a synthetic fluorinated hectorite clay depended on the proximity of water molecules to interlayer cations.[113] This results in slower water molecule movements when they are near cations. In a similar study employing oriented synthetic sodium and calcium smectite clays that were analyzed by three-axis neutron scattering coupled with molecular dynamics simulations, Michot, et al. investigated the effects of different interlayer cations on water molecule motions.[99] They reported that, compared to bulk water, water molecule diffusion coefficients were reduced more for clays containing calcium than for those containing sodium, and that the time spent by water molecules in cation hydration spheres was longer for calcium ions than for sodium ions.[99] These trends may be attributed to stronger electrostatic interactions between calcium ions and neighboring water molecules. Assuming no change in mass transfer processes, stronger interactions

would have the effect of delaying water desorption to higher temperatures during TG-MS analyses of CaMMT compared to NaMMT samples, which is consistent with the m/z 18 temperature profiles shown in Figure 4.2. Consequently, the m/z 18 ion signal intensity profile for the CaMMT sample contains two overlapping contributions, whereas the profile for NaMMT appears to be a single asymmetric distribution. The maximum for the NaMMT profile occurs at about the same temperature as the maximum for the first CaMMT profile component (~62 °C), suggesting that this evolution is mainly due to loss of water molecules hydrogen bonded to other water molecules but having negligible interactions with interlayer cations. The high temperature contribution to the CaMMT m/z 18 ion signal intensity profile likely results from water molecules that are interacting with calcium ions in addition to being hydrogen bonded to other water molecules. Desorption temperatures for water molecules interacting with sodium ions were evidently not shifted to sufficiently higher temperatures to produce a discernible overlapping contribution. This could be due to weaker interactions between water molecules and sodium ions, which would result in shorter times spent by water molecules in the sodium ion hydration sphere when compared to predicted calcium ion hydration sphere dynamics.

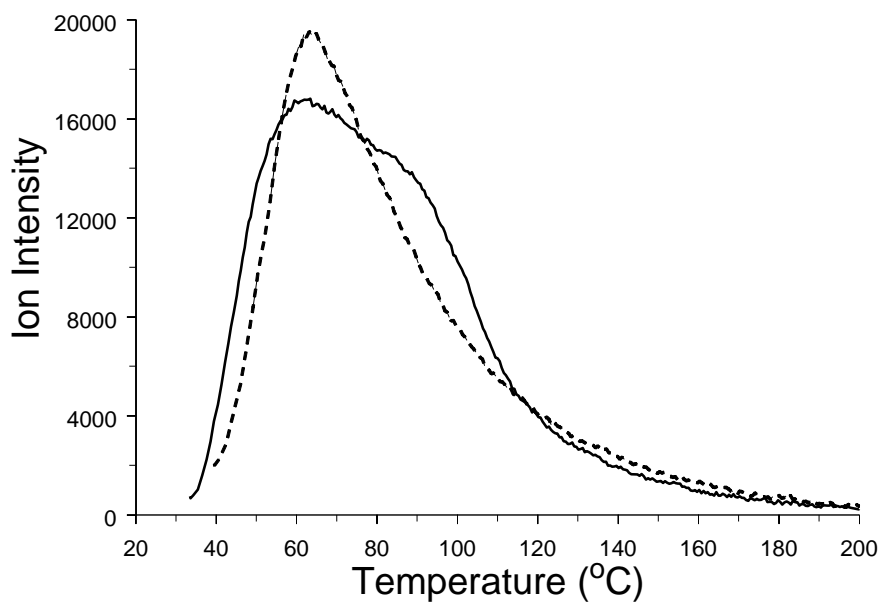


Figure 4.2 Mass spectrometric m/z 18 ion signal intensity profiles representing water desorption from sodium (dashed line) and calcium (solid line) montmorillonite

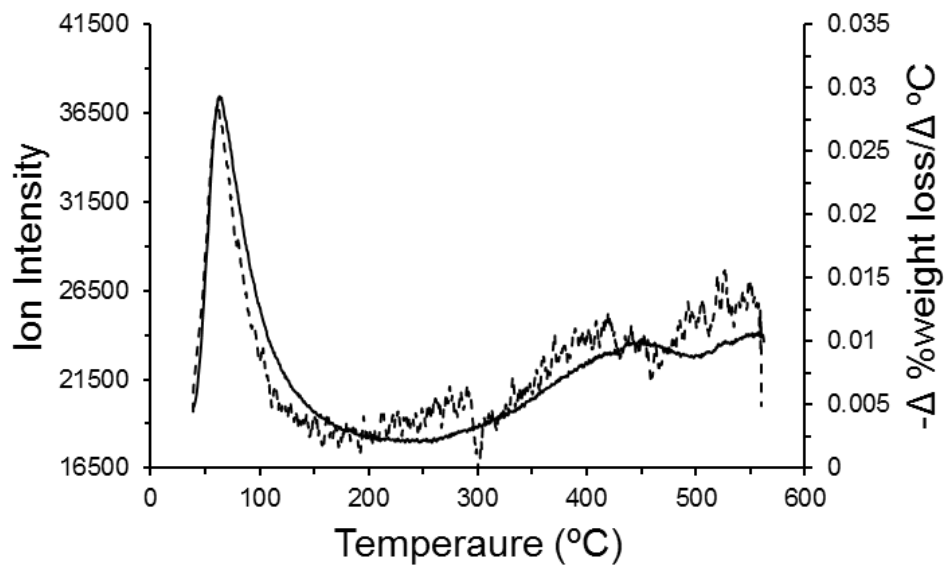


Figure 4.3 Neat sodium montmorillonite mass spectrometric m/z 18 ion signal intensity profile (solid line) overlaid with first derivative of weight loss curve (dashed line)

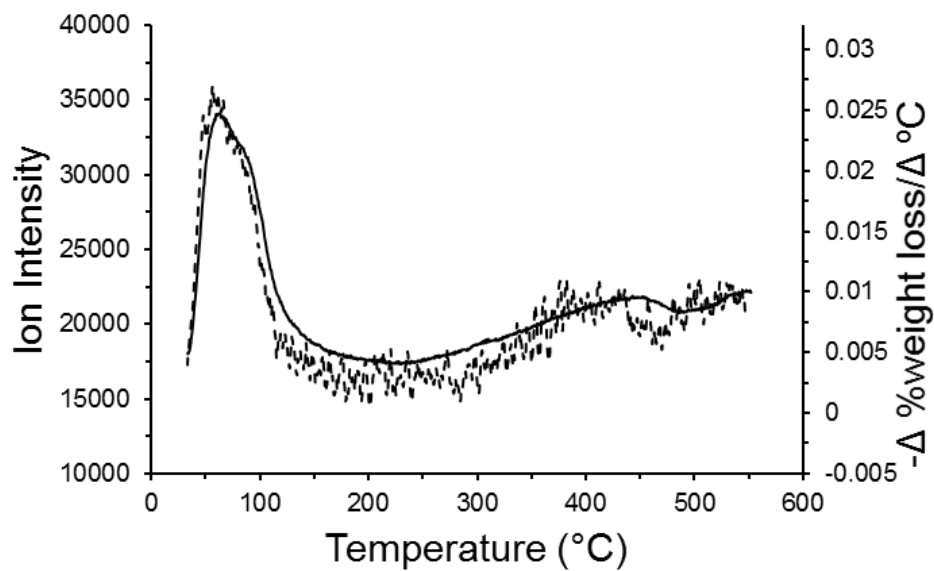


Figure 4.4 Neat calcium montmorillonite mass spectrometric m/z 18 ion signal intensity profile (solid line) overlaid with first derivative of weight loss curve (dashed line)

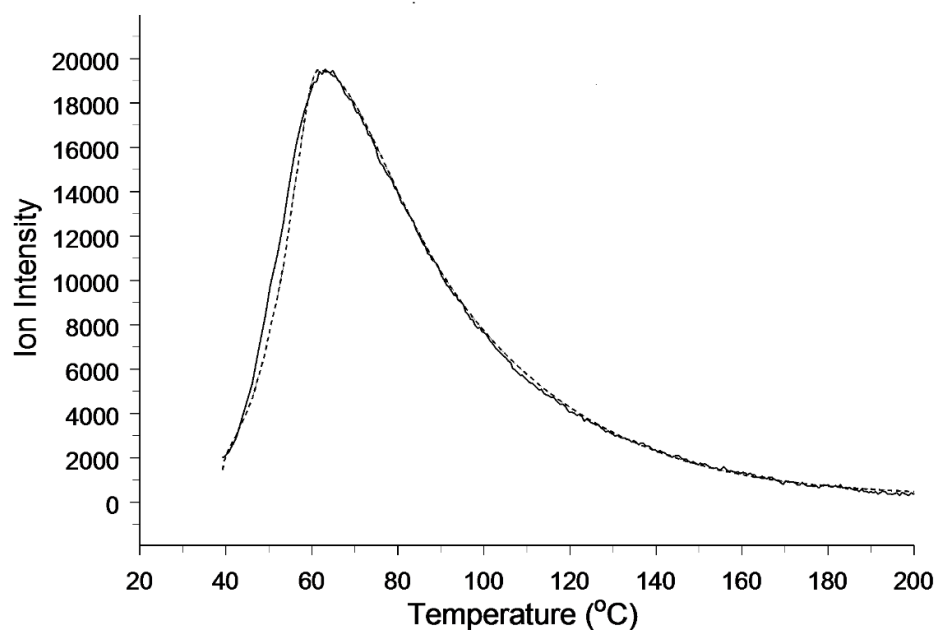


Figure 4.5 Curve fitting for the neat sodium montmorillonite m/z 18 ion intensity temperature profile

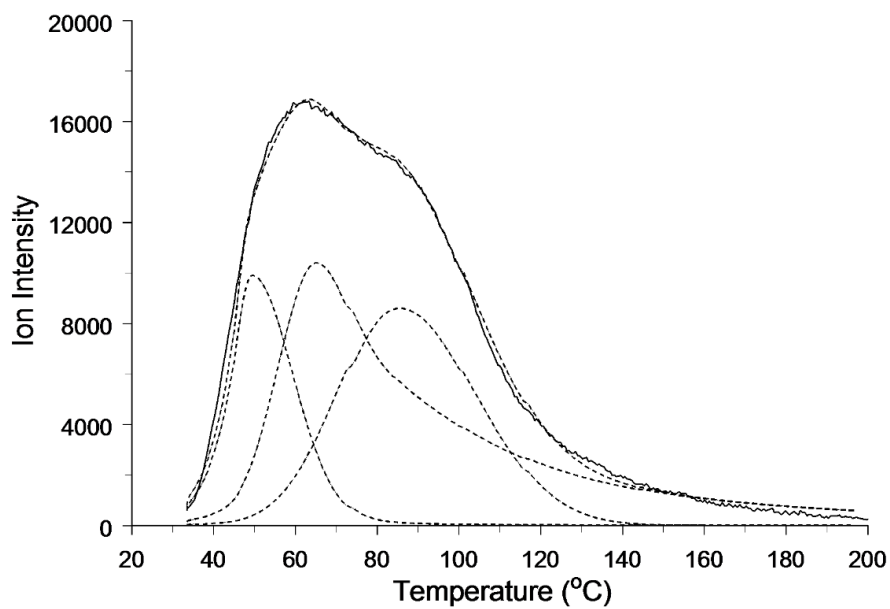


Figure 4.6 Curve fitting for the neat calcium montmorillonite m/z 18 ion intensity temperature profile

Comparisons of previously published thermogravimetric mass loss curves for neat montmorillonite and the same clay containing adsorbed benzoic acid indicate that adsorbate loadings of at least 15% (w/w) can be achieved. [18] To assure that adsorbate concentrations were below saturation, clay samples prepared for studies described here contained at most 10% (w/w) benzoic acid. Mass loss curves for the NaMMT and CaMMT samples containing 10% (w/w) benzoic acid are shown in Figure 4.7. For reference, vertical arrows denote specific mass losses over the same temperature ranges that were highlighted for the neat clay samples (Figure 4.1). Like the neat clay results, the mass loss curves are qualitatively similar. Both profiles exhibit a gradual mass loss due to water evolution, with additional mass losses between 150 and 250 °C, and between 400 and 500 °C, which can be attributed to loss of adsorbed benzoic acid in addition to water loss. Total mass loss at 550 °C was about 11% for both samples, suggesting that not all of the benzoic acid was removed by heating and/or that samples evolved less water than the corresponding neat clays. Because of the complexity of the mass loss curves shown in Figure 4.7 and the fact that, unlike the neat clays, multiple concurrent thermal processes were responsible for mass losses, characterizations of discrete mass loss steps were primarily based on mass spectrometric evolved gas analysis results.

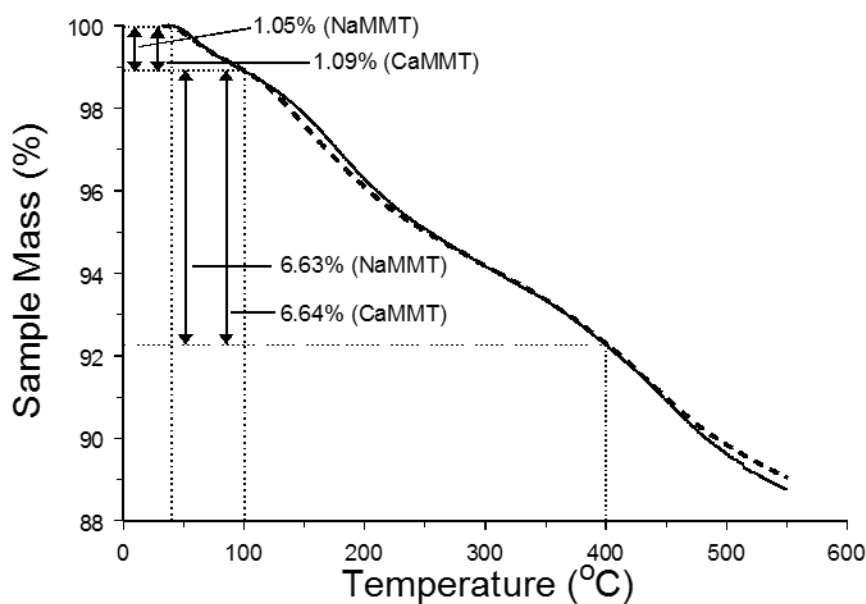


Figure 4.7 Mass loss curves for samples containing 10% (w/w) benzoic acid adsorbed on sodium (dashed line) and calcium (solid line) montmorillonites

TG-MS water desorption temperature profiles (i.e. m/z 18 ion signal intensity) obtained during mass loss below 200 °C for 10% (w/w) benzoic acid/clay samples are shown in Figure 4.8. The ion profiles are similar in size and shape and show only slight variations. Unlike the m/z 18 ion signal intensity temperature profiles for the neat clays (Figure 4.2), water evolution for samples containing benzoic acid adsorbed on clays appears to be independent of the nature of the cation and exhibits a significantly higher desorption rate (i.e. m/z 18 ion signal intensity) above 120 °C compared to the neat clays. This is indicative of a change in water molecule environment relative to the neat clay, in

which inter-molecular hydrogen bonded water molecules are also interacting with cations, to one in which interlayer cations have less influence on water molecule desorption energies. It has been postulated that a water bridge between benzoic acid and cations can form inside the interlayer clay space. [24, 25] If so, these bridges could disrupt interactions between cations and water molecules in the ion hydration sphere. These new interactions could not only disrupt the water molecule environment characteristic of neat clays, but also cause bridging water molecules to be more tightly bound, resulting in higher thermal desorption temperatures. In fact, the presence of a water bridge between benzoic acid molecules and interlayer cations is supported by our recent infrared spectroscopic study in which spectral changes were correlated with interlayer water desorption temperatures (Chapter 3). [28] It was found that thermal desorption of interlayer water from the same 10% (w/w) benzoic acid/clay samples described here caused shifts in benzoic acid vibration frequencies and changes in absorbance band intensities that were consistent with disruption of a benzoic acid – water – cation arrangement. These spectral changes were detected at sample temperatures below 100 °C, which is below the energy required for benzoic acid desorption (vide infra). Furthermore, the observed infrared spectral changes revealed that only a fraction of the adsorbed benzoic acid molecules (initially 10% w/w) were involved in water bridges to cations (Chapter 3). [28]

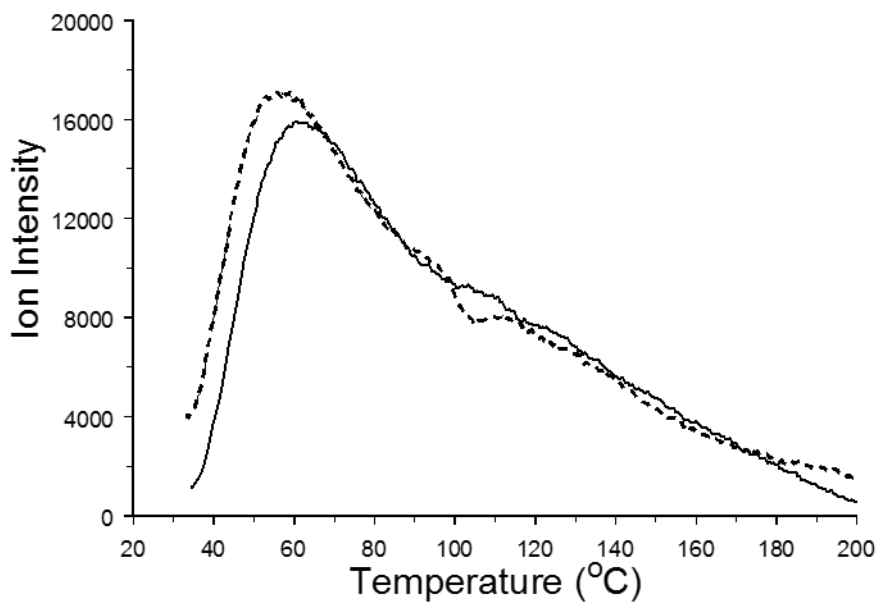


Figure 4.8 Mass spectrometric m/z 18 ion signal intensity profiles representing water desorption from samples containing 10% (w/w) benzoic acid adsorbed on sodium (dashed line) and calcium (solid line) montmorillonites

To further investigate changes in water evolution (m/z 18 ion intensity profiles) observed during thermal analysis of samples containing 10% (w/w) benzoic acid adsorbed on clays, additional samples prepared with varying % (w/w) benzoic acid loadings were analyzed by TG-MS. Results obtained from samples containing different benzoic acid loadings are shown in Figure 4.9 - Figure 4.12. Low temperature (<200 °C) m/z 18 ion profiles shift in shape with lower % benzoic acid loadings toward a shape consistent with the neat clays. The shift for the benzoic acid loaded calcium

montmorillonite m/z 18 profile (Figure 4.9) is more easily discerned than the shift for the benzoic acid loaded sodium montmorillonite m/z 18 profile (Figure 4.11). It is likely that benzoic acid molecules adsorbed onto the clays in the 10% (w/w) benzoic loaded clays disturb only some of the water molecules. The amount of water molecules interacting with benzoic acid likely decreases with decreasing benzoic acid loadings. Thus, water molecules not associated with benzoic acid should interact with interlayer cations much like they do in neat clays. Differences in water desorption profiles of benzoic acid loaded Na^+ (Figure 4.10) and Ca^{2+} (Figure 4.12) clays at higher temperature ($>200\text{ }^\circ\text{C}$) was also observed. Water evolution at high temperature also appears to be correlated with benzoic acid loading. An increase in water desorption from benzoic acid loaded clays compared to neat clays is observed at approximately $450\text{ }^\circ\text{C}$. However, unlike the water evolution peaks at low temperatures, the water evolution profile intensity and shape at high temperatures appears to be unrelated to the % (w/w) benzoic acid loaded onto the clays. The water evolution profile for the sample containing 1% benzoic acid loaded on sodium montmorillonites resembles the high temperature water evolution profile for neat sodium montmorillonites.

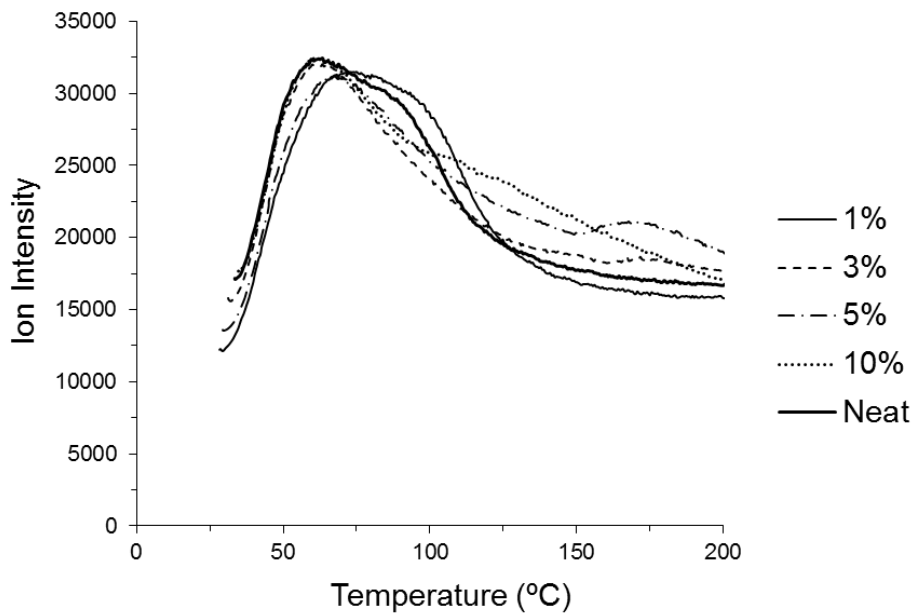


Figure 4.9 Low temperature mass spectrometric m/z 18 ion signal intensity profile overlays for benzoic acid loaded calcium montmorillonites

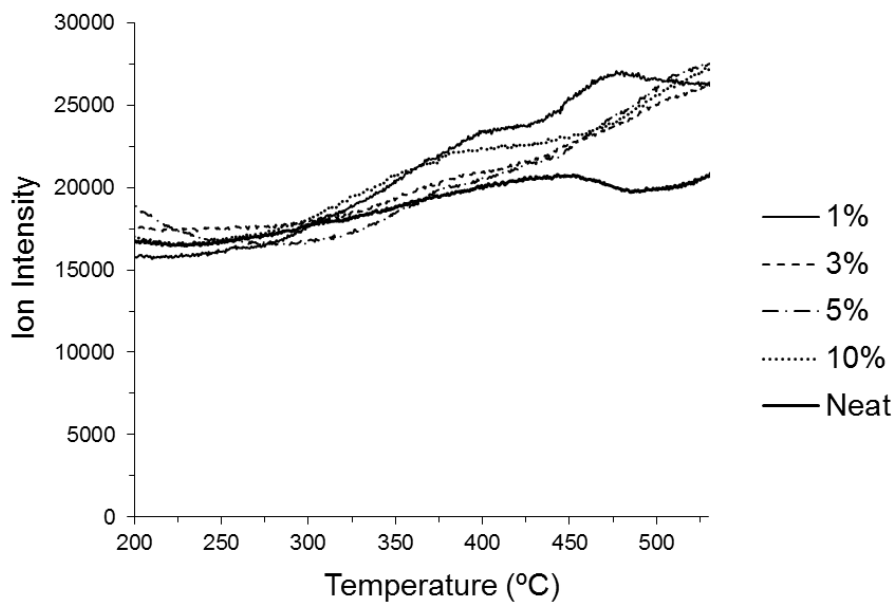


Figure 4.10 High temperature mass spectrometric m/z 18 ion signal intensity profile overlays for benzoic acid loaded calcium montmorillonites

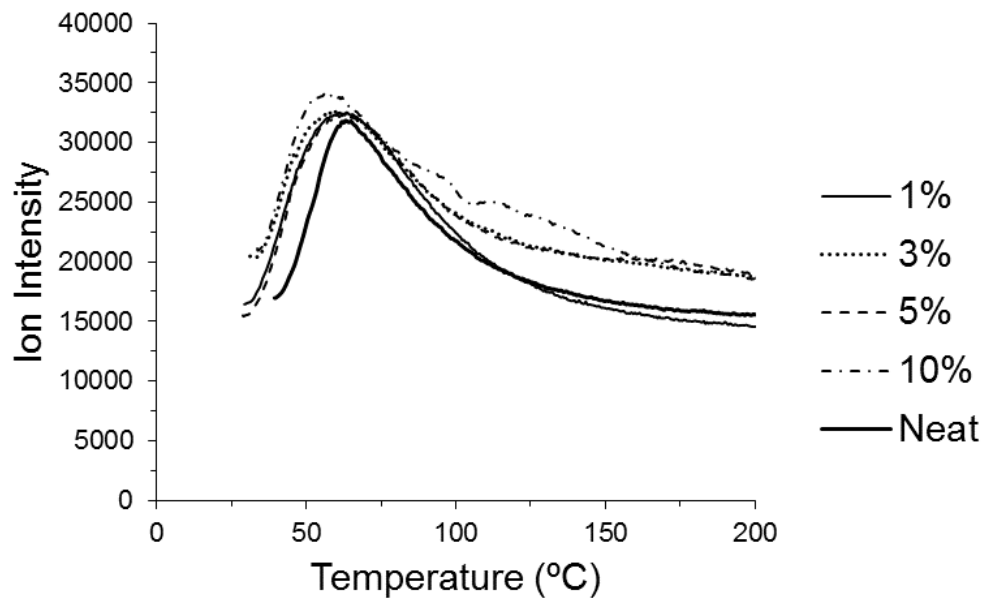


Figure 4.11 Low temperature mass spectrometric m/z 18 ion signal intensity profile overlays for benzoic acid loaded sodium montmorillonites

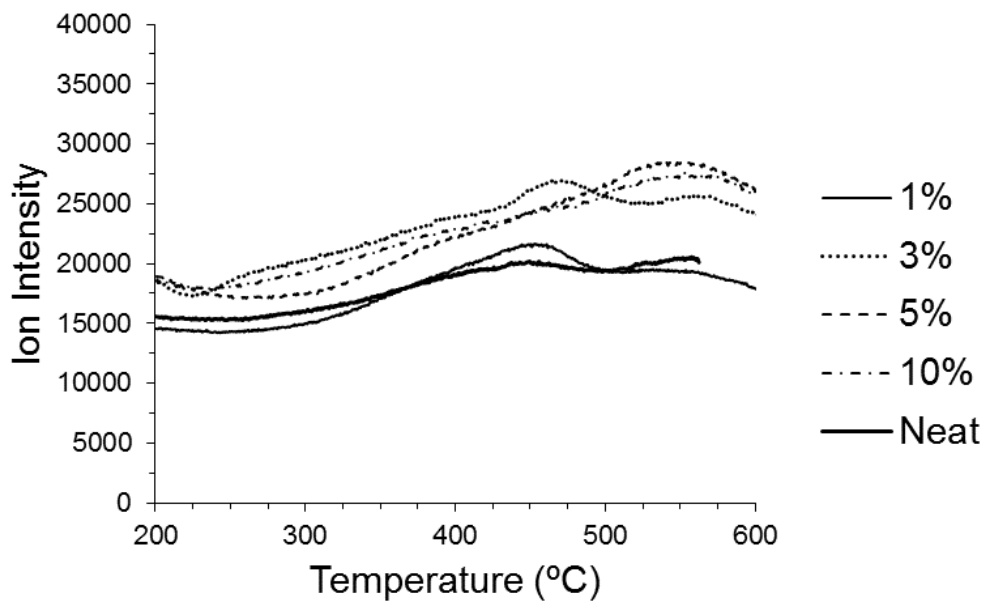


Figure 4.12 High temperature mass spectrometric m/z 18 ion signal intensity profile overlays for benzoic acid loaded sodium montmorillonites

Figure 4.13 shows temperature-dependent TG-MS ion profiles representing the primary volatiles detected while heating NaMMT and CaMMT clays containing adsorbed benzoic acid (10% w/w). Profiles for water (m/z 18), benzoic acid (m/z 122), benzene (m/z 78) and carbon dioxide (m/z 44) are shown. Due to its rigid structure, benzoic acid has a relatively intense molecular ion at m/z 122. In fact, all of the ions chosen for profiling correspond to molecular ions for the species represented. It should be noted that the ion signal intensity values plotted in Figure 4.13 do not accurately represent the relative concentrations of selected species in evolved gases. In addition to concentration in the vapor entering the mass spectrometer, ion signals depend on molecular ionization cross-sectional areas, ionization energies, and degree of fragmentation, which differ for each substance responsible for the ions shown in Figure 4.13. In addition, m/z 44 and m/z 78 are fragment ions in benzoic acid mass spectra. Therefore, intensities for these ions at the same temperatures at which m/z 122 was detected are at least partially due to evolution of benzoic acid. In contrast to results reported by Lu et al.[18], which were based on mass loss measurements and indicated that benzoic acid desorption occurred over a relatively narrow temperature range, Figure 4.13 shows that benzoic acid evolution began at approximately 100 °C and continued to a temperature of at least 450 °C for both samples. The initial rise in m/z 122 ion signal intensity occurred at about 95 °C for the sample containing sodium montmorillonite and at about 110 °C for the sample containing calcium montmorillonite. It is evident that m/z 122 temperature profiles obtained for both samples consist of at least two overlapping contributions. The low temperature benzoic acid contribution is more significant than the higher temperature contribution. However, the low temperature benzoic acid contribution is somewhat broader for the sample

containing NaMMT clay. The low temperature benzoic acid desorption contribution maximized at approximately 175 °C for the NaMMT sample and at approximately 185 °C for the CaMMT sample. This 10 °C temperature difference suggests that benzoic acid was more tightly bound to the clay containing Ca²⁺. Based on the ion signal intensity profiles in Figure 4.13, the ~1% mass losses for both benzoic acid/clay samples detected between 40 and 100 °C (Figure 4.7) can be attributed to interlayer water desorption. These losses are about the same as the neat NaMMT sample and somewhat less than the neat CaMMT sample over this temperature range (Figure 4.1). To insure that benzoic acid was not adsorbed to the clay outside surfaces, 3% (w/w) benzoic acid was loaded onto silver powder. Figure 4.14 shows mass spectral ion intensity (m/z 122) temperature plots for desorption of benzoic acid from silver powder. Desorption of benzoic acid begins at a much lower temperature, and peaks at 100 °C. This suggests that very little, if any benzoic acid desorbs from clay surfaces.

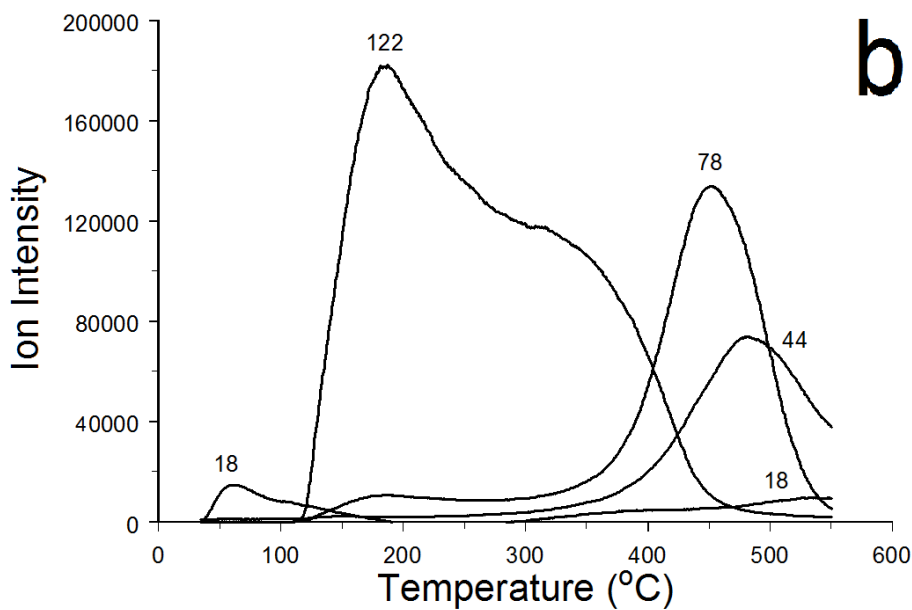
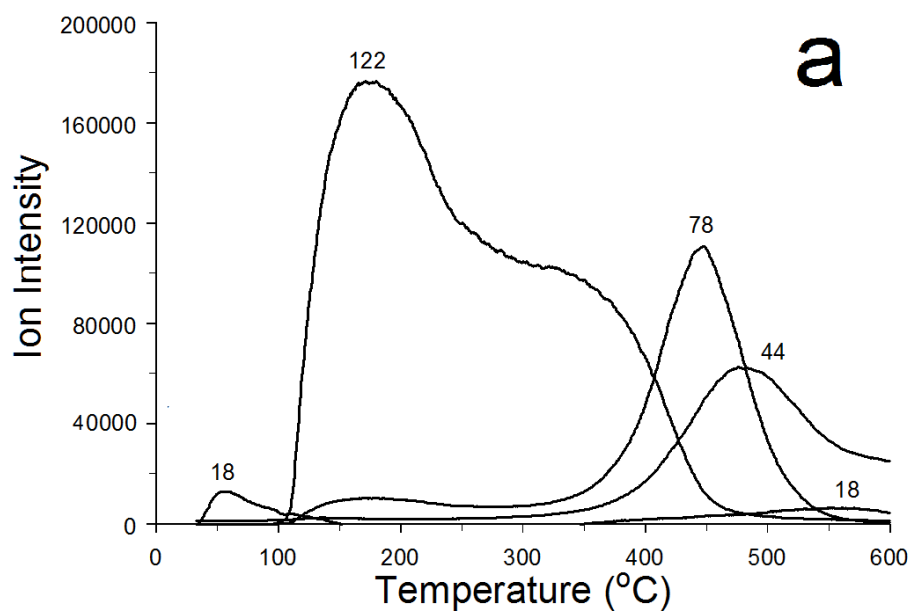


Figure 4.13 Mass spectrometric ion signal intensity profiles representing water (18), benzoic acid (122), benzene (78), and carbon dioxide (44) measured during TG-MS analysis of samples containing 10% (w/w) benzoic adsorbed on (a) sodium and (b) calcium montmorillonite

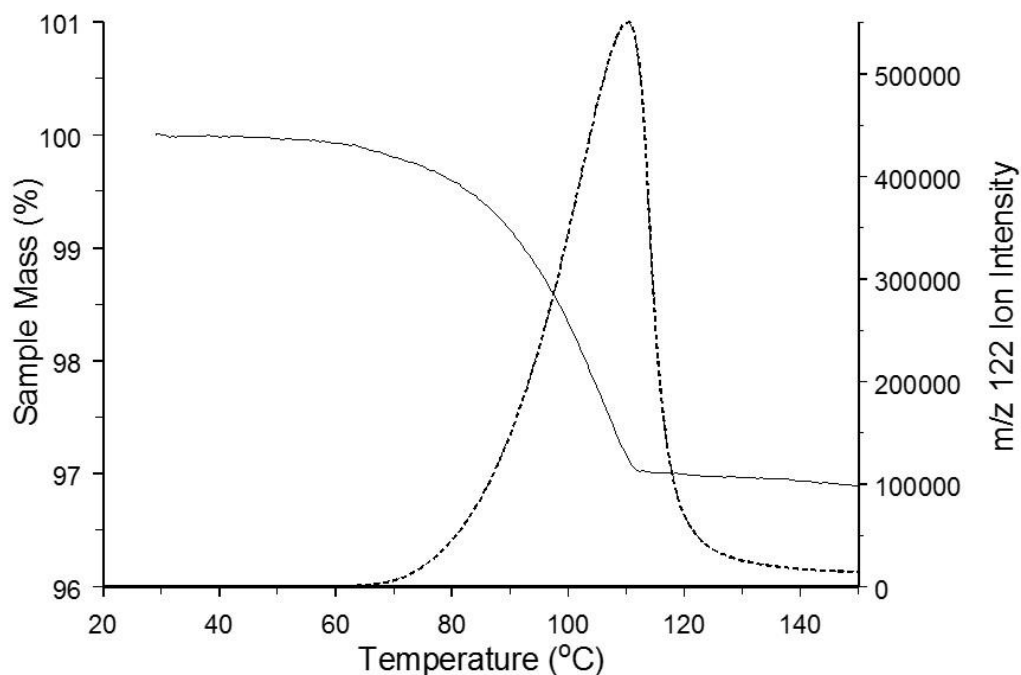


Figure 4.14 TG-MS analysis of Benzoic Acid Deposited on Silver Powder

Figure 4.13 shows that, in addition to benzoic acid desorption, TG-MS analyses detected significant amounts of benzene (m/z 78) and carbon dioxide (m/z 44), which evolved between 300 and 600 °C for both samples. These decomposition products are obtained by benzoic acid decarboxylation at temperatures above 300 °C. [74] The maximum rate of carbon dioxide (m/z 44) evolution occurred near the temperature corresponding to the maximum benzene evolution rate. However, the carbon dioxide evolution maximum temperature was slightly higher than the benzene evolution maximum for both clay samples. This may have been due to the fact that carbon dioxide can strongly adsorb on clay surfaces, which could delay desorption. [115-120] The fact

that these substances were detected above 300 °C and the correlation between m/z 78 and m/z 44 evolution profiles suggest that benzoic acid present in clays at high temperatures decomposed to form benzene and carbon dioxide.

To further investigate the overlapping m/z 122 contributions observed during the thermal analysis of samples containing 10% (w/w) benzoic acid adsorbed on clays, additional samples prepared with varying benzoic acid loadings were analyzed by TG-MS. Results obtained from samples containing different benzoic acid loadings are shown in Figure 4.15. Vertical reference lines at 200 and 400 °C are provided to emphasize temperature profile differences and aid comparisons. The lower temperature benzoic acid desorption contribution for both NaMMT and CaMMT samples was found to decrease with decreasing benzoic acid loading. The m/z 122 ion signal intensity profiles for the 3% benzoic acid NaMMT sample and the 1% benzoic acid CaMMT sample consist of only one contribution, corresponding to the higher temperature component. TG-MS analysis of the sample containing 1% (w/w) benzoic acid on NaMMT yielded negligible m/z 122 ion signal, but m/z 78 and m/z 44 were detected, confirming that benzoic acid was present. The m/z 122 ion signal intensity profile obtained for the 3% loading on the CaMMT clay still contained the low temperature component, suggesting that the number of cations present in interlayer spaces was important in determining this distribution. The sample containing 1% (w/w) benzoic acid adsorbed on CaMMT exhibited an m/z 18 profile with a discernible shoulder, similar to that for the neat CaMMT sample shown in Figure 4.2, and did not exhibit an increase in water evolution at 450 °C, suggesting that this low benzoic acid loading had little impact on interlayer water molecule dynamics. It is not likely a coincidence that the 1% (w/w) benzoic acid loaded clay m/z 18 ion intensity

profile closely resembles neat clay and did not contain a discernable m/z 122 ion intensity profile. Because the CaMMT sample was prepared by ion exchange from the same clay that was used to prepare the NaMMT sample, the negative surface charges inside of interlayer spaces should be about the same. Therefore, assuming near complete ion exchange, the number of Na^+ ions present in interlayer spaces should be approximately twice the number of Ca^{2+} ions. Thus, if the high temperature m/z 122 ion signal intensity profile component involves interactions between benzoic acid molecules and cations with a stoichiometry that does not depend on cation charge, it would be expected that fewer adsorbate molecules would be required to saturate these orientations for CaMMT compared to NaMMT. The high temperature m/z 122 component maximized at about 370 °C for the sample containing 3% (w/w) benzoic acid adsorbed on NaMMT and at 395 °C for the 1% (w/w) benzoic acid on CaMMT sample. The higher maximum evolution temperature for the CaMMT clay compared to the NaMMT clay is consistent with a stronger interaction between benzoic acid and the clay containing cations with higher charge. Thus, maximum evolution temperatures for both the low and high temperature contributions to the m/z 122 ion signal intensity profiles show a dependence on cation charge, with maxima shifted to higher temperatures for clays containing Ca^{2+} . Apparently, because the higher temperature benzoic acid adsorption environment is more stable, only after all of these orientations are filled, will benzoic acid occupy orientations corresponding to the less stable, lower temperature, environments.

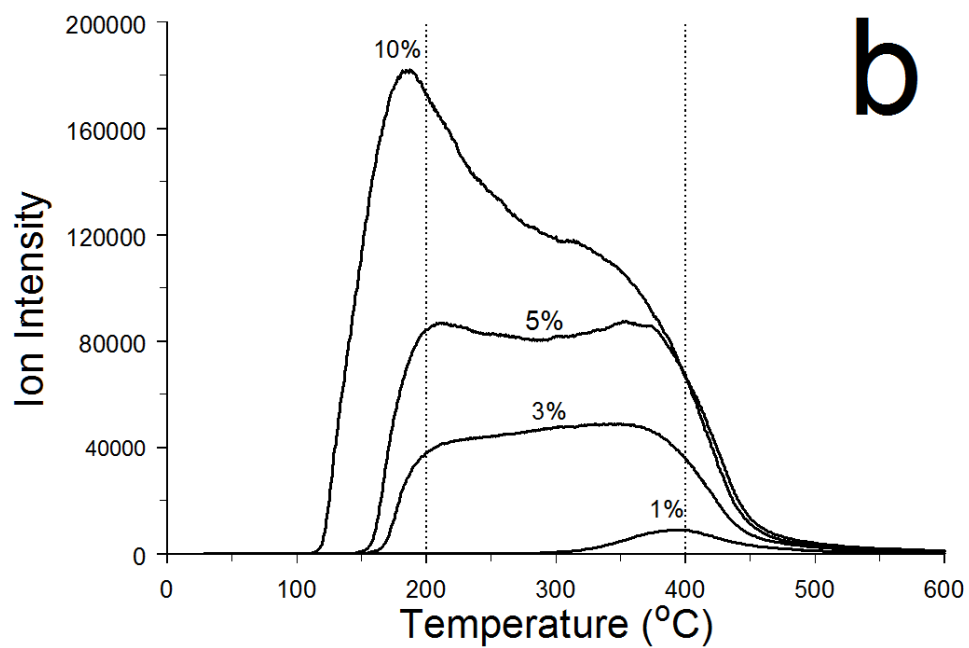
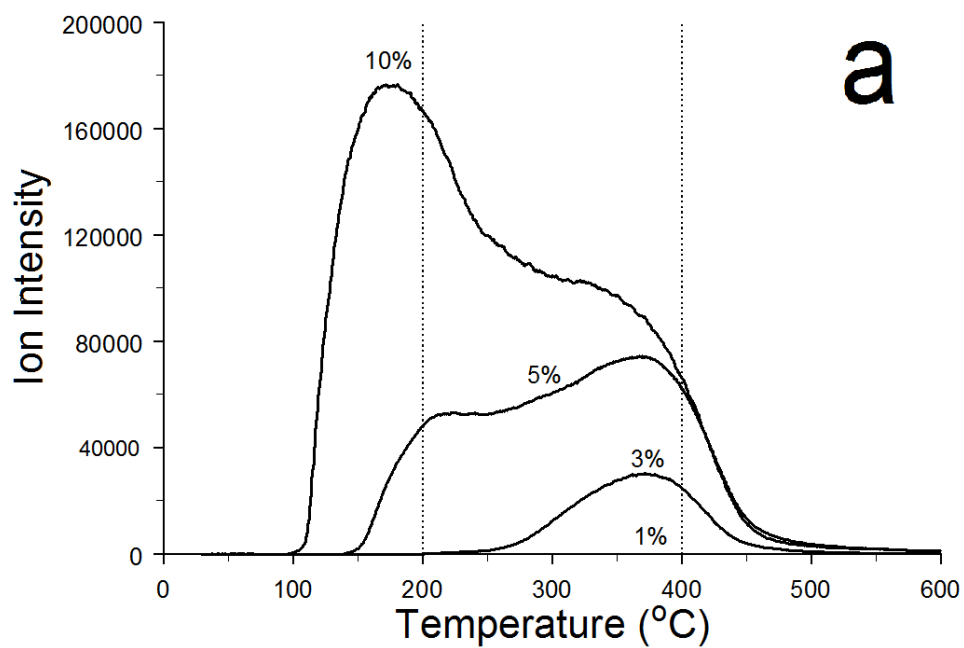


Figure 4.15 Mass spectrometric m/z 122 ion signal intensity temperature profiles for samples containing different amounts of benzoic acid adsorbed on (a) sodium and (b) calcium montmorillonites

The benzene (m/z 78) and carbon dioxide (m/z 44) volatiles detected for clay samples containing 10% (w/w) benzoic acid (Figure 4.13) were also detected during TG-MS analyses of samples containing lower benzoic acid loadings (Figure 4.16-Figure 4.19). Unlike the m/z 122 profiles in Figure 4.15, maximum ion signal intensities for m/z 78 and m/z 44 did not correlate with benzoic acid loading. In addition, m/z 78 and m/z 44 relative ion signal intensities varied from sample to sample, which is inconsistent with the assertion that both volatiles were produced from a single process, namely benzoic acid decarboxylation. However, when samples initially containing adsorbed benzoic acid were removed from the TG-MS apparatus after analyses, they often exhibited a darker color, ranging from light gray to black. This was not observed for TG-MS analyses of neat clay samples that were heated in the same manner. Moreover, replicate analyses obtained by using powders derived from clays containing the same benzoic acid loadings did not have the same color after heating. The presence of darker color after TG-MS analysis suggests that high temperature benzoic acid decomposition reactions resulted in char formation for these samples, and that the amount of char produced was not reproducible. Thus, one explanation for the lack of correlation between m/z 78 and m/z 44 ion signal intensities could be that some of the benzoic acid that persisted to high temperatures was converted to char after decarboxylation, which remained with the solid sample. Some was converted to benzene, which evolved from the sample and was detected by MS. Significant char formation would explain why mass losses for samples initially containing 10% (w/w) benzoic acid were less than expected. As shown in Figure 4.7, both samples lost about 6.6% mass between 100 and 400 °C, which, as indicated by the ion signal intensity profiles in Figure 4.13, can be attributed to most of the benzoic acid desorption and some benzene

and carbon dioxide evolution along with water desorption, which may contribute as much as 1.4% (Figure 4.1) to the 6.6% total.

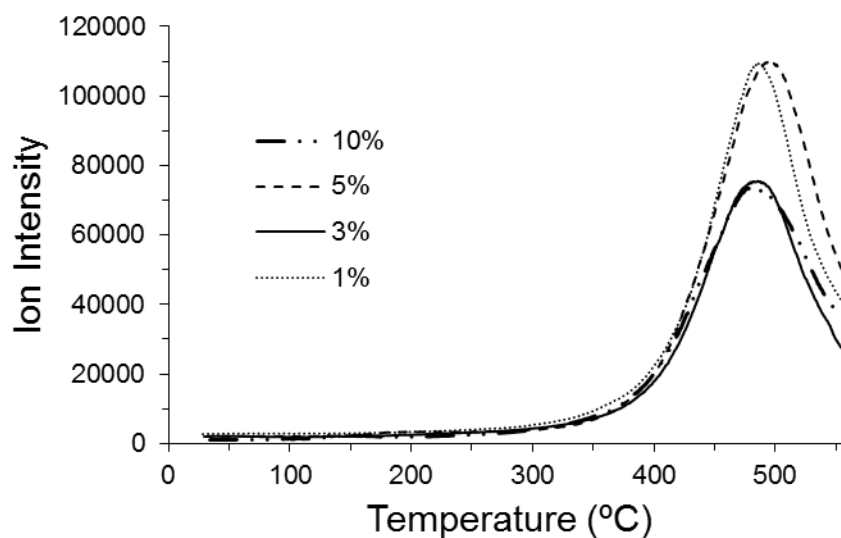


Figure 4.16 Mass spectrometric m/z 44 ion signal intensity temperature profiles for samples containing different amounts of benzoic acid adsorbed on calcium montmorillonites

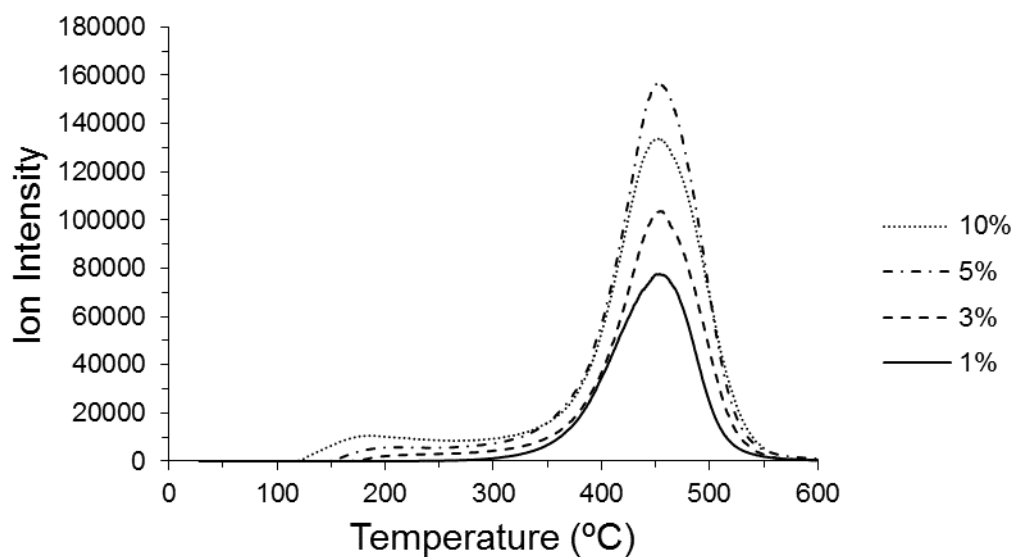


Figure 4.17 Mass spectrometric m/z 78 ion signal intensity temperature profiles for samples containing different amounts of benzoic acid adsorbed on calcium montmorillonites

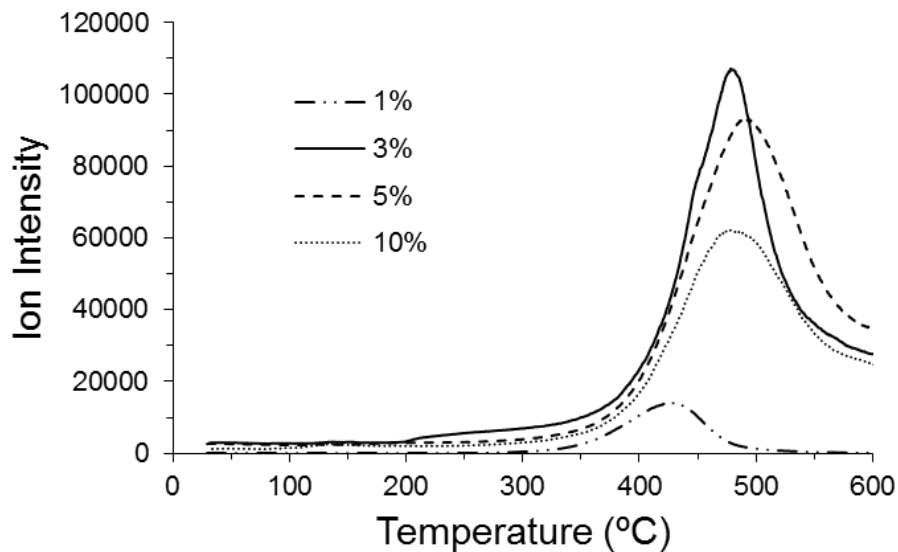


Figure 4.18 Mass spectrometric m/z 44 ion signal intensity temperature profiles for samples containing different amounts of benzoic acid adsorbed on sodium montmorillonites

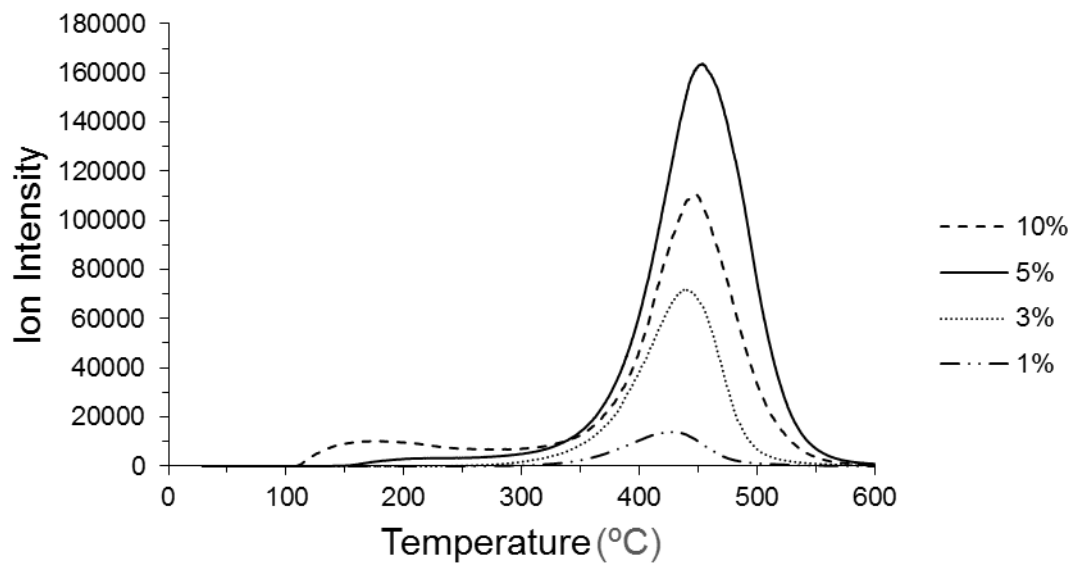


Figure 4.19 Mass spectrometric m/z 78 ion signal intensity temperature profiles for samples containing different amounts of benzoic acid adsorbed on sodium montmorillonites

4.3 Conclusions

Based on TG-MS analysis results described here, the following conclusions may be drawn regarding the adsorption of benzoic acid on montmorillonites and the temperature dependencies of adsorbate thermal desorption/decomposition processes. The high ionic strength and confined interlayer water environment provided by the clay structure uniquely enhances benzoic acid uptake. For comparison, in bulk water at 25 °C, benzoic acid solubility is limited to a relatively small mole fraction (5×10^{-4}). [121] Assuming that the clays employed for studies described here contained 4% (w/w) water (Figure 4.1) along with 10% (w/w) benzoic acid, the mole fraction of benzoic acid in hydrated interlayer spaces would be 0.27, which is about 540 times its bulk water solubility. This dramatic increase in mole fraction is a consequence of the strong molecular interactions between benzoic acid molecules and montmorillonite interlayer environments.

It was determined that the low temperature thermal desorption of interlayer water was affected by interactions with benzoic acid, which disrupt water – cation interactions. Some adsorbate interactions likely involve the formation of benzoic acid – water – cation bridging. These effects are more pronounced for CaMMT than NaMMT. Furthermore, benzoic acid thermal desorption profiles exhibit trends that depend on the nature of the cation present in montmorillonite clay interlayer spaces. Stronger benzoic acid – cation interactions were found to occur with Ca^{2+} , presumably because of its higher charge relative to Na^+ . At low adsorbate loadings, benzoic acid molecules occupy interlayer space sites that provide the highest stability, likely involving direct interactions with cations. After saturating these sites, which are limited by the number of interlayer cations,

benzoic acid occupies less stable sites, which also exhibit a stability dependence on cation charge. These sites likely involve longer range adsorbate – cation interactions than the more stable sites. Interlayer water desorption caused by heating samples containing adsorbed benzoic acid results in clay interlayer space contraction, resulting in increased confinement of adsorbed molecules. In fact, the basal spacing for smectites after removal of the hydration layer is estimated to be about 1 nm. [122] Thus, after most of the interlayer water has been removed, benzoic acid molecules are effectively trapped in this confined space, with motion perpendicular to basal planes restricted by the octahedral smectite sheets and in plane motion hindered by multiple surrounding cations. At sample temperatures above 300 °C, these confined benzoic acid molecules thermally decompose to benzene and carbon dioxide, which can escape the confined space. In parallel high temperature reaction paths, benzoic acid decomposition reactions result in char formation, which remains within the dehydrated interlayer space of the solid clay sample.

Chapter 5: Variable Temperature Infrared Spectroscopy

Investigations of Benzoic Acid Desorption from Sodium and Calcium Montmorillonite Clays

5.1 Introduction

Specific molecular interactions between benzoic acid and montmorillonite clays were previously characterized by thermo-IR [24] and thermogravimetry. [18] By using thermo-IR, Yariv et al. reported that the -C=O stretching vibration frequency of benzoic acid adsorbed on montmorillonite is dependent on the cation present in the clay interlayer space and the extent of clay dehydration. [24] They proposed a model to explain their spectroscopic findings in which a water molecule bridges between the acid and cation. This model was supported by results from recent variable temperature diffuse reflection infrared Fourier transform spectroscopy (VT-DRIFTS) studies of interactions between benzoic acid and montmorillonite clay interlayer water molecules, which were conducted at low temperatures (< 100 °C) to avoid benzoic acid desorption (Chapter 3). [28] In a thermogravimetry study of benzoic acid/clay interactions, Lu et al. reported that benzoic

acid desorption from sodium montmorillonite maximized at 140 °C, which was lower than when the clay contained calcium interlayer cations (179 °C). [18] They attributed the higher desorption temperature to stronger interactions between calcium ions and benzoic acid molecules. In the study described in Chapter 4 in which volatiles were selectively detected by mass spectrometry, evidence for multiple benzoic acid adsorption sites was obtained. [30] To characterize benzoic acid-clay interactions in more detail, in-situ thermal analyses were conducted by using VT-DRIFTS. Unlike results described in Chapter 3, [28] the results presented here were obtained at higher sample temperatures, and focus on benzoic acid desorption from montmorillonite interlayer spaces.

5.2 Results and Discussion

Infrared spectroscopic measurements of heated samples were employed to characterize temperature-dependent molecular environments of adsorbed benzoic acid on montmorillonite clays. By subtracting infrared spectra obtained at different temperatures, small spectral variations caused by heating were isolated from bulk infrared spectra. Difference spectra calculated by subtracting a selected spectrum from one acquired at higher temperature contain information regarding functional groups lost by the sample (negative bands) and gained by the sample (positive bands) over the corresponding temperature range. If spectral band intensity variations can be attributed to specific substances or functional groups, negative difference spectra bands represent adsorbate molecular vibrations at specific sites before desorption.

Figure 5.1 shows a comparison of ambient temperature DRIFTS spectra for sodium and calcium montmorillonites containing 10% (w/w) adsorbed benzoic acid (middle) along with calcium montmorillonite (top) and neat benzoic acid (bottom) for reference. The DRIFTS spectrum for sodium montmorillonite is nearly identical to calcium montmorillonite, so only one of these clay spectra is shown in Figure 5.1. Table 5.1 contains a listing of the more intense neat benzoic acid vibration frequencies measured by DRIFTS along with previously reported values for the dimer and monomer. Solid benzoic acid is dimeric, so it is not surprising that DRIFTS band frequencies correlate well with previously published dimer values. However, there are some interesting variations between the DRIFTS results and previously reported values. For instance, the 936 cm^{-1} DRIFTS band, which is assigned to out of plane -C-O-H bending, was previously reported by Bakker et al. at 962 cm^{-1} . [123] The vibration frequency of this band is particularly sensitive to acid group hydrogen bonding interactions. In fact, the large shift for this vibration from 962 cm^{-1} for the dimer to 571 cm^{-1} for the monomer is primarily attributed to loss of intermolecular hydrogen bonding in the dimer. [123] The 962 cm^{-1} literature value was obtained from gas phase measurements, [110, 123] where only dimeric hydrogen bonds affected frequencies. In contrast, the study that employed a pressed KBr pellet sample yielded a lower frequency for this vibration (936 cm^{-1})[70], which matches the DRIFTS value (Table 5.1). Apparently, interactions between benzoic acid molecules and diluent can affect dimer hydrogen bonding. The -C=O stretching vibration band in the neat benzoic acid DRIFTS spectrum consists of two overlapping features, at 1682 and 1700 cm^{-1} (Figure 5.1). In contrast, the frequency for this vibration was reported by Boczar et al. to be 1688 cm^{-1} [70] and by Bakker et al. to be 1709 cm^{-1} .

[123] The frequency of this vibration is very sensitive to hydrogen bonding, as evidenced by the fact that the monomer -C=O stretching vibration occurs at much higher frequency (1752 cm^{-1}). Thus, differences between -C=O absorbance band frequencies reported here and literature values are also most likely due to differences in sample composition.

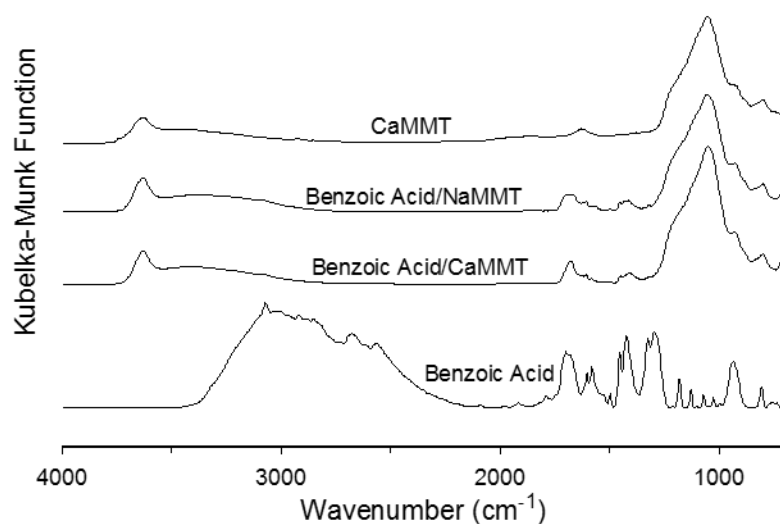


Figure 5.1 Ambient temperature DRIFTS spectra for benzoic acid/clay samples and for neat clay (top) and benzoic acid (bottom)

Table 5.1 Benzoic Acid Vibration Band Assignments (cm⁻¹)

DRIFTS (Dimer)	Dimer [70]	Dimer [110, 123]	Monomer [110, 123]	Monomer [124]	Assignment
705	708	708	710	711	C-C-H b
809	810	810			C-C-H b
936	936	962	571	568	C-O-H b
1073	1073	1066	1063	1066	C-C-H b
1129	1129	1126	1084	1086	C-C-H b
1184	1187	1176	1173	1169	C-C-H b
1296	1294	1297	1187	1185	C-C-H/C-O-H b
1325	1327	1322			C-O-H b
1426	1426	1432	1347	1347	C-O-H b
1455	1454	1453	1455	1456	C-O-H b
1498	1497	1498			C-O-H b
1583	1584	1591	1591	1590	C-C str
1604	1603	1618	1609	1606	C-C str
1700/1682	1688	1709	1752	1752	C=O str

As shown in Figure 5.1, DRIFTS spectra for samples containing clay are dominated by a broad, intense absorbance band at about 1050 cm⁻¹, assigned to inorganic oxide vibrations, a less intense, broad -O-H stretching vibration absorbance band in the 2000-3500 cm⁻¹ range, primarily due to hydrogen bonded water, and a more narrow absorption band near 3600 cm⁻¹, representing moderately hydrogen bonded hydroxyl functionalities, associated with the inorganic oxide clay component. With the exception of the -C=O stretching vibration (~1700 cm⁻¹) and the -C-O-H bending vibration (1400-1500 cm⁻¹), absorbance bands associated with benzoic acid are not readily apparent in the two middle

plots in Figure 5.1. Comparing benzoic acid/clay DRIFTS spectral features to the neat benzoic acid spectrum suggests that strong interactions between benzoic acid adsorbate and montmorillonite result in dramatic changes to absorbance band relative intensities. In particular, the intense 2200-3400 cm^{-1} absorbance due to overlapping -C-H and -O-H stretching vibrations, which dominates the neat benzoic acid spectrum, is not evident in DRIFTS spectra for benzoic acid/clay samples. In addition, the neat benzoic acid DRIFTS spectrum exhibits absorbance in the 1400-1500 cm^{-1} region that is more intense than the -C=O stretching vibration band near 1700 cm^{-1} . In contrast, the -C=O stretching vibration band intensities in DRIFTS benzoic acid/clay spectra are greater than the intensities of bands in the 1400-1500 cm^{-1} range. Similar effects were found in thin film spectra reported by Yariv et al. for samples comprising benzoic acid adsorbed on sodium and calcium montmorillonites. [24]

As previously reported in Chapter 3, initial heating of 10% (w/w) benzoic acid/clay samples results in water desorption, but benzoic acid evolution is not immediately detected. [28] Above 100 °C, significant benzoic acid loss from 10% (w/w) benzoic acid/clay samples was confirmed by thermogravimetry – mass spectrometry (TG-MS) measurements (Chapter 4). [30] Benzoic acid desorption above 100 °C results in detectable VT-DRIFTS spectra changes, which may be described as continuously decreasing benzoic acid absorbance band intensities with increasing temperature. However, within the temperature range corresponding to benzoic acid band intensity loss, three distinct regions were identified over which vibrational frequencies remained fairly constant, indicating distinctly different environments. These temperature ranges were identified by subtracting selected VT-DRIFTS spectra from spectra measured at

successively higher temperatures and tracking specific difference spectrum changes. Spectral changes resulting from initial benzoic acid desorption are represented by the difference spectra shown in Figure 5.2. The lower temperature spectrum used for difference spectra calculations was the same as the high temperature spectrum employed in the previous study of benzoic acid/water interactions using these same clay samples (Chapter 3). [28] These temperatures were selected because they are above the temperatures at which the maximum water evolution rate occurs (~60 °C) but lower than temperatures required for benzoic acid desorption (~100 °C). Upper plots in Figure 5.2 are overlays of the VT-DRIFTS spectra that were employed for subtraction and lower plots show subtraction results. Results for the benzoic acid/CaMMT sample appear on the right side of the figure and results for the benzoic acid/NaMMT sample are on the left. Difference spectra contain broad negative features between 2800 and 3800 cm^{-1} primarily associated with interlayer water loss, which began as soon as samples were heated and continued through sample temperatures at which benzoic acid desorbed. Both difference spectra contain small positive peaks near 3700 cm^{-1} , that can be assigned to hydroxyl groups that have lost hydrogen bonding partners. In addition, several features appear in difference spectra that can be assigned to adsorbed benzoic acid. A small negative peak at 3077 cm^{-1} superimposed on the large, negative -O-H stretching vibration band in both spectra can be assigned to benzoic acid aromatic ring -C-H stretching vibrations. The wavenumber for this negative band can be correlated with a sharp peak on top of the broad band in the neat benzoic acid spectrum (Figure 5.1 bottom). The most intense negative features in difference spectra for both benzoic acid/clay samples resulted from loss of -C=O vibration band intensity. For the benzoic acid/CaMMT sample, this

loss occurred at 1685 cm^{-1} , which is 13 cm^{-1} higher than the corresponding loss for the benzoic acid/NaMMT sample (1672 cm^{-1}). In addition, several negative bands associated with benzoic acid loss were detected at frequencies below the -C=O stretching vibration band frequencies for both samples. Small, sharp negative peaks near 1600 cm^{-1} can be assigned to aromatic ring -C-C- stretching vibrations. Difference spectra frequencies assigned to loss of these bands did not significantly vary from the neat benzoic acid values listed in Table 5.1, suggesting that the clays had minimal impact on these in-plane aromatic ring vibrations. Broader negative peaks with minima at 1430 (CaMMT) and 1420 (NaMMT) cm^{-1} likely correspond to in plane -C-O-H bending vibrations, which exhibit a maximum absorbance at 1426 cm^{-1} in the neat dimer. The corresponding frequency for this vibration is at 1347 cm^{-1} in the monomer. The fact that difference spectra features match the dimer more closely than the monomer suggests that benzoic acid adsorbed on the clays had a hydrogen bonding environment more similar to the dimer configuration. Negative features at 1250 (CaMMT) and 1270 (NaMMT) cm^{-1} most closely match the 1296 cm^{-1} vibration for the neat benzoic acid dimer. This vibration appears in the monomer spectrum at a significantly lower frequency (1187 cm^{-1}). Again, the closer correlation with the dimer frequency for this vibration suggests that benzoic acid adsorbed on the clays experiences a local environment (i.e hydrogen bonding) more like the dimer than the monomer. The negative bands at 925 (CaMMT) and 930 (NaMMT) cm^{-1} may be assigned to out of plane -C-O-H bending vibrations. Unfortunately, these bands overlap negative bands at 935 cm^{-1} that were detected by VT-DRIFTS analyses of the neat clays, and therefore were not considered when characterizing adsorption sites. Negative bands at 720 cm^{-1} for both samples may

correspond to out of plane aromatic ring –C-C-H bending vibrations. However, these bands also may overlap neat clay difference spectra negative features, and were therefore not used for characterizations. Overall, the difference spectra features shown in Figure 5.2 suggest that benzoic acid adsorbed on the clays exists in an environment more closely resembling the dimer than the monomer, which would be expected due to hydrogen bonding interactions with neighboring water molecules in clay interlayer spaces. Furthermore, the nature of the interlayer cation affects vibrations associated with the acid group more than those attributed to the aromatic ring. This suggests that benzoic acid molecules are oriented within the interlayer space so that the carboxylic acid functionalities align with interlayer cations.

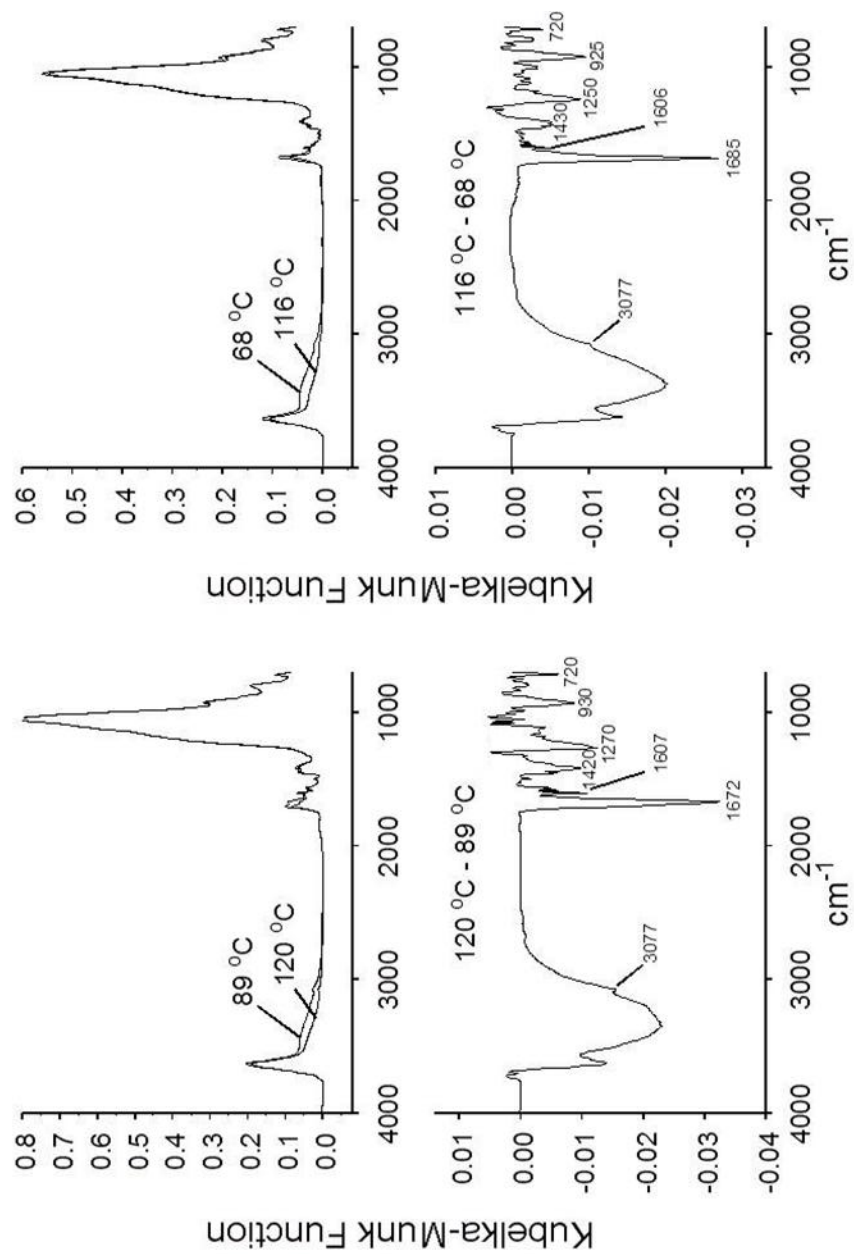


Figure 5.2 VT-DRIFTS spectra for sodium (left) and calcium (right) montmorillonites containing 10% (w/w) benzoic acid. The overlaid spectra shown at the top were subtracted to produce the difference spectra at the bottom

Figure 5.3 shows VT-DRIFTS spectra representing the second temperature range over which lost vibration band frequencies remained fairly constant. Difference spectra representing changes at these higher temperatures indicated less water loss than was detected at the lower temperatures (Figure 5.2). The negative peaks assigned to loss of aromatic -C-H stretching vibration intensity are more evident in difference spectra because they overlap smaller absorption bands attributed to water loss. The largest negative features in Figure 5.3 difference spectra can be assigned to -C=O stretching vibrations. For the CaMMT sample, this loss occurs at 1673 cm^{-1} , which is 12 cm^{-1} less than the corresponding negative band in the Figure 5.2 spectrum (1685 cm^{-1}). This -C=O stretching vibration red shift suggests that benzoic acid molecules lost at higher temperatures were interacting more strongly with their local environments. The negative band assigned to the -C=O stretching vibration for the NaMMT sample split into a doublet, with maxima at 1710 and 1675 cm^{-1} . In contrast to the CaMMT results, the 1710 cm^{-1} band represents a significant blue shift when compared to the lower temperature difference spectrum in Figure 5.2. Clearly, the -C=O functional group environments for benzoic acid molecules adsorbed on CaMMT and NaMMT were significantly different. In addition to the -C=O vibration band loss, VT-DRIFTS difference spectra for both benzoic acid/clay samples contain negative features corresponding to the other vibrations labeled in Figure 5.2. The negative peaks at 1430 (CaMMT) and 1420 (NaMMT) cm^{-1} , which can be assigned to in plane -C-O-H bending vibrations, are split into overlapping contributions in Figure 5.3. The two overlapping bands can be correlated with similar overlapping bands in the neat benzoic acid DRIFTS spectrum located at 1426 and 1455 cm^{-1} . It is possible that these overlapping absorbance bands were also in the Figure 5.2

difference spectra, but that the signal-to-noise ratios for those spectra were too low for them to be distinguished. Although not labeled in Figure 5.3 difference spectra, both plots exhibit narrow negative bands near 1605 cm^{-1} , which can be assigned to aromatic – C-C- stretching vibrations.

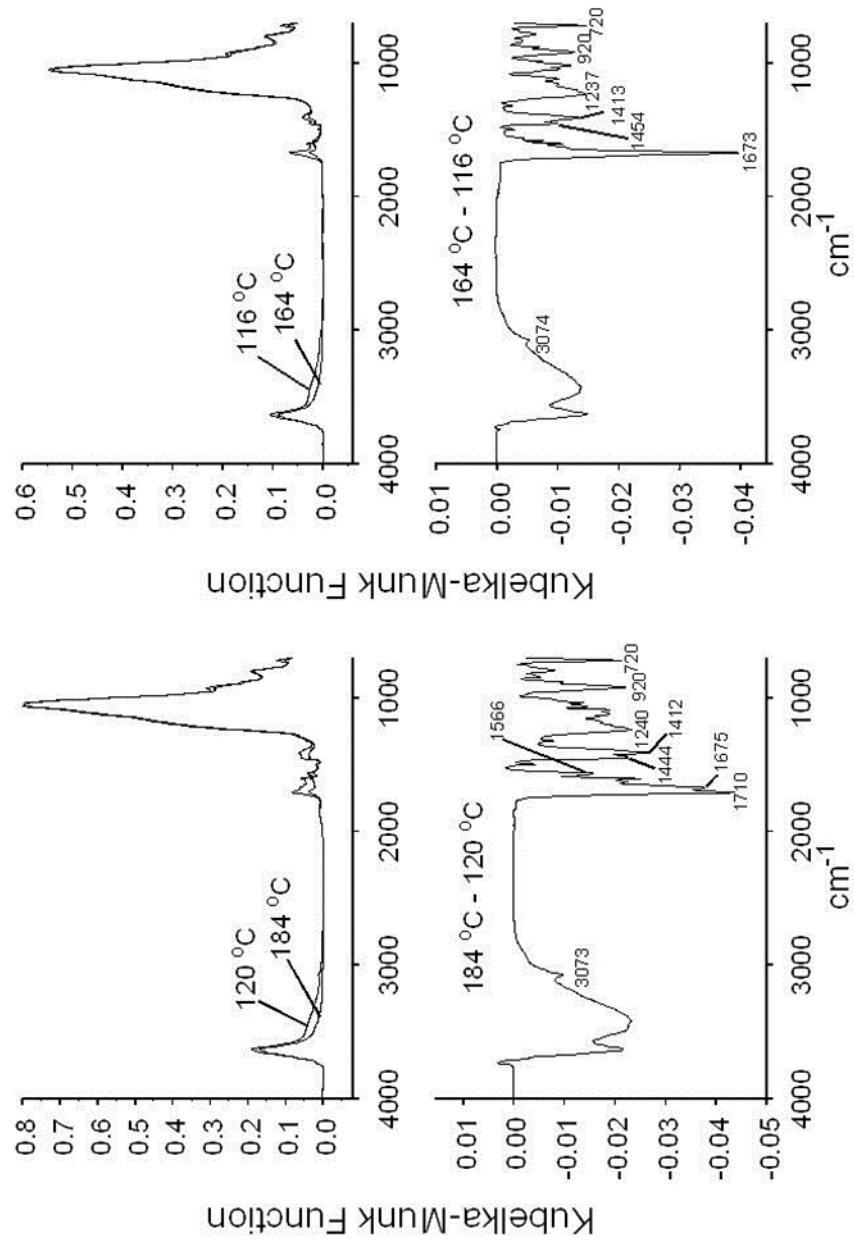


Figure 5.3 VT-DRIFTS spectra for sodium (left) and calcium (right) montmorillonites containing 10% (w/w) benzoic acid. The overlaid spectra shown at the top were subtracted to produce the difference spectra at the bottom

The Figure 5.3 benzoic acid/NaMMT difference spectrum contains a negative peak at 1566 cm^{-1} that is not found in the benzoic acid/CaMMT spectrum. This band can be attributed to the presence of benzoate anions. [125] The loss of 1566 cm^{-1} band intensity may be correlated with the appearance of the 1710 cm^{-1} contribution to the C=O stretching vibration doublet. Benzoate anions trapped within clay interlayer spaces would be expected to be strongly associated with cations by electrostatic attractions. Thus, the strengths of interactions between benzoic acid molecules interacting with cations associated with benzoate anions would be diminished, resulting in somewhat higher C=O stretching vibration frequencies (e.g. 1710 cm^{-1}).

Figure 5.4 shows VT-DRIFTS spectral differences calculated for spectra measured at about $260\text{ }^{\circ}\text{C}$ and spectra measured at $164\text{ }^{\circ}\text{C}$ (CaMMT) and $184\text{ }^{\circ}\text{C}$ (NaMMT). The negative O-H stretching vibration band can be attributed to loss of hydroxyl functionalities that had few hydrogen bonding partners. Due to the high frequency shift in this band compared to Figure 5.2 and Figure 5.3, the negative aromatic C-H stretching vibration band appears as a small peak that is no longer superimposed on the broad negative hydroxyl stretching vibration band. Negative features below 2000 cm^{-1} for the benzoic acid/CaMMT sample correspond to the same spectral changes that were assigned for the spectra shown in Figure 5.3. Compared to Figure 5.3, the negative C=O stretching vibration contribution for the benzoic acid/NaMMT sample at 1675 cm^{-1} is absent, but the negative benzoate anion band at 1565 cm^{-1} remains, suggesting that benzoic acid molecules desorbing over the $184\text{-}262\text{ }^{\circ}\text{C}$ temperature range were predominately those interacting with Na^+ ions associated with benzoate anions. Unlike

the lower temperature ranges, VT-DRIFTS difference spectra representing changes over the 164-260 °C (benzoic acid/CaMMT) and 184-262 °C (benzoic acid/NaMMT) temperature ranges contained a positive feature at 970 cm⁻¹. This feature is most likely associated with the formation of inorganic oxide -M-O-M- bridges that result from inorganic oxide dehydroxylation reactions, which produce water. In fact, this band was also detected by VT-DRIFTS analyses of the neat clays. From TG-MS data, it is known that benzoic acid desorption continues above 260 °C. However, due to the necessity for highly diluted samples, spectral features at higher temperatures were not reliably detected. Like the TG-MS studies described in Chapter 4, investigations using lower % (w/w) benzoic acid loadings were performed. Results from these studies were consistent with 10% (w/w) benzoic acid loading results. Additionally, changes in spectral features for lower % (w/w) adsorbed benzoic acid were much smaller and were not readily detected at high temperatures.

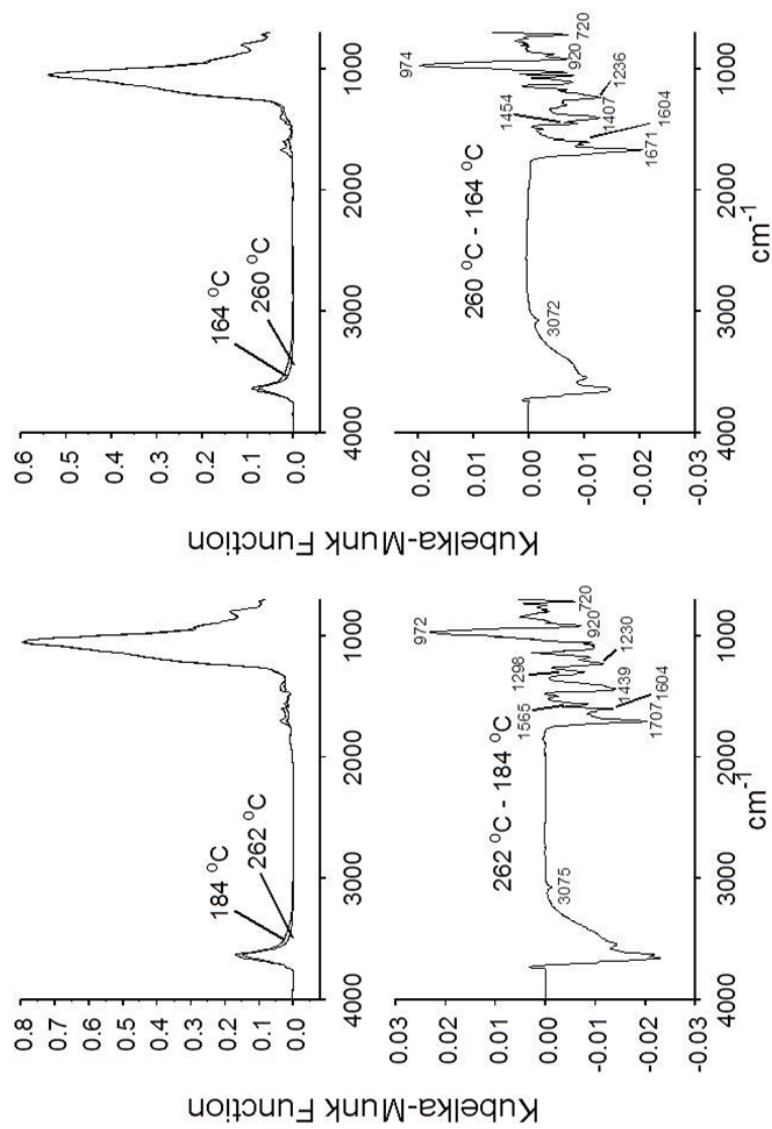


Figure 5.4 VT-DRIFTS spectra for sodium (left) and calcium (right) montmorillonites containing 10% (w/w) benzoic acid. The overlaid spectra shown at the top were subtracted to produce the difference spectra at the bottom

The specific VT-DRIFTS spectra selected for computing the difference spectra shown in Figure 5.2-Figure 5.4 were chosen to produce high signal-to-noise ratio subtraction results. Thus, the widest temperature gap between subtracted spectra was desired, as long as difference peak frequencies did not significantly vary. Due to inadequate signal-to-noise ratio, most infrared absorbance bands associated with benzoic acid desorption could not be discerned when successively acquired spectra were subtracted. However, it was possible to detect -C=O stretching vibration intensity losses when subtracting successively measured spectra (i.e. at 5 °C increments). Difference spectra -C=O stretching vibration band frequencies obtained by subtracting successively acquired spectra are plotted as a function of temperature for both benzoic acid/clay samples in Figure 5.5. These plots exhibit increasing noise at the temperature extremes due to low benzoic acid evolution rates at the beginning and end of the thermal desorption profile. Figure 5.5a shows that the -C=O stretching vibration frequencies for benzoic acid molecules lost from NaMMT between 50 and 125 °C were between 1670 and 1675 cm^{-1} . Above 125 °C, the -C=O stretching vibration band split into two components, one that trended to lower wavenumber and one that trended to higher wavenumber. As described previously, the higher wavenumber contribution can be correlated with benzoate loss and may be explained by loss of benzoic acid molecules interacting with cations that were simultaneously involved in benzoate anion interactions. The -C=O band component trending to lower wavenumbers likely represents loss of benzoic acid molecules interacting with cations that were not associated with benzoate anions. Figure 5.5b shows the corresponding -C=O band frequency versus temperature plot for the

benzoic acid/CaMMT sample. At low temperatures, the negative -C=O stretching vibration band is near 1685 cm^{-1} , which is significantly higher than the corresponding frequency for the benzoic acid/NaMMT sample (Figure 5.5a). A significant red shift occurs near $125\text{ }^{\circ}\text{C}$, after which it decreases to 1672 cm^{-1} . Figure 5.5 plots suggest that a transition between benzoic acid adsorption site environments occurs at about $125\text{ }^{\circ}\text{C}$ for both samples.

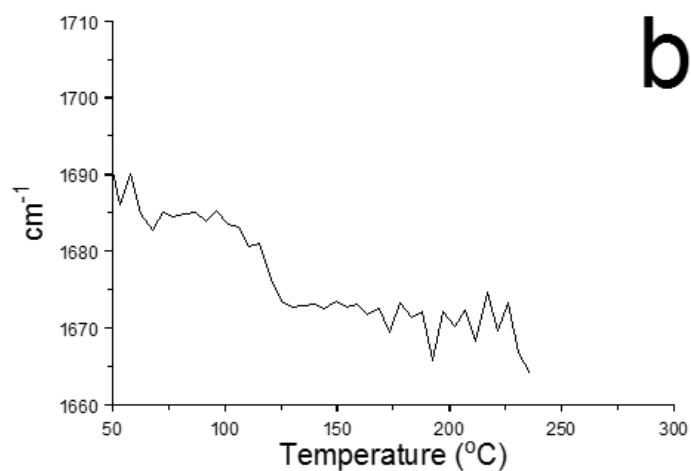
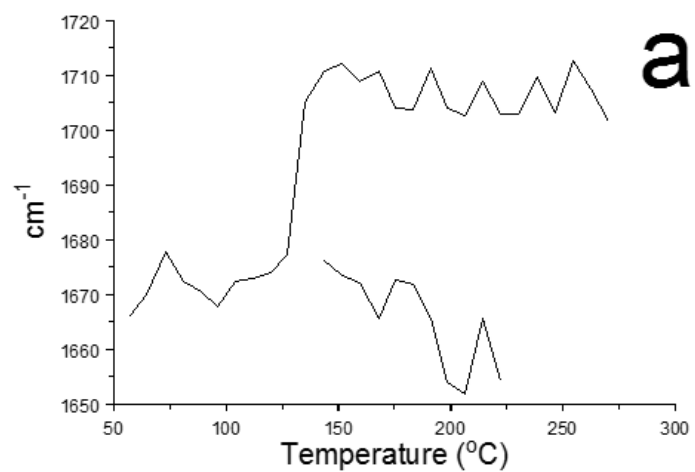


Figure 5.5 Plots of -C=O stretching vibration band wavenumber as a function of sample temperature obtained from VT-DRIFTS analyses of samples containing 10% (w/w) benzoic acid adsorbed on (a) sodium and (b) calcium montmorillonites

5.3 Conclusions

When heated under the same conditions employed for VT-DRIFTS analyses of benzoic acid/clay samples, spectral bands for a 5% (w/w) neat benzoic acid dispersed in silver powder sample (Figure 5.1, bottom) decreased without significant frequency shifts or relative changes in absorptivity until they were completely absent at about 100 °C. Therefore, the VT-DRIFTS spectral features shown in Figure 5.2-Figure 5.4 can be attributed solely to changes in benzoic acid/clay interactions. Difference spectra bands near 1600 and 3075 cm^{-1} match infrared absorbance band wavenumbers corresponding to $-\text{C}-\text{C}-$ and $-\text{C}-\text{H}$ stretching vibrations for benzoic acid monomer and dimer (Table 5.1). The invariability of these stretching vibration frequencies, which primarily involve aromatic ring motions, suggests that the aromatic ring is not significantly affected by benzoic acid/clay interactions. In contrast, vibrations associated with the carboxylic acid group exhibit temperature-dependent wavenumber shifts. For example, the $-\text{C}-\text{O}-\text{H}$ bending vibration bands that appear in Figure 5.2 difference spectra at 1250 (benzoic acid/CaMMT) and 1270 cm^{-1} (benzoic acid/NaMMT) shift to 1237 and 1240 cm^{-1} respectively in Figure 5.3. The shift to lower wavenumbers for these vibrations may be explained by loss of hydrogen bonding interactions for the adsorbate carboxylic acid group. Indeed, these trends represent $-\text{C}-\text{O}-\text{H}$ bending vibration frequency shifts away from those typical of the dimer and towards those characteristic of the monomer (Table 5.1). The loss of hydrogen bonding indicated by these band shifts would be expected due to loss of clay interlayer water, which occurs continuously while heating benzoic acid/clay samples. This loss of hydrogen bonding is inconsistent with the fact that higher

temperatures are required to desorb benzoic acid molecules. However, red shifts in $\text{C}=\text{O}$ stretching vibration frequencies with increasing sample temperature are indicative of strengthening interactions between carbonyl functionalities and local clay environments. This is likely due to stronger interactions between benzoic acid molecules and interlayer cations. However, at the same temperature, $\text{C}=\text{O}$ stretching vibration band frequencies were lower for benzoic acid/NaMMT samples than for benzoic acid/CaMMT samples, which is the opposite of what would be expected if benzoic acid molecules were directly interacting with the cations. Instead, these trends are consistent with a model in which benzoic acid interacts with cations through water bridges. [24, 25, 28]

The dramatic shift in $\text{C}=\text{O}$ stretching vibration frequencies for benzoic acid molecules lost when samples were heated to 125 °C suggests that the adsorbate local environment changed significantly at this temperature. This may be a result of an abrupt decrease in interlayer thickness resulting from water loss, resulting in increased benzoic acid confinement and facilitating more intense benzoic acid – water - cation interactions.

Although sample preparation procedures were employed to add adsorbate in its acid form to the clays, some benzoate, identified by its characteristic carboxylate stretching vibration at 1565 cm^{-1} , was present in the benzoic acid/NaMMT sample. The temperature range over which benzoate loss was detected correlated with the appearance of $\text{C}=\text{O}$ stretching vibration difference spectrum bands at wavenumbers above 1700 cm^{-1} . Interactions between benzoate anions and interlayer cations could result in increased $\text{C}=\text{O}$ stretching vibration frequencies because cation-water-benzoic acid interactions would be diminished. TG-MS studies described in Chapter 4 have shown that benzoic

acid decomposition occurs at temperatures above 300 °C, resulting in the formation of benzene and carbon dioxide volatile products. [30] Although this VT-DRIFTS study provided no information regarding sample changes that occurred above 260 °C, samples were darker in color after analyses, like those used for TG-MS analyses, which is indicative of char formation, most likely from subsequent reactions of benzoic acid decomposition products.

Chapter 6: Conclusions and Future Implications

Results described here illustrate the power of combining a sample perturbation (i.e. temperature change) approach with the high reproducibility afforded by diffuse reflection Fourier transform infrared spectroscopy to study complex solid sample structure changes. This technique should be well suited for soil contamination studies. [101] VT-DRIFTS analyses were used here to study sequential changes to a single sample, eliminating effects from sample-to-sample variations that occur when spectra are derived from different materials. Consequently, very small spectral changes were reliably detected. In fact, some of the difference spectra features described here could not be discerned from the VT-DRIFTS spectra that were employed for subtractions. Thermogravimetry is often used to characterize clays and recently has been used to characterize clay contaminants. By combining this well-established technique with the high sensitivity of mass spectrometry, mass loss steps were correlated with specific volatiles and species specific temperature profiles were used to characterize molecular interactions between benzoic acid and clays. The combination of these two powerful techniques, VT-DRIFTS and TG-MS, facilitated investigations of contaminated clays. While experimental results obtained by using the techniques described here leave some aspects of molecular interactions open

for speculation, the approach should be applicable to future studies of a variety of organic contaminants with various soil constituents.

6.1 Benzoic Acid and Water Molecular Environments

Conclusive assignments of benzoic acid orientations cannot be obtained from the data presented here and are therefore left open to speculation. Several different interlayer space configurations may be consistent with the experimental results, including various benzoic acid locations, bulk water distributions, and water bridge orientations. Although specific benzoic acid environments cannot be determined by the analytical techniques utilized here, some aspects of the interlayer space composition can be inferred from this work and previous literature. Le Caer et al proposed that neat clay interlayer water can be categorized into three types: bulk water, water molecules that interact with exchangeable cations, and water molecules that interact with siloxane surface groups. [126] Redistributions of interlayer clay water molecules among these classifications has been reported. [127] Theoretical calculations by Michot et al demonstrated that interlayer water molecules likely exist in close proximity to doubly charged interlayer cations longer than singly charged cations. [99] These results indicate that interlayer water is strongly influenced by interlayer cation charge. Benzoic acid may form hydrogen bonds with water molecules from any of these three categories. Benzoic acid molecules could also form hydrogen bonds with other benzoic acid molecules and with inorganic oxide hydroxyl groups in the interlayer space. It is also possible that benzoic acid interacts with

siloxane surface groups and/or interlayer cations. The range of possible interactions illustrates the complexity of possible contaminant-clay interlayer interactions. In fact, it is very likely that benzoic acid exists in multiple environments.

Li et al showed that tetracycline adsorption was greater for clays with exchangeable cations than for clays without cations. [128] Therefore, the clay cations located within the interlayer space are most likely responsible for stabilizing tetracycline molecules. From these results, it can be inferred that cation interactions contribute more to stabilizing polar contaminant adsorptions than inorganic oxide surface interactions. Based on this, the dominant benzoic acid interactions in clay interlayer spaces are most likely with cations, either directly or indirectly through water bridges. Results shown in Figure 4.13 and Figure 4.15 suggest that distinct benzoic acid losses occur at three sample temperatures, either desorbing intact or after decomposition. Although this may indicate that benzoic acid occupies at least three different environments within interlayer spaces, this desorption phenomenon may also be explained by changes to interlayer space with temperature. Two possible scenarios for benzoic interactions with interlayer cations can be postulated.

As described in Chapter 3, at least some benzoic acid adsorbed onto montmorillonite is involved in cation-water molecule interactions. Two possible orientations are represented in Figure 6.1. At ambient temperature, the hydrated montmorillonite interlayer spacing could accommodate benzoic acid monomers with a variety of orientations. With respect to the inorganic oxide sheets that define the interlayer space, the parallel and perpendicular orientations shown in Figure 6.1 represent extremes for these configurations. The perpendicular orientation places benzoic acid ring

hydrogens in close proximity to clay silicate sheets, where they may interact with negative charges. The parallel configuration places benzoic acid molecules closer to the middle of the interlayer space, where they interact primarily with cations. When montmorillonite is heated, the interlayer spacing decreases to a minimum spacing of 1 nm due to dehydration. [97, 114] Molecular calculations indicate that benzoic acid monomers have a length of approximately 7 angstroms and a width of about 5 angstroms. Therefore, benzoic acid molecules oriented so that their molecular planes are parallel to clay silicate layers may not be significantly affected by a decrease in interlayer spacing with heating. In contrast, the perpendicular orientation would be disrupted, requiring a molecular rotation to the parallel position and possibly contributing to adsorbate desorption if this rotation is sterically hindered. If multiple benzoic acid molecules are interacting with interlayer cations, desorption pathways may be blocked for benzoic acid molecules oriented parallel to clay silicate layers. At high temperatures, decreased clay interlayer spacing may produce benzoic acid environments where desorption is physically hindered. At these high temperatures, sufficient energy may be available for molecules in the parallel orientation to be released, possibly accounting for the higher temperature benzoic acid desorption shown in Figure 4.13. At higher temperatures (>400 °C) decomposition of trapped benzoic acid molecules may contribute to volatile products. Sample-to-sample variability in the amount of desorption, relative yields in desorption and decomposition products, and desorption/decomposition temperature variations can be ascribed to differences in clay compositions. In summary, different benzoic acid orientations and temperature induced changes to the interlayer space dimensions may be responsible for the benzoic acid desorption/decomposition trends reflected in the results described here.

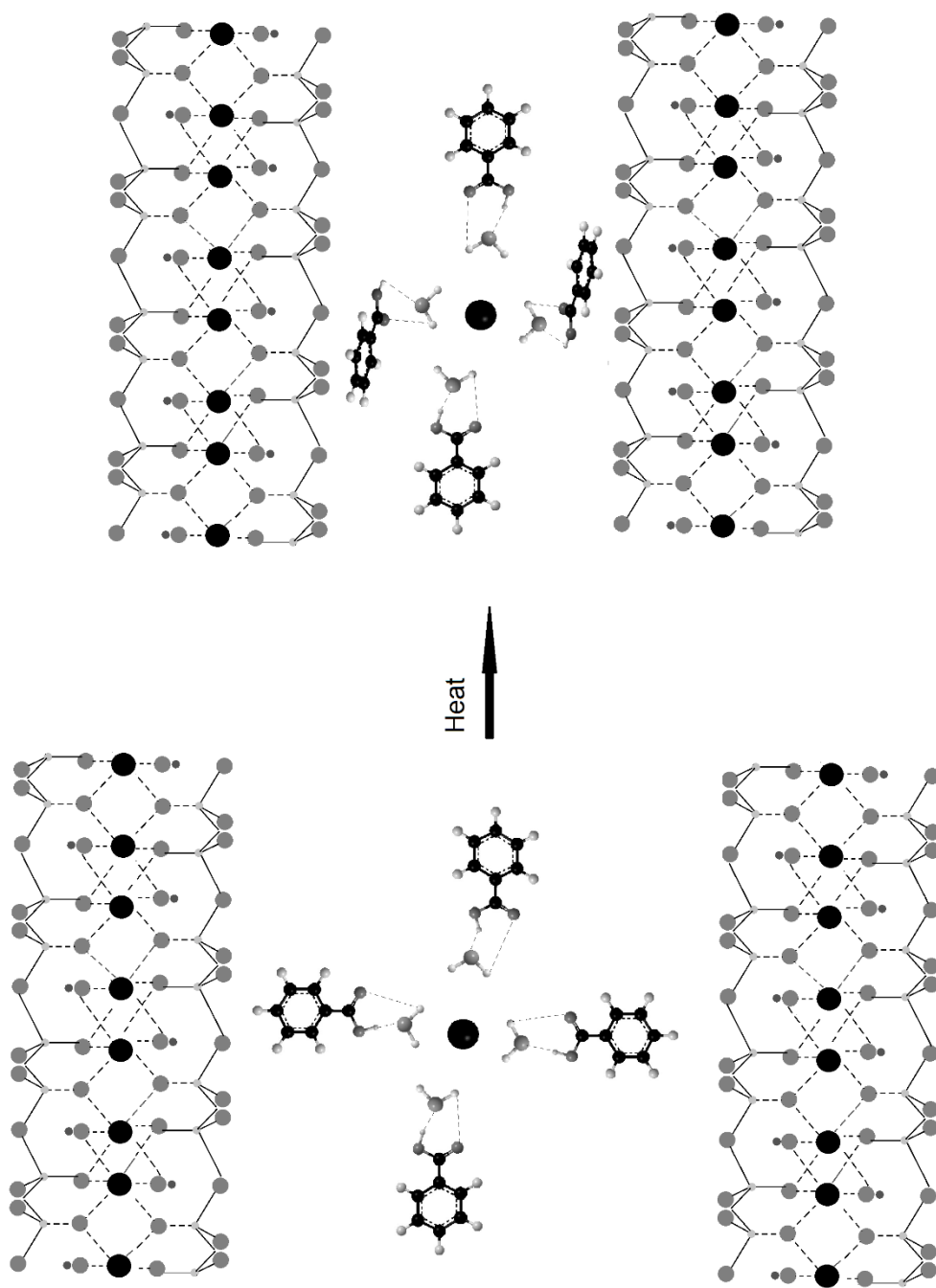


Figure 6.1 Adsorbed Benzoic Acid

As shown in Figure 6.2, it is likely that benzoic acid clusters in multiple layers around clay interlayer cations. This would lead to a range of hydrogen bonding environments, depending on benzoic acid molecule location. Benzoic acid molecules farther from cations would experience fewer interactions with the cation, and would form longer hydrogen bonds with bridging water molecules. Adjacent benzoic acid molecules may also hydrogen bond, but molecular orientations in the vicinity of cations may sterically limit the strength of this bonding. Therefore, benzoic acid molecules undergoing long range interactions with cations would be held less tightly. Due to weaker interactions, these molecules may require less energy to desorb from the clay. In contrast, benzoic acid molecules involved in cation-water bridging would be in a more stable environment, requiring higher temperatures for desorption. Benzoic acid molecules coordinated with the interlayer cation so that its molecular plane is parallel to clay silicate sheets would be the most stable configuration, requiring the highest temperatures for desorption. Presumably, when small amounts of benzoic acid are first added to the clay, equilibrium would favor the formation of orientations involving the closest interactions with cations. After these environments have been filled, benzoic acid molecules would occupy locations farther from the cations, but with maximum hydrogen bonding interactions with neighboring water and benzoic acid molecules.

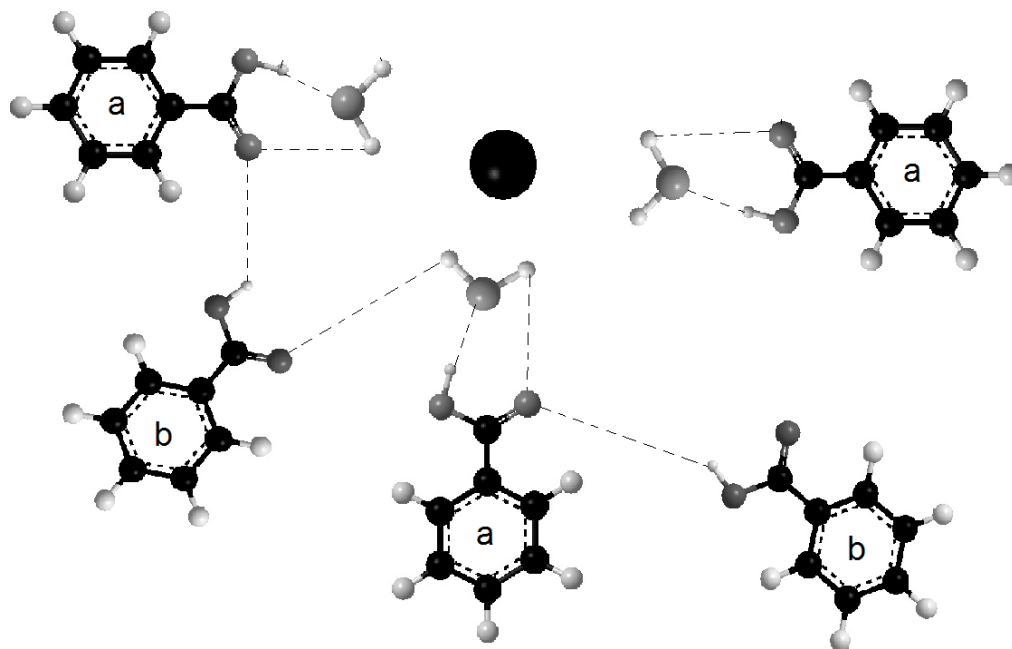


Figure 6.2 Clustered Benzoic Acid: (a) benzoic acid interacting through a water bridge, (b) benzoic acid interacting through long range hydrogen bonding

Evidence of benzoate in VT-DRIFTS difference spectra appears at 1566 cm^{-1} for benzoic acid adsorbed on Na^+ montmorillonite (Figure 5.3). The 1566 cm^{-1} absorbance band is characteristic of the carboxylate stretching vibration. This carboxylate stretching was not detected in VT-DRIFTS spectra for benzoic acid adsorbed on Ca^{2+} montmorillonite. Detection of benzoate in infrared spectra for samples containing benzoic acid adsorbed on montmorillonite clays was previously reported by Yariv et al. [25] In contrast to the results described here, Yariv et al observed benzoate when clay samples contained Ca^{2+} but not for clays containing Na^+ . The Yariv et al study employed samples made in a similar manner as those used for the measurements described here.

Thus, it is likely that benzoate was formed as a result of inconsistent sample preparation rather than due to a stabilizing effect from the cation. Strong interactions between benzoate molecules and interlayer cations is to be expected due to the benzoate negative charge. In addition to the 1566 cm^{-1} absorbance band, benzoic acid adsorbed on sodium montmorillonite exhibited a distinct split in -C=O stretching vibrations in VT-DRIFTS difference spectra (Figure 5.5). An increase in wavenumber for the benzoic acid -C=O stretching vibration to 1710 cm^{-1} indicates a less stable benzoic acid confirmation which was not detected for the calcium montmorillonite sample. This may be explained by benzoic acid molecules interacting with cations that are simultaneously involved in interactions with benzoate anions, as shown in Figure 6.3. Strong interactions between clay interlayer sodium cations and benzoate anions would diminish the stabilizing effects of these cations through benzoic acid-water bridge interactions, which may result in the observed wavenumber increase for the -C=O stretching vibration band. It is likely that benzoate may have existed in calcium montmorillonite samples, but at much lower concentrations, so that the effects from these anions on -C=O stretching vibration frequencies were not detected.

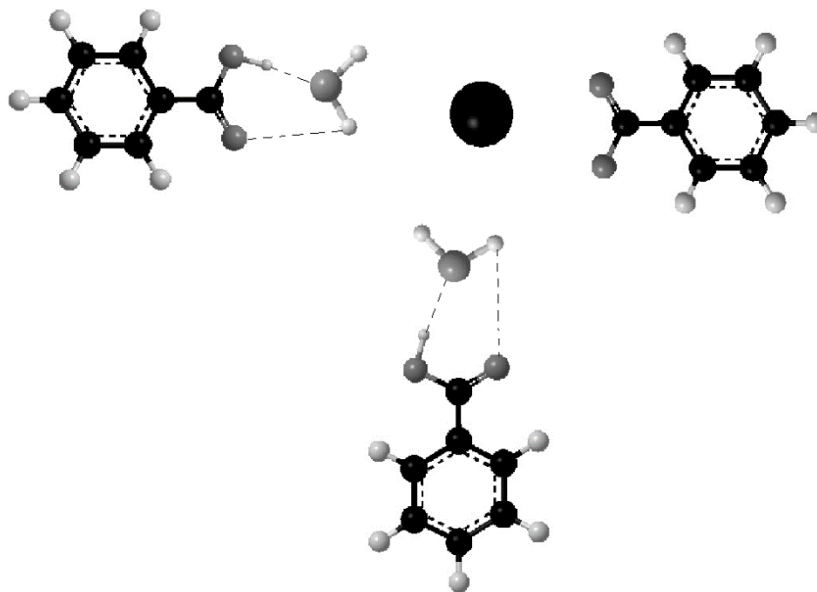


Figure 6.3 Benzoate-Cation Interaction

As illustrated by water thermal desorption profiles (Figure 4.2), addition of benzoic acid molecules to clay interlayer spaces alters water molecule environments. After benzoic acid is deposited on clays, water evolution profiles differ from what is observed for the neat clays. Although water desorption profiles for neat clays containing Na^+ and Ca^{2+} are different, the temperature profiles for samples containing benzoic acid are similar (Figure 4.8). This suggests that interlayer space water molecule environments are similar after benzoic acid adsorbed on Na^+ and Ca^{2+} montmorillonites. In the neat clays, the primary difference in water molecule potential energy can be ascribed to differences in the strengths of interactions with Na^+ and Ca^{2+} . Benzoic acid interactions with cations through water bridging would significantly change the potential energies of hydration sphere water molecules. Furthermore, these interactions would be expected to reduce the

influence of the cation on water molecule potential energy, resulting in similar environments regardless of the interlayer cation.

The benzoic acid-water-cation bridging configuration was first postulated by Yariv [24]. Molecular modeling was employed in the work described here to examine this bridging in greater detail. Calculations based on Yariv's postulated water bridge orientation, in which water oxygen atoms are directed toward the cations, did not produce vibration frequencies that matched measured values. However, when the bridging water molecule was oriented so that the hydrogens faced the interlayer cation (Figure 2.6), calculated frequencies matched experiment derived frequencies very well (Table 3.2 & Table 3.3). Molecular modeling calculations did not include montmorillonite silicate sheets, which might have altered predicted frequencies. Calculations were also only performed with the cation-water-benzoic acid bridge in a planar orientation. However, the calculations were performed for two different water bridging orientations: with the oxygen on the water facing the cation and the hydrogen atoms on the water molecule facing the cation. These molecular modeling calculations indicate that hydrogen bonding interactions between benzoic acid and the bridging water molecule were mostly responsible for the water orientation. This is an unexpected finding, but it may be a result of using an inadequate representation of the interlayer space for computing molecular vibration frequencies.

Figure 6.3 illustrates the water molecule environment disruption that may occur near cations after addition of benzoic acid. In this scheme, hydration sphere water molecules would be incorporated into benzoic acid interactions by forming bridges between the adsorbate and cation. Water molecules that are hydrogen bonded primarily

to other water molecules or involved in interactions with negative charges on inorganic oxide sheets would be largely unaffected by the introduction of benzoic acid.

Water desorption profile shapes are a reflection of the thermal energies required to disrupt water molecule interactions for the three classes of water molecule environments. Bulk water and water molecule interactions with inorganic oxide sheets should be relatively unchanged when benzoic acid is added. The fact that similar water desorption profile shapes are obtained after addition of benzoic acid suggests that benzoic acid-water-cation orientations provide water molecule environments that are not significantly influenced by the cation charge.

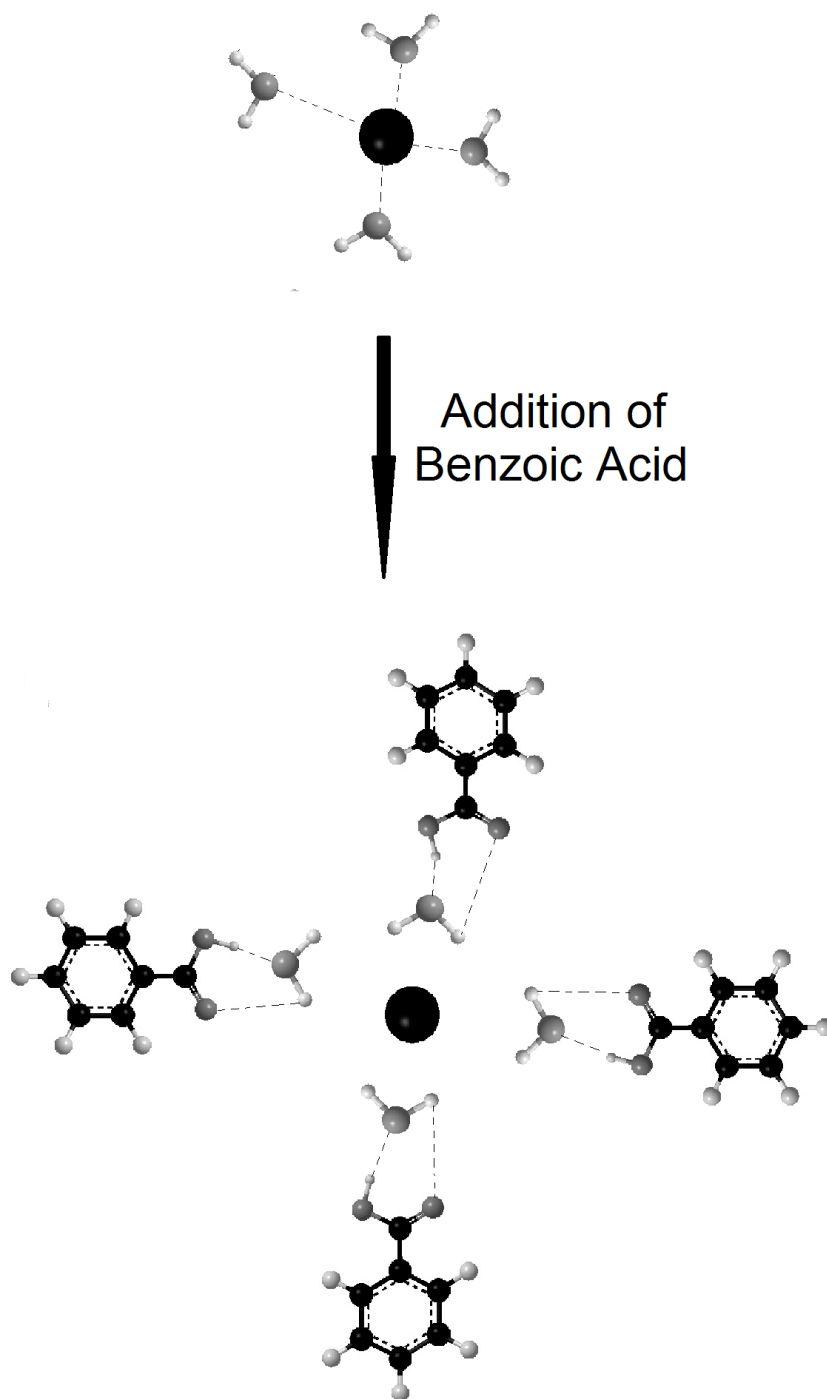


Figure 6.4 Water Bridge

Yariv et al postulated benzoic acid orientations within clay interlayer spaces that are similar to those proposed here. In their investigations, benzoic acid was deposited onto clay thin films for infrared analysis. Placing the sample at a 45° orientation to the infrared beam increased the –C-O-H in- plane band by 36%, while the out of plane C-O-H band was unaffected. [25] The montmorillonite thin films that Yariv et al employed for studies were orientated, making adsorbed benzoic acid molecules also oriented if they interacted in the same manner. Thus, rotating the thin film would change the orientation of the adsorbed benzoic acid molecules with respect to the infrared beam, which would affect the coupling between the radiation oscillating electric field and the oscillating vibration. The in plane –C-O-H bending vibration absorbance was found to be sensitive to orientation, whereas, the out of plane bending vibration was not. This would be expected if the in plane –C-O-H bending vibration was predominantly aligned parallel to the inorganic sheets defining the clay interlayer space, much like the orientations depicted in the figures shown here. TG-MS results presented here indicated that benzoic acid exists in multiple environments. Therefore, Yariv’s proposed orientation may account for some interlayer benzoic acid orientations, possibly even the majority of them, but does not explain why TG-MS analyses yield more than one desorption peak. To further characterize benzoic acid interlayer orientation in relation to clay silicate sheets, additional experiments are necessary. As discussed in Section 1.1.2, NMR may be an appropriate technique for providing more details regarding benzoic acid orientations. However, sample pretreatments to remove bulk water or to replace water molecules with D₂O might be necessary for these investigations.

6.2 Subsequent Soil Contaminant Investigations

The benzoic acid-montmorillonite studies outlined here represent the first attempts to apply VT-DRIFTS and TG-MS to studies related to soil contamination. Benzoic acid was selected as the initial model compound for these studies because it has a simple structure and has been studied extensively. Part of the motivation for conducting the experiments described here was to evaluate VT-DRIFTS as a thermal analysis technique for soil studies and to work out the methodologies needed for conducting these types of studies. Future studies should focus on adsorption of molecules that are considered to be environmental contaminants. To facilitate comparisons to the benchmark studies described here, good choices for contaminant molecules for studies should involve those with structures similar to benzoic acid. As shown by the list in Table 1.1, acetylsalicylic acid, which is essentially a derivative of benzoic acid, is considered to be a significant environmental contaminant. Acetylsalicylic acid readily decomposes to salicylic acid and acetic acid by environmental decomposition mechanisms. Due to this ease of decomposition, acetylsalicylic acid is often found in the environment as its decomposition products, salicylic acid and acetic acid. Salicylic acid, which has a structure even closer to benzoic acid, is found in over-the-counter personal care products, and is also considered an environmental pollutant. Thus, it makes sense to study salicylic acid-montmorillonite interactions because salicylic acid has a larger environmental impact than benzoic acid, and there should be similarities with what has been learned regarding benzoic acid adsorption. Like benzoic acid, salicylic acid has been well characterized. Theoretical and experimental IR frequencies for neat salicylic acid have been reported

[129, 130] and thermal decomposition products have been identified. Salicylic acid decomposes to phenol and carbon dioxide at temperatures as low as 200°C. [74] This is significantly lower than the temperature at which benzoic acid begins to decompose (350 °C). [74]

6.2.1 Thermogravimetric-Mass Spectrometric Data Predictions for Salicylic Acid loaded montmorillonites

Thermogravimetry- mass spectrometry studies of desorption of salicylic acid from Na⁺ and Ca²⁺ montmorillonites would likely yield results similar to those obtained for desorption of benzoic acid from the same clays. It is likely that the hydroxyl group in the salicylic acid structure may associate with bulk water molecules in the interlayer, making interactions with montmorillonites somewhat different than for benzoic acid. In particular, water desorption temperature profiles below 150 °C for samples containing salicylic acid loaded on montmorillonite should differ from those characteristic of the benzoic acid-montmorillonite system. Due to the lower decomposition temperature of salicylic acid compared to benzoic acid, mass spectrometric ion profiles would likely be significantly different, even if interactions between adsorbate and the clays are similar. Assuming that salicylic acid interacts with montmorillonite clays and desorbs similarly to benzoic acid, desorption of the intact salicylic acid should appear as a single peak in mass spectrometric ion profiles due to a significantly lower decomposition temperature. Decomposition products (e.g. phenol and carbon dioxide) should be detected at sample

temperatures above 200 °C. As predicted for benzoic acid (Figure 6.1), interactions between salicylic acid and clay interlayer environments should hold the acid on the clay until temperatures at which the molecule decomposes.

6.2.2 *Variable Temperature- Diffuse Reflection Infrared Fourier Transform*

Spectroscopy Data predictions for salicylic acid loaded montmorillonites

Salicylic acid has a much more complex infrared spectrum than benzoic acid. Therefore, spectra of salicylic acid adsorbed on clays will likely contain more overlapping features, making specific assignments more difficult than for benzoic acid. Calculated and experimental frequencies for neat salicylic acid dimer are listed below in Table 6.1. The carboxylic acid functionality of benzoic acid was primarily responsible for stabilizing interactions within the clay interlayer space. The carboxylic acid functionality of salicylic acid would be expected to interact similarly. However, the salicylic acid structure contains a hydroxyl group in addition to the carboxylic acid. Thus, VT-DRIFTS spectra obtained while salicylic acid desorbs from the clays may exhibit absorbance band shifts that are associated with the hydroxyl group in addition to the acid functionality. It would be interesting to compare the trends for vibrational bands assigned to the carboxylic acid functionality of salicylic acid and benzoic acid. It may be that the acid group is less affected by neighboring hydrogen bonding (both inter- and intra-molecular) partners because of an increase in hydrogen bonding for the hydroxyl group.

Table 6.1 Salicylic Acid Predicted and Experimental Infrared Frequencies

Vibration	Salicylic Acid Dimer Experimental Values [130]	Salicylic Acid Dimer B3LYP/cc-pVTZ Calculated Values [130]
-C=O Stretch	1658	1655
In-Plane Carboxylic Acid -C-O-H Bend	1249/1296	1247/1315
Out-Of-Plane Carboxylic Acid -C-O-H Bend	698/759	700/760
In-Plane Ring -C-O-H Bend	1484/1579	1486/1583
Out-of-Plane Ring -C-O-H Bend	NA	NA
In Plane Both Ring -C-O-H Bend	1325/1466	1330/1459
Out-Of-Plane Both Ring -C-O-H Bend	965/1211	941/1224

6.3 Future Applications

The results presented here have been used to predict molecular interactions between benzoic acid and montmorillonites. Additional experiments could be conducted to further elucidate these types of interactions for other adsorbates. In a similar study, Morillo et al investigated the adsorption of 3-aminotriazole on Mg^{2+} montmorillonite. They reported that O-H stretching vibration band frequencies associated with clay interlayer water

molecules shifted after adsorption of 3-aminotriazole. However, their experimental data interpretations were largely limited to this observation because they did not employ perturbation techniques to study their samples in more detail. Clearly more detail regarding water molecule environment changes caused by adsorbate addition to the clay sample could be obtained by using VT-DRIFTS for analysis of their samples. Due to the numerous interactions involving O-H functionalities and adsorbate molecules, the O-H stretching vibration band is very broad (2000-3500 cm^{-1}), consisting of many overlapping bands. This is apparent in both VT-DRIFTS measurements and difference spectra (Figure 3.3 & Figure 5.2). Although the presence of the broad O-H stretching vibration band in VT-DRIFTS data was mentioned here, experiments designed to focus on changes in this spectral region due to the addition of adsorbate to the clays were not performed. VT-DRIFTS studies in which the amount of water contained within clay interlayer spaces is varied may provide information regarding the types of interactions that water molecules are involved in for neat clays and clays containing adsorbates.

Although it may seem logical that water molecules occupying cation hydration spheres or serving as bridges between benzoic acid molecules and cations would require more energy for desorption than bulk water molecules, this claim cannot be substantiated by the results obtained from the studies described here. Alternatively, the water bridge environment might be inferred by tracking changes to spectral features for adsorbate functional groups that interact with these bridging waters. For example, VT-DRIFTS results indicate that the benzoic acid C=O stretching vibration is affected by the loss of clay interlayer water. At room temperature, the C=O stretching vibration frequency for benzoic acid loaded on Na^+ montmorillonite is at a lower wavenumber than for benzoic

acid loaded on Ca²⁺ montmorillonite. This trend is consistent with the presence of a water bridge. However, if the water bridge is lost by heating the sample, the benzoic acid C=O stretching vibration frequency should occur at higher wavenumber when benzoic acid interacts with Na⁺ montmorillonite compared to Ca²⁺ montmorillonite. Unfortunately, the positive difference spectra features that would represent these changes could not be discerned in VT-DRIFTS results because of the large change in absorptivity for this band. To determine the nature of the bridging water molecules and how they change with temperature, additional VT-DRIFTS studies focusing on O-H spectral changes should be conducted. Spectral subtractions of neat clays would reveal information regarding the O-H vibrations associated with water molecules interacting with bulk water and clay constituents. Careful comparisons between trends detected when analyzing neat clays and results obtained for samples containing adsorbates may provide information regarding interactions between adsorbates and water molecules, in particular, bridging water molecules. These studies would require careful planning of VT-DRIFTS measurements because, unlike the procedures described here, data interpretations would involve comparisons between two different samples (i.e. neat clays and clays containing adsorbates). The VT-DRIFTS studies of benzoic acid loaded clays presented here involved the use of a 5 °C/min linear heating ramp. The VT-DRIFTS apparatus can also be used with a heating profile in which sample temperatures are held for specific durations before heating to higher temperatures. Heating samples at slower ramp rates and/or utilizing stepwise heating functions could potentially yield higher quality VT-DRIFTS data and allow for differentiation of bridging water molecule spectral features.

Development of new techniques for investigation of soil contaminants is imperative. The number of pharmaceuticals and personal care products detected in the environment continues to increase at a rapid rate and PPCP production rates continuously increase. The scope of the environmental impacts associated with these contaminants has yet to be fully realized. Understanding the mechanism by which contaminants are stabilized in the environment and concentrate in soils is imperative for the development of effective low-cost remediation approaches. Further improvements in the techniques described here may be attained by investigating interactions involving more complex adsorbates. Ultimately, “pharmacoecovigilance” may lead to the implementation of more informed regulations for landfilling and waste water treatment methods with regard to PPCPs and the environment.

References

1. Stumm-Zollinger, E. and G.M. Fair, *Biodegradation of Steroid Hormones*. J. Water Poll. Cont. Fed., 1965. **37**(11): p. 1506-1510.
2. Eckel, W.P., B. Ross, and R.K. Isensee, *Pentobarbital found in groundwater*. Ground Water, 1993. **31**(5): p. 801-804.
3. Holm, J.V., K. Ruge, P.L. Bierg, and T.H. Christensen, *Occurances and Distribution of pharmaceutical organic-compounds in the groundwater downgradient of a landfill (Grindsted, Denmark)*. Environ. Sci. and Technology, 1995. **29**(5): p. 1415-1420.
4. Ternes, T.A., R. Hirsch, J. Mueller, and K. Haberer, *Methods for the determination of neutral drugs as well as betablockers and α 2-sympathomimetics in aqueous matrices using GC/MS and LC/MS/MS*. Fresen. J. Anal. Chem., 1998. **362**: p. 329-340.
5. Ternes, T.A., *Occurrence of drugs in German sewage treatment plants and rivers*. Wat. Res., 1998. **32**(11): p. 3245-3260.
6. Snyder, S.A., T.L. Keith, D.A. Verdrugge, E.M. Snyder, T.S. Gross, K. Kannan, and J.P. Giesy, *Analytical methods for detection of selected estrogenic compounds in aqueous mixtures*. Environ. Sci. and Technol., 1999. **33**: p. 2814-2820.
7. Pedersen, J.A., M. Soliman, and I.H. Suffet, *Human Pharmaceuticals, Hormones, and Personal Care Product Ingredients in Runoff from Agricultural Fields Irrigated with Treated Wastewater*. J. Agric. Food Chem., 2005. **53**: p. 1625-1632.
8. Routledge, E.J., D. Sheahan, C. Desbrow, G.C. Brighty, M. Waldock, and J.P. Sumpter, *Identification of Estrogenic Chemicals in STW Effluent. 2. In Vivo Responses in Trout and Roach*. Environ. Sci. Technol., 1998. **32**: p. 1559-1565.
9. Desbrow, C., E.J. Routledge, G.C. Brighty, J.P. Sumpter, and M. Waldock, *Identification of Estrogenic Chemicals in STW Effluent. 1. Chemical Fractionation and in Vitro Biological Screening*. Environ. Sci. and Technology, 1998. **32**(11): p. 1549-1558.
10. Ahel, M. and I. Jelcic, *Phenazone analgesics in soil and groundwater below a municipal solid waste landfill*. ACS Symp. Ser., 2001. **791**(Pharmaceuticals and Personal Care Products in the Environment): p. 100-115.

11. Hachat, K., N. Potter, and C.H. Lisse. *Development of analytical methods for detection of pharmaceutical pollution of surface water in Georgia using purge-n-trap GC/MS*. 2015. American Chemical Society.
12. Simazaki, D., R. Kubota, T. Suzuki, M. Akiba, T. Nishimura, and S. Kunikane, *Occurrence of selected pharmaceuticals at drinking water purification plants in Japan and implications for human health*. *Water Res.*, 2015: p. Ahead of Print.
13. Cai, M.-Q., R. Wang, L. Feng, and L.-Q. Zhang, *Determination of selected pharmaceuticals in tap water and drinking water treatment plant by high-performance liquid chromatography-triple quadrupole mass spectrometer in Beijing, China*. *Environ. Sci. Pollut. Res.*, 2015. **22**(3): p. 1854-1867.
14. Ferrer, I. and E.M. Thurman. *Analysis of pharmaceuticals in drinking water, groundwater, surface water, and wastewater*. 2013. Elsevier B.V.
15. *Pharmaceuticals in drinking-water*. 2012, World Health Organization: France.
16. Ryu, J., J. Oh, S.A. Snyder, and Y. Yoon, *Determination of micropollutants in combined sewer overflows and their removal in a wastewater treatment plant (Seoul, South Korea)*. *Environ Monit Assess*, 2014. **186**: p. 3239-3251.
17. Fatta, D., A. Achilleos, A. Nikolaou, and S. Meric, *Analytical methods for tracing pharmaceutical residues in water and wastewater*. *TrAC, Trends Anal. Chem.*, 2007. **26**(6): p. 515-533.
18. Lu, L., R.L. Frost, and J. Cai, Liu, Y., Zhang, L., *Desorption of Benzoic and Stearic Acid Adsorbed upon Montmorillonites: A Thermogravimetric Study*. *J. Therm. Anal. Calorim.*, 2010. **99**: p. 377-384.
19. Meier, D.W., A. Urakawa, and A. Baiker, *Adsorption Behavior of Salicylic, Benzoic, and 2-Methyl-2-Hexenoic Acid on Alumina: an in situ Modulation excitation PM-IRRAS Study*. *Phys. Chem. Chem. Phys*, 2009. **11**: p. 10132-10139.
20. Zhao, X. and Y. Fang, *Raman Experimental and DFT Theoretical Studies on the Adsorption Behavior of Benzoic Acid on Silver Nanoparticles*. *J. Mol. Struct.*, 2006. **789**: p. 157-161.
21. Lu, L., J. Cai, and R.L. Frost, *Near Infrared Spectroscopy of Benzoic Acid Adsorbed on Montmorillonite*. *Spectrosc. Lett.*, 2010. **43**: p. 266-274.
22. Hagaman, E.W., B. Chen, J. Jiao, and W. Parsons, *Solid-State ¹⁷O NMR Study of Benzoic Acid Adsorption on Metal Oxide Surfaces*. *Solid State Nucl. Magn. Reson.*, 2012. **41**: p. 60-67.

23. Chefetz, B., S. Eldad, and T. Polubesova, *Interactions of Aromatic Acids with Montmorillonite: Ca²⁺ and Fe³⁺ Saturated Clays versus Fe³⁺ - Ca²⁺ clay System*. Geoderma, 2011. **160**: p. 608-613.
24. Yariv, S., *IR Spectroscopy and Thermo-IR Spectroscopy in the Study of the Fine Structure of Organo-Clay Complexes*. Organo-Clay Complexes and Interactions. 2002, New York: Marcel Dekker, Inc.
25. Yariv, S., J.D. Russell, and V.C. Farmer, *Infrared Study of Adsorption of Benzoic Acid and Nitrobenzene in Montmorillonite*. Isr. J. Chem., 1966. **4**(5-6): p. 201-213.
26. Thomas, J.E. and M.J. Kelley, *Interaction of Mineral Surfaces with Simple Organic Molecules by Diffuse Reflectance IR Spectroscopy (DRIFT)*. J. Colloid Interface Sci., 2008. **322**(2): p. 516-526.
27. Yan, L.G., J. Wang, H.Q. Yu, Q. Wei, B. Du, and X.Q. Shan, *Adsorption of Benzoic Acid by CTAB Exchanged Montmorillonite*. Appl. Clay Sci., 2007. **37**: p. 226-230.
28. Nickels, T.M., A.L. Ingram, D.K. Maraoulaite, and R.L. White, *Variable Temperature Infrared Investigation of Benzoic Acid Interactions with Montmorillonite Clay Interlayer Water*. Appl. Spectrosc., 2015: p. in press.
29. Nickels, T.M., A.L. Ingram, D.K. Maraoulaite, and R.L. White, *Variable Temperature Infrared Spectroscopy Investigations of Benzoic Acid Desorption from Sodium and Calcium Montmorillonite Clays*. Appl. Spectrosc.: p. submitted.
30. Nickels, T.M., A.L. Ingram, D.K. Maraoulaite, and R.L. White, *Thermogravimetry – Mass Spectrometry Investigation of Benzoic Acid Interactions with Sodium and Calcium Montmorillonite Clays* Thermochem. Acta: p. submitted.
31. Bendz, D., N.A. Paxeus, T.R. Ginn, and F.J. Loge, *Occurrence and fate of pharmaceutically active compounds in the environment, a case study: Hoeje River in Sweden*. J. Hazard. Mater., 2005. **122**(3): p. 195-204.
32. Ternes, T.A., A. Joss, and H. Siegrist, *Scrutinizing pharmaceuticals and personal care products in wastewater treatment*. Environ. Sci. Technol., 2004. **38**(20): p. 392A-399A.
33. Smil, V., *Detonator of the population explosion*. Nature (London), 1999. **400**(6743): p. 415.

34. Speidel, J.J., D.C. Weiss, S.A. Ethelston, and S.M. Gilbert, *Population policies, programmes and the environment*. Philos Trans R Soc Lond B Biol Sci, 2009. **364**(1532): p. 3049-65.
35. Heeb, F., H. Singer, B. Pernet-Coudrier, W. Qi, H. Liu, P. Longree, B. Muller, and M. Berg, *Organic Micropollutants in Rivers Downstream of the Megacity Beijing: Sources and Mass Fluxes in a Large-Scale Wastewater Irrigation System*. Environ. Sci. Technol., 2012. **46**(16): p. 8680-8688.
36. Tran, N.H., J. Li, J. Hu, and S.L. Ong, *Occurrence and suitability of pharmaceuticals and personal care products as molecular markers for raw wastewater contamination in surface water and groundwater*. Environ. Sci. Pollut. Res., 2014. **21**(6): p. 4727-4740.
37. Lunde, G., J. Gether, N. Gjøs, and M.B.S. Lande, *Organic Micropollutants in Precipitation in Norway*. Atmos. Environ., 1977. **11**: p. 1007-1014.
38. Kumar, A., B. Chang, and I. Xagorarakis, *Human health risk assessment of pharmaceuticals in water: issues and challenges ahead*. Int. J. Environ. Res. Public Health, 2010. **7**: p. 3929-3953.
39. Heberer, T., *Occurrence, fate, and removal of pharmaceutical residues in the aquatic environment: a review of recent research data*. Toxicol. Lett., 2002. **131**(1-2): p. 5-17.
40. Bound, J.P. and N. Voulvoulis, *Household disposal of pharmaceuticals as a pathway for aquatic contamination in the United Kingdom*. Environ Health Perspect, 2005. **113**(12): p. 1705-11.
41. Lubick, N., *Drugs in the environment: do pharmaceutical take-back programs make a difference?* Environ Health Perspect, 2010. **118**(5): p. A210-4.
42. Daughton, C.G., *Cradle-to-cradle stewardship of drugs for minimizing their environmental disposition while promoting human health. II. Drug disposal, waste reduction, and future directions*. Environ. Health Perspect., 2003. **111**(5): p. 775-785.
43. Heerenklage, J. and R. Stegmann, *SARDINIA '97 - Sixth International Landfill Symposium. Cagliari/Italy, October 13-17, 1997*. Environ Sci Pollut Res Int, 1998. **5**(2): p. 117-8.
44. Stegmann, R. *Landfilling: MBP waste landfills*. 2011. John Wiley & Sons Ltd.
45. Odunlami, M.O., *Investigation of groundwater quality near a municipal landfill site (IGQMLS)*. Int. J. Chem. Eng. Appl., 2012. **3**(6): p. 366-369.

46. Heyer, K.-U. and R. Stegmann. *Landfill systems, sanitary landfilling of solid wastes, and long-term problems with leachate*. 2005. Wiley-VCH Verlag GmbH & Co. KGaA.
47. Rahman, S.Z., R.A. Khan, V. Gupta, and M. Uddin, *Pharmacoenvironmentology--a component of pharmacovigilance*. Environ Health, 2007. **6**: p. 20.
48. Cooper, E.R., T.C. Siewicki, and K. Phillips, *Preliminary Risk Assessment Database and Risk Ranking of Pharmaceuticals in the Environment*. Sci. Total Environ., 2008. **398**: p. 26-33.
49. Agerstrand, M., C. Berg, B. Bjorlenius, M. Breitholtz, B. Brunstrom, J. Fick, L. Gunnarsson, D.G.J. Larsson, J.P. Sumpter, M. Tysklind, and C. Ruden, *Improving environmental risk assessment of human pharmaceuticals*. Environ. Sci. Technol., 2015: p. Ahead of Print.
50. Willis, H.H., J.M. Gibson, R.A. Shih, S. Geschwind, S. Olmstead, J. Hu, A.E. Curtright, G. Cecchine, and M. Moore, *Prioritizing environmental health risks in the UAE*. Risk Anal, 2010. **30**(12): p. 1842-56.
51. Etchepare, R. and J.P. van der Hoek, *Health risk assessment of organic micropollutants in greywater for potable reuse*. Water Res., 2015. **72**: p. 186-198.
52. Wibbertmann, A., J. Kielhorn, G. Koennecker, I. Mangelsdorf, and C. Melber, *Benzoic Acid and Sodium Benzoate*. 2000: Geneva, Switzerland. p. 1-48.
53. *CRC Handbook of Chemistry and Physics*, ed. R.C. Weast. Vol. 65. 1984, Boca Raton, FL: CRC Press, Inc.
54. Sparks, D.L., *Milestones in Soil Chemistry*. Soil Science, 2006. **171**(Suppl. 1): p. S47-S50.
55. MacEwan, D.M.C., *Identification of the Montmorillonite Group of Minerals by X-Rays*. Nature, 1944. **154**: p. 577-578.
56. Bradley, W.F., *Molecular Associations between Montmorillonite and some Polyfunctional Organic Liquids*. Journal of the American Chemical Society, 1945. **67**(6): p. 975-981.
57. Lu, L., J. Cai, and R.L. Frost, *Near Infrared Spectroscopy of Benzoic Acid Adsorbed on Montmorillonite*. Spectroscopy Letters, 2010. **43**(4): p. 266-274.
58. Sanz, J. and J.M. Serratos, *Nuclear Magnetic Resonance Spectroscopy of Organo-Clay Complexes*. Organo-Clay Complexes and Interactions. ed. S. Yariv and H. Cross. 2002, New York: Marcel Dekker, Inc.

59. Simpson, A.J., D.J. McNally, and M.J. Simpson, *NMR Spectroscopy in Environmental Research: From Molecular Interactions to Global Processes*. Prog. Nucl. Mag. Res. Spectrosc., 2011. **58**: p. 97-175.
60. Chen, J.S. and C.Y. Chiu, *Characterization of Soil Organic Matter in Different Particle-Size Fractions in Humid Subalpine Soils by CP/MAS ¹³C NMR*. Geoderma, 2003. **117**: p. 129-141.
61. Hatcher, P.G., K.J. Dria, S. Kim, and S.W. Frazier, *Modern Analytical Studies of Humic Substances*. Soil Science, 2001. **166**(11): p. 770-794.
62. Plante, A.F., J.M. Fernandez, and J. Leifeld, *Application of Thermal Analysis Techniques in Soil Science*. Geoderma, 2009. **153**: p. 1-10.
63. Yariv, S., *Study of the Adsorption of Organic-Molecules on Clay-Minerals by Differential Thermal-Analysis*. Thermochimica Acta, 1985. **88**(1): p. 49-68.
64. Yariv, S. and I. Lapidés, *Thermo-Infrared-Spectroscopy Analysis of Dimethyl-Sulfoxide-Kaolinite Intercalation Complexes*. J. Therm. Anal. Calorim., 2008. **94**: p. 433-440.
65. Yariv, S., *Thermo-IR-Spectroscopy Analysis of the Interactions between Organic Pollutants and Clay Minerals*. Thermochim. Acta, 1996. **274**: p. 1-35.
66. Farmer, V.C. and M.M. Mortland, *An Infrared Study of Co-Ordination of Pyridine and Water to Exchangeable Cations in Montmorillonite and Saponite*. Journal of the Chemical Society a -Inorganic Physical Theoretical, 1966(3): p. 344-351.
67. Kubicki, J.D., L.M. Schroeter, M.J. Itoh, B.N. Nguyen, and S.E. Apitz, *Attenuated Total Reflectance Fourier-Transform Infrared Spectroscopy of Carboxylic Acids Adsorbed onto Mineral Surfaces*. Geochimica Et Cosmochimica Acta, 1999. **63**(18): p. 2709-2725.
68. Capkova, P., M. Pospisil, M. Valaskova, D. Merinska, M. Trchova, Z. Sedlakova, Z. Weiss, and J. Simonik, *Structure of Montmorillonite Cointercalated with Stearic Acid and Octadecylamine: Modeling, Diffraction, IR Spectroscopy*. Journal of Colloid and Interface Science, 2006. **300**(1): p. 264-269.
69. Fillaux, F., M.H. Limage, and F. Romain, *Quantum Proton Transfer and Interconversion in the Benzoic Acid Crystal: Vibrational Spectra, Mechanism and Theory*. Chem. Phys., 2002. **276**: p. 181-210.
70. Boczar, M., K. Szczeponek, M.J. Wojcik, and C. Paluszkiwicz, *Theoretical Modeling of Infrared Spectra of Benzoic Acid and its Deuterated Derivative*. J. Mol. Struct., 2004. **700**: p. 39-48.

71. Wilson, C.C., N. Shankland, and A.J. Florence, *Direct determination of the temperature dependence of proton transfer in the benzoic acid dimer by single crystal neutron diffraction*. Chem. Phys. Lett., 1996. **253**(1,2): p. 103-107.
72. Wilson, C.C., N. Shankland, and A.J. Florence, *A single-crystal neutron diffraction study of the temperature dependence of hydrogen-atom disorder in benzoic acid dimers*. J. Chem. Soc., Faraday Trans., 1996. **92**(24): p. 5051-5057.
73. Cai, W. and A. Katrusiak, *Pressure effects on H-ordering in hydrogen bonds and interactions in benzoic acid*. CrystEngComm, 2012. **14**(13): p. 4420-4424.
74. Lindquist, E. and Y. Yang, *Degradation of Benzoic Acid and its Derivatives in Subcritical Water*. J. Chromatogr. A, 2011. **1218**: p. 2146-2152.
75. Kong, C.H., P. Wang, Y. Gu, X.H. Xu, and M.L. Wang, *Fate and Impact on Microorganisms of Rice Allelochemicals in Paddy Soil*. J. Agric. Food Chem., 2008. **56**: p. 5043-5049.
76. Strobel, B.W., *Influence of Vegetation on Low-Molecular-Weight Carboxylic Acids in Soil Solution - A Review*. Geoderma, 2001. **99**: p. 169-198.
77. Fountain, D.W., C.A. Cornford, and G.J. Shaw, *Benzoic Acid and Hydroxylated Benzoic Acids in Pollen*. Grana, 1995. **34**: p. 213-216.
78. Kaur, H., Inderjit, and S. Kaushik, *Cellular Evidence of Allelopathic Interference of Benzoic Acid to Mustard (Brassica Juncea L.) Seedling Growth*. Plant Physiol. Biochem., 2005. **43**: p. 77-81.
79. Baziramakenga, R., R.R. Simard, and G.D. Leroux, *Effects of Benzoic and Cinnamic Acids on Growth, Mineral Composition, and Chlorophyll Content of Soybean*. J. Chem. Ecol., 1994. **20**: p. 2821-2833.
80. Kawamura, K., L.L. Ng, and I.R. Kaplan, *Determination of Organic Acids (C1-C10) in the Atmosphere, Motor Exhausts, and Engine Oils*. Environ. Sci. Technol., 1985. **19**(11): p. 1082-1086.
81. Helmig, D., J. Muller, and W. WKlein, *Volatile Organic Substances in a Forest Atmosphere*. Chemosphere, 1989. **19**(8/9): p. 1399-1412.
82. Jalal, M.A.F. and D.J. Read, *The Organic Acid Composition of Calluna Heathland Soil with Special Reference to phyto- and fungitoxicity I. Isolation and Identificaiton of Organic Acids*. Plant and Soil, 1983. **70**: p. 257-272.
83. Cakir, R. and A. Cagri-Mehmetoglu, *Sorbic and benzoic acid in non-preservative-added food products in Turkey*. Food Addit. Contam., Part B, 2013. **6**(1): p. 47-54.

84. Toyoda, M., Y. Ito, K. Isshiki, K. Onishi, T. Kato, M. Kamikura, Y. Shiroishi, Y. Harada, Y. Hukasawa, T. Yokoyama, M. Yoneda, and M. Iwaida, *Daily intake of preservatives, benzoic acid, dehydroacetic acid, propionic acid and their salts, and esters of p-hydrobenzoic acid in Japan*. J. Jap Soc of Nut, 1983. **96**: p. 467-480.
85. Lu, P.-Y. and R.L. Metcalf, *Environmental fate and biodegradability of benzene derivatives as studied in a model aquatic ecosystem*. Environ. Health Perspect., 1975(10): p. 269-84.
86. Barker, J.F., J.E. Barbash, and M. Labonte, *Groundwater contamination at a landfill sited on fractured carbonate and shale*. J. Contam. Hydrol., 1988. **3**(1): p. 1-25.
87. Kawamura, K. and I.R. Kaplan, *Biogenic and anthropogenic organic compounds in rain and snow samples collected in southern California*. Atmos. Environ., 1986. **20**(1): p. 115-24.
88. Inderjit and P.C. Bhowmik, *Sorption of Benzoic Acid onto Soil Colloids and its Implications for Allelopathy Studies*. Biol. Fertil. Soils, 2004. **40**: p. 345-348.
89. Harpstead, M.I. and D.H. Francis, *Soil Science Simplified*. 1980, Ames, Iowa, U.S.A.: Iowa State University Press.
90. Bhattacharya, K.G. and S.S. Gupta, *Adsorption of a Few Heavy Metals on Natural and Modified Kaolinite and Montmorillonite: A Review*. Adv. Colloid Interface Sci., 2008. **276**: p. 181-210.
91. Foth, H.D., *Fundamentals of Soil Science*. 1984: John Wiley & Sons, Inc.
92. Hinrich, B., B.L. McNeal, and G.A. O'Conner, *Soil Chemistry*. 1979: John Wiley & Sons, Inc.
93. Gieseking, J.E., *Soil Components*. Inorganic Components. Vol. 2. 1975.
94. FitzPatrick, E.A., *Soils*. 1980, New York City, NY, U.S.A.: Longman, Inc.
95. Deer, W.A., R.A. Howie, and J. Zussman, *Rock-Forming Minerals*. Vol. 1-5. 1962-1963, London: Longmans.
96. Hurlbut, C.S., *Dana's Manual of Mineralogy*. 1952, New York: Wiley.
97. Hendricks, S.B.N., R. A.; Alexander, L. T., *Hydration Mechanism of the Clay Mineral Montmorillonite Saturated with Various Cations*. Journal of the American Chemical Society 1940. **62**: p. 1457-64.

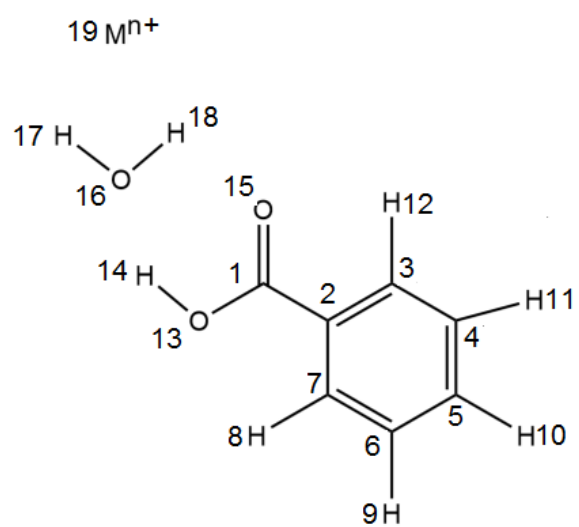
98. Ferrage, E., Bruno Lanson, Natalie Malikove, Alain Plancon, Boris A. Sakharov, and Victor A. Drits, *New Insights on the Distribution of Interlayer Water in Bi-Hydrated Smectite from X-ray Diffraction Profile Modeling of 00l Reflections*. Chem. Mater., 2005. **90**: p. 3499-3512.
99. Michot, L.J., E. Ferrage, M. Jimenez-Ruiz, M. Boehm, and A. Delville, *Anisotropic Features of Water and Ion Dynamics in Synthetic Na- and Ca-Smectites with Tetrahedral Layer Charge. A Combined Quasi-elastic Neutron Scattering and Molecular Dynamics Simulations Study*. J. Phys. Chem. C, 2012. **116**: p. 16619-16633.
100. Angell, C.L., J.R. Ferraro, R.H. Hall, G. Horlick, K. Krishnan, L.A. Nafie, D.W. Vidrine, and W.K. Yuen, *Fourier Transform Infrared Spectroscopy*. Techniques Using Fourier Transform Interferometry, ed. J.R. Ferraro and L.J. Basile. Vol. 3. 1982, New York: Academic Press.
101. Horta, A., B. Malone, U. Stockmann, B. Minasny, T.F.A. Bishop, A.B. McBratney, R. Pallasser, and L. Possz, *Potential of Integrated Field Spectroscopy and Spatial Analysis for Enhanced Assessment of Soil Contamination: A Prospective Review*. Geoderma, 2015. **241-242**: p. 180-209.
102. Schwartz, G., G. Eshel, and E. Ben-Dor, *Reflectance Spectroscopy as a Tool for Monitoring Contaminated Soils*.
103. Mielenz, R.C., N.C. Schieltz, and M.E. King. *Thermogravimetric analysis of clay and claylike minerals*. in *Clays and Clay Minerals*. 1953. Denver, CO: Natl. Acad. Sci.-Natl. Research Council.
104. Stanley, D.A. and B.J. Scheiner, *Flocculation and Dewatering of Montmorillonite Modified by Ion Exchange - RI 9021*. 1986, Avondale, MD: U.S. Dept of Interior, Bureau of Mines.
105. Stanley, D.A., S.W. Webb, and B.J. Scheiner, *Rheology of Ion-Exchanged Montmorillonite Clays - RI 8895*. 1984, Avondale, MD: U.S. Dept. of Interior, Bureau of Mines. 17.
106. Lahav, N., Y. Chen, and B. Bar-Yosef, *Clay Suspensions in a Drying-Out Process*. Soil Sci., 1967. **106**(4): p. 297-302.
107. Fitzsimmons, R.F., A.M. Posner, and J.P. Quirk, *Electron Microscopic and Kinetic Study of the Flocculation of Calcium Montmorillonite*. Israel Journal of Chemistry, 1970. **8**: p. 301-314.
108. Hapke, B., *Theory of Reflectance and Emittance Spectroscopy*. 2nd ed. 2012: Cambridge University Press.

109. White, D.R. and R.L. White, *Isoconversion Effective Activation Energy Profiles by Variable Temperature Diffuse Reflection Infrared Spectroscopy*. Appl. Spectrosc., 2008. **62**: p. 116-120.
110. Antony, J., G. Von Helden, G. Meijer, and B. Schmidt, *Anharmonic Midinfrared Vibrational Spectra of Benzoic Acid Monomer and Dimer*. J. Chem. Phys., 2005. **123**: p. 14305-14311
111. Nandi, C.K., M.K. Hazra, and T. Chakraborty, *Vibrational Coupling in Carboxylic Acid Dimers*. J. Chem. Phys., 2005. **123**: p. 124310-124317.
112. Morodome, S.a.K.K., *Swelling Behavior of Na- and Ca- Montmorillonite Up to 150C By In Situ X-Ray Diffraction Experiments*. Clays and Clay Minerals, 22009. **57**(2): p. 150-160.
113. Marry, V., E. Dubois, N. Malikova, J. Breu, and W. Haussler, *Anisotropy of Water Dynamics in Clays: Insights from Molecular Simulations for Experimental QENS Analysis*. J. Phys. Chem. C, 2013. **117**: p. 15106-15115.
114. Handy, R.L., T. Demirel, T. Ruenkairergsa, and T. Olson, *Adsorption Energies and Swelling Pressures of Montmorillonite*. 1973. p. 1-87.
115. Loring, J.S., E.S. Ilton, J. Chen, C.J. Thompson, P.F. Martin, P. Benezeth, K.M. Rosso, A.R. Felmy, and H.T. Schaef, *In Situ Study of CO₂ and H₂O partitioning between Na-Montmorillonite and Variably Wet Supercritical Carbon Dioxide*. Langmuir, 2014. **30**(21): p. 6120-6128.
116. Rother, G., E.S. Ilton, D. Wallacher, T. Haub, H.T. Schaef, D. Qafoku, K.M. Rosso, A.R. Felmy, E.G. Krukowski, A.G. Stack, N. Grimm, and R.J. Bodnar, *CO₂ sorption to Subsingle Hydration Layer Montmorillonite Clay Studied by Excell Sorption and Neutron Diffraction Measurements*. Environ. Sci. Technol., 2013. **47**(1): p. 205-211.
117. Schaef, H.T., V. Glezakou, A.T. Owen, S. Ramprasad, P.F. Martin, and B.P. McGrail, *Surface Condensation of CO₂ onto Kaolinite*. Environ. Sci. Technol. Lett., 2014. **1**(2): p. 142-145.
118. Ilton, E.S., H.T. Schaef, O. Qafoku, K.M. Rosso, and A.R. Felmy, *In Situ X-Ray Diffraction Study of Na⁺ Saturated Montmorillonite Exposed to Variabley Wet Super Critical CO₂*. Environ. Sci. Technol., 2012. **46**(7): p. 4241-4248.
119. Loring, J.S., H.T. Schaef, R.V.F. Turcu, C.J. Thompson, Q.R.S. Miller, P.F. Martin, J. Hu, D.W. Hoyt, O. Qafoku, E.S. Ilton, A.R. Felmy, and K.M. Rosso, *In Situ Molecular Spectroscopic evidence for CO₂ intercalation into montmorillonite in supercritical carbon dioxide*. Langmuir, 2012. **28**(18): p. 7125-7128.

120. Schaefer, H.T., E.S. Ilton, O. Qafoku, P.F. Martin, A.R. Felmy, and K.M. Rosso, *In Situ XRD Study of Ca²⁺ Saturated Montmorillonite (STX-1) Exposed to Anhydrous and Wet Supercritical Carbon Dioxide*. *Internat. J. Greenhouse Gas Cont.*, 2012. **6**: p. 220-229.
121. Zhu, J.Q., M.P. Sheng, Z. Huan, X.S. Qian, W. Qiang, and Q. Yan, *The Effect of Temperature on the Solubility of Benzoic Acid Derivatives in Water*. *Fluid Phase Equil.*, 2006. **250**: p. 165-172.
122. Villar, M.V., R. Gomez-Espina, and G.-N. L., *Basal spacings of smectite in compacted bentonite*. *Appl. Clay Sci.*, 2012. **65**: p. 95-105.
123. Bakker, J.M., L. Mac Aleese, G. von Helden, and G. Meijer, *The Infrared Absorption Spectrum of the Gas Phase Neutral Benzoic Acid Monomer and Dimer*. *J. Chem. Phys.*, 2003. **119**(21): p. 11180-11185.
124. Stepanian, S.G., I.D. Reva, E.D. Radchenko, and G.G. Sheina, *Infrared Spectra of Benzoic Acid Monomers and Dimers in Argon Matrix*. *Vibrational Spectrosc.*, 1996. **11**: p. 123-133.
125. Borawska, M.H., P. Koczon, J. Piekut, R. Swislocka, and W. Lewandowski, *Vibrational Spectra and Antimicrobial Activity of Selected Bivalent Cation Benzoates*. *J. Mol. Struct.*, 2009. **17**: p. 284-289.
126. Le Caer, S., M. Lima, D. Gosset, D. Simeone, F. Bergaya, S. Pommeret, J.P. Renault, and R. Righini, *Dynamics of Water Confined in Clay Minerals*. *J. Phys. Chem. C*, 2012. **116**(23): p. 12916-12925.
127. Pitman, M.C. and A.C.T. van Duin, *Dynamics of Confined Reactive Water in Smectite Clay-Zeolite Composites*. *J. Am. Chem. Soc.*, 2012. **134**(6): p. 3042-3053.
128. Li, Z., L. Schulz, C. Ackley, and N. Fenske, *Adsorption of tetracycline on kaolinite with pH-dependent surface charges*. *J. Colloid Interface Sci.*, 2010. **351**(1): p. 254-260.
129. Boczar, M., L. Boda, and M.J. Wojcik, *Theoretical modeling of infrared spectra of hydrogen-bonded crystals of salicylic acid*. *Spectrochim. Acta, Part A*, 2006. **64A**(3): p. 757-760.
130. Boczar, M., L. Boda, and M.J. Wojcik, *Theoretical model for a tetrad of hydrogen bonds and its application to interpretation of infrared spectra of salicylic acid*. *J. Chem. Phys.*, 2006. **124**(8): p. 084306/1-084306/12.

Appendix I: Molecular Modeling

Numbered Three-Body Model



X, Y, Z coordinates for Na⁺ Three-Body Model

Number	Atom	X	Y	Z
1	C	0.00000	0.00000	0.00000
2	C	1.46959	-0.21230	0.00732
3	C	1.96006	-1.52029	0.00665
4	C	3.32868	-1.74894	0.01349
5	C	4.21408	-0.67390	0.02112
6	C	3.72905	0.63092	0.02181
7	C	2.36010	0.86444	0.01493
8	H	1.97394	1.87453	0.01540
9	H	4.41847	1.46644	0.02772
10	H	5.28280	-0.85346	0.02654
11	H	3.70693	-2.76399	0.01292
12	H	1.25616	-2.34204	0.00073
13	O	-0.37351	1.26573	0.00181
14	H	-1.37561	1.33420	-0.00642
15	O	-0.79471	-0.93855	-0.00723
16	O	-2.22400	-0.04831	0.02227
17	H	-3.13232	0.23301	0.03624
18	H	-2.21509	-0.99844	0.06137
19	Na	-4.30346	-0.82653	0.01964

Predicted Infrared Frequencies for Na⁺ Three-Body Model

Frequency (cm ⁻¹)	Intensity	Assignment
704.0383	9.0557	Ring bend
715.9829	26.8924	Ring Stretch
735.0352	55.8259	C-C-H oop bend
803.8426	23.8569	COOH scissor + ring stretch
829.6635	30.4908	C-C-H oop bend + C-O-H oop bend
862.7097	68.7641	C-O-H oop bend
877.6543	0.4913	C-C-H oop bend
983.2872	0.9844	C-C-H oop bend
1015.5097	0.0039	C-C-H oop bend
1021.7330	5.3220	Ring Stretch
1042.2730	0.0053	C-C-H oop bend
1050.8282	4.0076	Ring Stretch
1108.3114	11.1415	Ring Stretch
1125.6173	45.3321	C-OH stretch + Ring Stretch
1194.6157	1.1873	C-C-H in plane bend
1207.8085	23.9164	C-C-H in plane bend
1269.5349	103.0477	C-O-H in plane bend
1296.2049	177.9231	C-O-H in plane bend
1345.1416	23.1744	C-O-H stretch + Ring Stretch
1359.7355	8.4719	Ring Stretch
1375.0024	260.5175	C-OH stretch + C-C-H in plane bend
1490.1229	34.6636	C-C-H in plane bend
1529.4777	0.7779	C-C-H in plane bend
1621.3749	132.1498	Ring Stretch
1634.4363	117.0545	Ring Stretch
1675.7023	1300.0325	C=O stretch + C-O-H in plane bend
1719.7859	125.9259	Water Molecule
3159.9545	0.0004	C-H stretching
3170.4960	3.3629	C-H stretching
3179.0571	5.9366	C-H stretching
3190.3148	3.4170	C-H stretching
3196.8780	1.5733	C-H stretching
3267.6529	84.4122	O-H stretching
3798.4551	1536.9232	Water Molecule
3892.5832	776.4267	Water Molecule

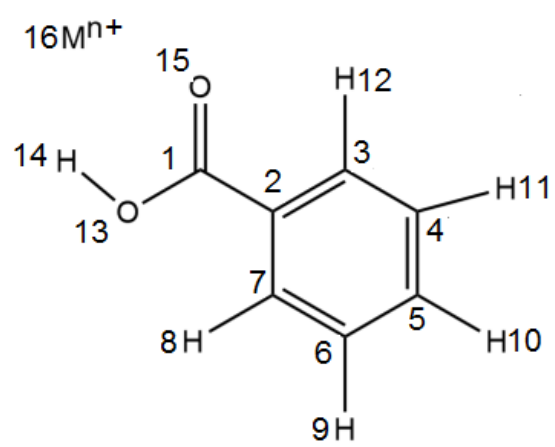
X, Y, Z coordinates for Ca²⁺ Three-Body Model

Number	Atom	X	Y	Z
1	C	0.00000	0.00000	0.00000
2	C	1.46309	-0.25324	0.00732
3	C	1.91687	-1.57440	0.00665
4	C	3.27857	-1.84116	0.01349
5	C	4.19363	-0.79125	0.02112
6	C	3.74520	0.52660	0.02181
7	C	2.38330	0.79824	0.01493
8	H	2.02548	1.81871	0.01540
9	H	4.45767	1.34255	0.02772
10	H	5.25692	-1.00057	0.02654
11	H	3.62835	-2.86637	0.01292
12	H	1.19030	-2.37619	0.00073
13	O	-0.33804	1.27566	0.00181
14	H	-1.33784	1.37207	-0.00642
15	O	-0.82059	-0.91600	-0.00723
16	O	-2.22448	0.01378	0.02227
17	H	-3.12460	0.32035	0.03624
18	H	-2.24210	-0.93623	0.06137
19	Ca	-4.32485	-0.70610	0.01964

Predicted Infrared Frequencies for Ca²⁺ Three-Body Model

Frequency (cm ⁻¹)	Intensity	Motion
702.5858	8.3841	Ring bend
704.6416	4.9273	Ring Stretch
734.1841	55.3155	C-C-H oop bend
799.0677	8.5712	COOH scissor + ring stretch
829.5317	28.6962	C-C-H oop bend + C-O-H oop bend
861.6072	55.8969	C-O-H oop bend
877.3662	0.2400	C-C-H oop bend
984.3752	0.6976	C-C-H oop bend
1016.9982	0.0002	C-C-H oop bend
1021.6105	8.3632	Ring Stretch
1044.5652	0.0243	C-C-H oop bend
1051.7544	3.4747	Ring Stretch
1109.2649	11.0281	Ring Stretch
1125.5268	93.2433	C-OH stretch + Ring Stretch
1195.8919	1.0678	C-C-H in plane bend
1209.3677	29.8129	C-C-H in plane bend
1284.3116	112.0565	C-O-H in plane bend
1296.2672	334.8411	C-O-H in plane bend
1349.6730	8.2900	C-O-H in plane bend + Ring Stretch
1362.4861	6.3822	C-C-H in plane bend
1393.7331	542.4893	C-OH stretch + C-C-H in plane bend
1490.8351	63.1599	C-C-H in plane bend
1529.9765	0.3860	C-C-H in plane bend
1621.4587	245.8033	Ring Stretch + C-O-H in plane bend
1633.3351	118.2854	Ring Stretch
1678.4495	1514.8273	C=O stretch + C-O-H in plane bend
1826.8162	164.7454	Water Molecule
3160.8651	0.0054	C-H stretching
3171.3041	2.4691	C-H stretching
3179.5932	5.1963	C-H stretching
3190.3751	2.4856	C-H stretching
3196.6569	1.5253	C-H stretching
3268.5162	183.3200	O-H stretching
3713.5079	245.8932	Water Molecule
3884.7133	2187.7638	Water Molecule

Numbered Two-Body Model



X, Y, Z coordinates for Na⁺ Three-Body Model

Number	Atom	X	Y	Z
1	C	0.00000	0.00000	0.00000
2	C	-1.47861	-0.13896	0.02344
3	C	-2.03317	-1.42089	0.02067
4	C	-3.41132	-1.58120	0.04213
5	C	-4.24191	-0.46351	0.06637
6	C	-3.69248	0.81553	0.06921
7	C	-2.31376	0.98068	0.04783
8	H	-1.87777	1.97028	0.04985
9	H	-4.33931	1.68426	0.08809
10	H	-5.31812	-0.58970	0.08303
11	H	-3.83966	-2.57614	0.03998
12	H	-1.37120	-2.27659	0.00163
13	O	0.43610	1.24555	0.00380
14	H	1.44030	1.26047	-0.00980
15	O	0.74683	-0.97687	-0.02108
16	Na	2.85009	-0.63158	0.10811

Predicted Infrared Frequencies for Na⁺ Two-Body Model

Frequency (cm⁻¹)	Intensity	Motion
698.5466	13.7594	C-C-H oop bend + C-O-H oop bend
727.5111	22.491	C-C-H oop bend + C-O-H oop bend
774.661	153.6217	C-O-H oop bend
798.2269	17.603	Ring Stretch + COOH Scissor
835.2387	0.2736	C-C-H oop bend
875.0897	0.0262	C-C-H oop bend
985.9977	0.8238	C-C-H oop bend
1018.493	0.0233	C-C-H oop bend
1022.1688	3.5456	Ring Stretch
1048.3892	0.0395	C-C-H oop bend
1053.6015	2.9579	Ring Stretch
1111.5747	10.5951	C-C-H in plane bend
1146.5467	7.0846	C-C-H in plane bend + Ring stretch
1198.3789	1.4691	C-C-H in plane bend
1212.5579	44.7023	C-C-H in plane bend
1277.6283	497.0888	C-O-H in plane bend
1356.2898	13.9081	C-O-H in plane bend + Ring Stretch
1366.9941	12.7221	C-C-H in plane bend
1420.4733	74.9972	C-O-H in plane bend
1490.4074	24.7961	C-C-H in plane bend + Ring stretch
1530.9921	0.5814	C-C-H in plane bend
1622.5472	60.9037	Ring Stretch
1632.2017	51.8759	C-C-H in plane bend + Ring stretch
1710.1281	474.3929	C=O stretch + C-O-H in plane bend
3163.0917	0.026	C-H stretching
3172.9038	1.5321	C-H stretching
3181.1144	1.5663	C-H stretching
3192.1114	1.3698	C-H stretching
3197.3486	0.6313	C-H stretching
3285.2685	6.9503	O-H stretching

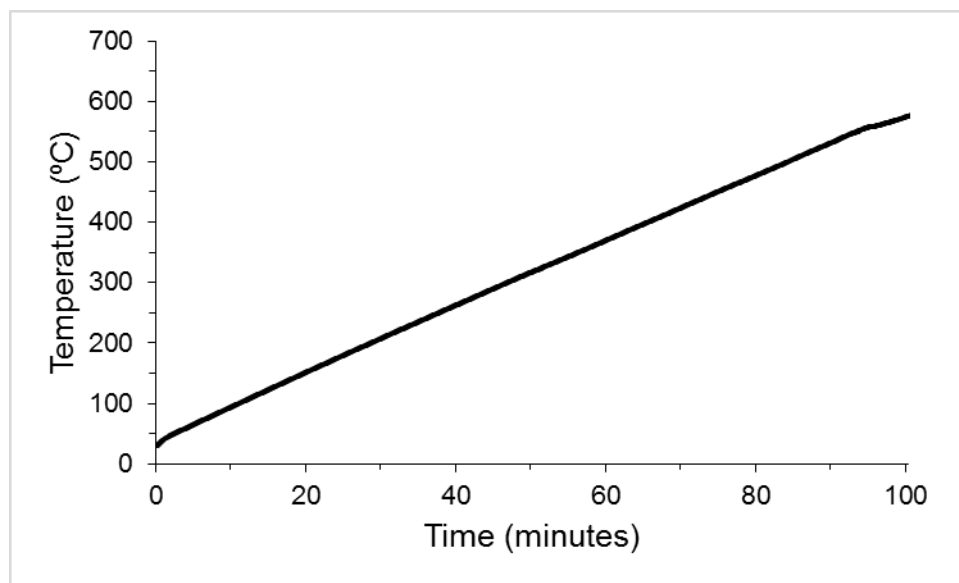
X, Y, Z coordinates for Ca²⁺ Three-Body Model

Number	Atom	X	Y	Z
1	C	0.00000	0.00000	0.00000
2	C	1.47251	-0.18890	-0.02901
3	C	1.98389	-1.48885	-0.02561
4	C	3.35574	-1.69570	-0.05220
5	C	4.22352	-0.60678	-0.08222
6	C	3.71763	0.69010	-0.08570
7	C	2.34537	0.90180	-0.05921
8	H	1.94307	1.90557	-0.06168
9	H	4.39336	1.53642	-0.10908
10	H	5.29478	-0.76932	-0.10288
11	H	3.75021	-2.70455	-0.04954
12	H	1.29346	-2.32165	-0.00204
13	O	-0.39376	1.25957	-0.00482
14	H	-1.39670	1.31205	0.01272
15	O	-0.77933	-0.95102	0.02621
16	Ca	-3.32553	-0.53612	-0.09013

Predicted Infrared Frequencies for Ca²⁺ Two-Body Model

Frequency (cm ⁻¹)	Intensity	Motion
693.2365	4.1500	C-C-H oop bend + C-O-H oop bend
715.9832	20.3733	C-C-H oop bend + C-O-H oop bend
747.8182	67.4950	C-O-H oop bend
799.2336	7.3063	Ring Stretch + COOH Scissor
832.9725	5.0966	C-C-H oop bend
875.8712	0.0008	C-C-H oop bend
985.6964	0.6610	C-C-H oop bend
1018.47	0.0009	C-C-H oop bend
1022.0293	6.0450	Ring Stretch
1047.9436	0.0409	C-C-H oop bend
1053.2943	5.9547	Ring Stretch
1110.7949	9.5719	C-C-H in plane bend
1146.1278	1.4220	C-C-H in plane bend + Ring stretch
1197.9602	1.9186	C-C-H in plane bend
1211.4944	68.3400	C-C-H in plane bend
1267.1549	337.7395	C-O-H in plane bend
1355.4614	7.7054	C-O-H in plane bend + Ring Stretch
1366.3549	8.4988	C-C-H in plane bend
1397.3017	439.9315	C-O-H in plane bend
1489.8036	30.9901	C-C-H in plane bend + Ring stretch
1530.3268	2.9439	C-C-H in plane bend
1621.9509	84.3290	Ring Stretch
1631.9295	69.6813	C-C-H in plane bend + Ring stretch
1698.6821	381.0135	C=O stretch + C-O-H in plane bend
3137.6152	1385.2084	C-H stretching
3162.7994	0.4584	C-H stretching
3172.8008	1.8294	C-H stretching
3180.9956	1.2434	C-H stretching
3191.7225	1.5920	C-H stretching
3197.4076	0.9752	O-H stretching

Appendix II: Thermogravimetry-Mass Spectrometry Time and Temperature Correlation



$$y = 5.3954374928x + 43.4785736407$$
$$R^2 = 0.9993348146$$

(Linear)

$$y = -0.0000000455x^5 + 0.0000096508x^4 - 0.0006544767x^3$$
$$+ 0.0103116019x^2 + 5.8238627407x + 34.7174456836$$

$$R^2 = 0.9999669113$$

(Polynomial)